

Promotoren: prof. dr. ir. Johan L. van Leeuwen,
hoogleraar in de experimentele zoölogie,

prof. dr. Jan W.M. Osse,
emeritus hoogleraar in de algemene dierkunde,

co-promotor: dr. Mees Muller,
universitair hoofddocent bij de leerstoelgroep Experimentele Zoölogie,

overige leden promotiecommissie: prof. dr. ir. Johan Grasman,
Wageningen Universiteit,

dr. Rob C. Peters,
Universiteit Utrecht,

prof. dr. Michael K. Richardson,
Universiteit Leiden,

prof. dr. Marten Scheffer,
Wageningen Universiteit,

prof. dr. Cees J. Weijer,
University of Dundee, United Kingdom.

OXYGEN DIFFUSION IN FISH EMBRYOS

Sander Kranenbarg

Proefschrift
ter verkrijging van de graad van doctor
op gezag van de rector magnificus
van Wageningen Universiteit, prof. dr. ir. L. Speelman,
in het openbaar te verdedigen
op woensdag 4 september 2002
des namiddags te vier uur in de Aula.

Kranenbarg, S. (2002). Oxygen diffusion in fish embryos. Doctoral thesis, Experimental Zoology Group, Wageningen University, P.O. Box 338, 6700 AH Wageningen, The Netherlands.

Subject headings: oxygen / diffusion / embryo / zebrafish / *Danio rerio* / teleost / model / *vegf*

ISBN: 90-5808-680-1

Contents

1	General Introduction	1
1.1	Developmental Biology	2
1.2	Biophysics and Diffusion	3
1.3	Vascular Development	4
1.4	Thesis Outline	5
2	The Phylotypic Egg Timer	9
2.1	Introduction	9
2.2	The Phylotypic Egg Timer	11
	Intermezzo I - A Brief History of the Diffusion Coefficient	15
3	Physical Constraints on Body Size in Teleost Embryos	19
3.1	Introduction	19
3.2	Model	21
3.2.1	Assumptions	21
3.2.2	Oxygen diffusion into embryos living in running water	22
3.2.3	Oxygen diffusion into embryos living in stagnant water	26
3.3	Parameter Values and Predictions on Morphogenesis	29
3.4	Discussion	34
4	Metabolic Constraints on Morphology of the Zebrafish Embryo (<i>Danio rerio</i>)	51
4.1	Introduction	51
4.2	Materials and Methods	52
4.2.1	Model	52
4.2.2	Experimental procedures	56
4.3	Results	56
4.3.1	Parameter values	56
4.3.2	Model output	59
4.4	Discussion	59
	Intermezzo II - Oxygen Transfer to a Sphere in Stokes Flow	63
5	Consequences of Forced Convection for the Constraints on Size and Shape in Embryos	69
5.1	Introduction	69
5.2	Theoretical Analysis	71
5.2.1	Optimal shape in forced convection with infinite or zero velocity	71
5.2.2	Effects of forced convection on size and shape; an analytical approach	74
5.2.3	Effects of forced convection on size and shape; a semi-empirical approach	76
5.3	Discussion	83

6	Oxygen Balance for Small Organisms: an Analytical Model	91
6.1	Introduction	92
6.2	The Model	93
6.2.1	Preliminaries	93
6.2.2	The model equations	96
6.2.3	Critical points and mean consumption rate	99
6.3	One-dimensional Cases	100
6.3.1	The infinite sheet	100
6.3.2	The infinite cylinder and the sphere	102
6.3.3	Limit cases and critical sizes	105
6.4	Higher Dimensional Cases	109
6.4.1	A formal solution	110
6.4.2	Three characteristic shapes	112
6.5	Critical Size for Differently Shaped Organisms	117
6.6	Discussion	122
	Intermezzo III - Diffusivity and solubility	125
7	Oxygen Profile in Zebrafish Embryo (<i>Danio rerio</i>) Elucidated by Theory and Experiment	127
7.1	Introduction	127
7.2	Materials and Methods	128
7.2.1	Oxygen measurements	128
7.2.2	Numerical simulation	129
7.2.3	Input parameter values	129
7.3	Results	130
7.4	Discussion	132
8	Effect of Oxygen Partial Pressure on <i>veg</i>f Expression in the Zebrafish Embryo (<i>Danio rerio</i>)	135
8.1	Introduction	135
8.1.1	Vasculogenesis and angiogenesis	135
8.1.2	Effect of hypoxia	136
8.1.3	Oxygen gradients and vessel development	137
8.2	Materials and Methods	138
8.2.1	Embryos and oxygen treatment	138
8.2.2	Whole mount <i>in situ</i> hybridisation and cryosectioning	138
8.2.3	Simulation of oxygen dynamics	139
8.3	Results	140
8.3.1	<i>veg</i> f expression	140
8.3.2	Simulation of oxygen dynamics	144
8.4	Discussion	145
	Summary	149
	Samenvatting	155
	Bibliography	160
	Dankwoord	179
	Curriculum Vitae	181
	Publication List	183

Chapter 1

General Introduction

If I were to describe the content of this thesis in only two words, they would be ‘passion fruit’. Not only is the work described here the result of four years of passionate work, but it really is the result of a marriage between two fields in biology, *viz.* developmental biology and biophysics. In the following sections, relevant background information on these two fields is given together with an explanation of how the two merge into an interesting research project.

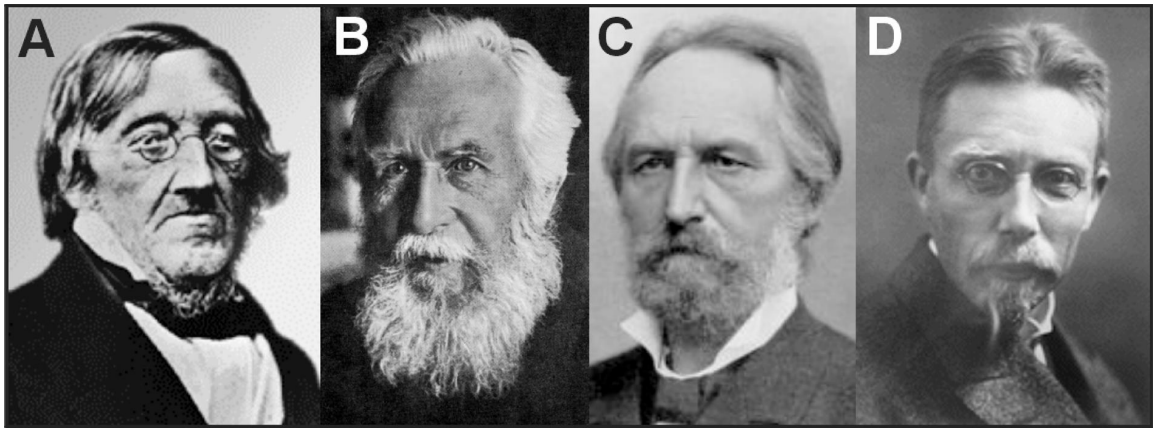


Figure 1.1: Four historical figures whose work provided the basis for an important part of this thesis. a) embryologist Karl Ernst von Baer (1792-1876), b) evolutionist Ernst Haeckel (1834-1919), c) physicist Adolf Fick (1829-1901) and d) physiologist August Krogh (1874-1949).

1.1 Developmental Biology

At the beginning of the 19th century, von Baer (Fig. 1.1) first observed a close resemblance among different vertebrates during early development and this idea was popularized by Haeckel's (Fig. 1.1) famous yet fraudulent drawings (Haeckel, 1877; Richardson *et al.*, 1997, 1998) (Fig. 1.2).

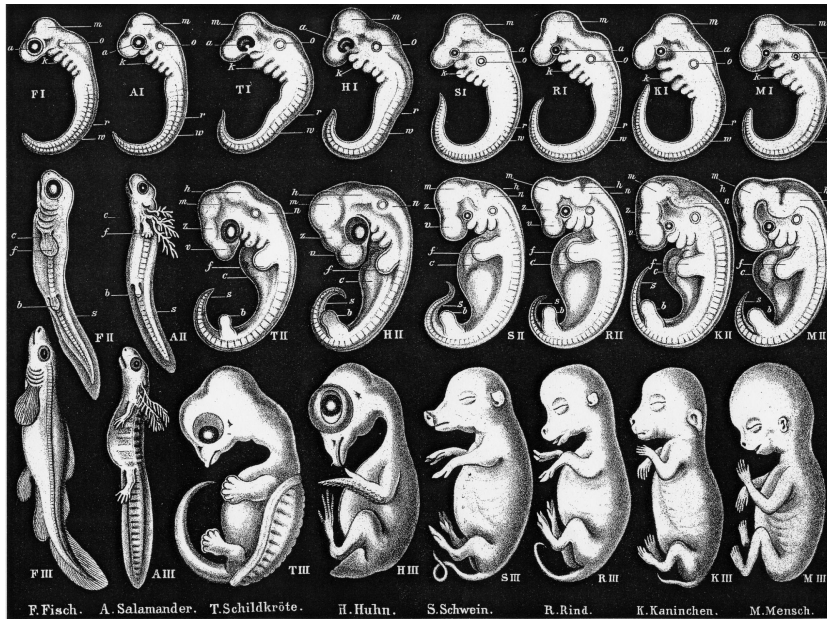


Figure 1.2: Haeckel's famous drawings (Haeckel, 1877) are somewhat idealized from reality to fit the theory. The drawings show the resemblance among vertebrates during early embryonic development. According to Haeckel (1877), the upper row represents a very early stage with gill slits and without bones, the middle row represents a somewhat later stage with gill slits and the first bone formation and the bottom row represents a still later stage with further bone development and loss of the gill slits in all species but the fish. From left to right, the embryos represent a teleost fish, salamander, turtle, chicken, pig, cow, rabbit and a human. Enveloping and appending parts of the embryos were not included in the drawings.

These drawings show human embryos to be similar to pig embryos, which greatly upset the late 19th century society. But even today, Haeckel's drawings keep disturbing many minds. In 2001 a bill was drafted in the state of Arkansas, USA, to prohibit the distribution of these drawings.

Haeckel's 'artist impression of vertebrate development' was put in perspective

by Richardson *et al.* (1997), who showed that vertebrate embryos are not virtually identical during a so-called phylotypic stage, as Haeckel suggested (upper row in Fig. 1.2). However, vertebrate development is characterized by a decrease in visible phenotypic diversity in mid-embryonic stages (Richardson, 1999). This developmental period of phenotypic similarity among vertebrates is known as the phylotypic period (Richardson *et al.*, 1997; Slack *et al.*, 1993). It is during the phylotypic period that organogenesis takes place and the basic vertebrate body plan is established (Duboule, 1994b).

The phylotypic period coincides with the expression of homeotic genes, encoding positional information and segment identity (Raff, 1996). Because the homeotic genes are very conserved among the vertebrates, their temporally colinear expression pattern has been suggested as a cause of the phylotypic period (Duboule, 1994b). The expression of homeotic genes during the phylotypic period provides an example of *phylogenetic constraints* on vertebrate development.

1.2 Biophysics and Diffusion

All vertebrate embryos develop in a watery environment and besides phylogeny, the ruling physical laws also constrain the developing embryos. If the embryo is small enough, diffusion through the skin is sufficient to meet its oxygen demands. Growth of the embryo, however, demands at some time the development of an internal oxygen transport mechanism as diffusion through the skin alone is not sufficient anymore to serve the increasing volume of cells. This is an example of a *physical constraint* on vertebrate development.

The process of diffusion was first mathematically described by Fick's (Fig. 1.1) laws (Fick, 1855), based on Fourier's equation for conduction of heat. Fick's first law describes stationary diffusion, while his second law (Fig. 1.3) incorporates time-dependent changes in the diffusion process. Fick provided a basis for the quantitative analysis of diffusion. While Fick considered diffusion to be an interesting *physical* phenomenon, it was Krogh (Fig. 1.1) who first pointed out the relevance of diffusion in *biological* phenomena. In 1919, Krogh published a paper on the rate of diffusion of gases through animal tissue. Warburg (1923) was the first to give a quantitative description of oxygen diffusion into a tissue slice. In '*The comparative physiology of respiratory mechanisms*', Krogh (1941) applied the physical description of diffusion to biological situations and formulated the general conclusion that "...diffusion alone

$$\frac{\partial y}{\partial t} = - k \frac{\partial^2 y}{\partial x^2}$$

Figure 1.3: Reproduction from Fick’s original publication ‘Ueber Diffusion’ (Fick, 1855). The picture represents Fick’s second law of diffusion, in which y is the concentration, t is time, k is the diffusion coefficient and x is distance. Note that the minus sign is incorrect (when k is positive) as a decrease in the oxygen gradient over a tissue slice (d^2y/dx^2 negative) leads to a decrease in the oxygen concentration in that slice (dy/dt negative).

can provide sufficient oxygen only to organisms of 1 mm diameter or less...”. Other examples of physical constraints in which diffusion plays a role are the distribution of nutrients and the removal of waste products in early embryos.

1.3 Vascular Development

The phylotypic period is a characteristic feature of vertebrate development and provides an interesting subject for biophysical research. During the phylotypic period, the circulatory system forms. This formation can be divided into two processes; vasculogenesis and angiogenesis (Weinstein, 1999). Vasculogenesis can be defined as “the differentiation of angioblasts from mesoderm and the formation of primitive blood vessels from angioblasts at or near the site of their origin” (Risau and Flamme, 1995). This process of vasculogenesis results in the formation of primitive major blood vessels and appears to be largely genetically determined (Weinstein, 1999).

Vasculogenesis is followed by “the vascularization of tissues as a result of sprouting of new vessels from preexisting ones” which is defined as angiogenesis (Maltepe and Simon, 1998; Risau and Flamme, 1995; Weinstein, 1999). The combination of vasculogenesis and angiogenesis leads to a proper development of the early primitive vessels into functional vascular networks. An increase in the relative importance of angiogenesis in the functional development of the axial vessels can be observed from

lower to higher vertebrates (Weinstein, 1999). In contrast to vasculogenesis, angiogenesis is largely dependent on environmental cues such as local oxygen concentration (Weinstein, 1999).

Prior to the development of a circulatory system, vertebrate embryos rely on diffusion through the skin for their oxygen supply. In adult vertebrates, the circulatory system plays an important role in the transport of oxygen to the respiring tissues. The research described in this thesis investigates whether circulatory system development in vertebrates is associated with reaching Krogh's 1 mm limit. In other words: does the circulatory system in vertebrates develop in order to instantly overcome oxygen shortage in the growing embryo (physical constraint) or is its formation largely determined by phylogenetic constraints (which might be physical constraints being incorporated in the genome)? Other functions of the circulatory system (*e.g.* waste removal, nutrient distribution) might provide other clues as to the proximate goal of its development.

1.4 Thesis Outline

Chapter 2 was published in a special issue of the Netherlands Journal of Zoology, entitled 'Adaptation and integration in vertebrates' (*Neth.J.Zool.* **50**(2): 289-294) on the occasion of the retirement of professor Jan W.M. Osse. That chapter gives further background information on the phylotypic period and can be seen as an elaboration of section 1.1.

In chapter 3 (published in the *Journal of Theoretical Biology* **204**(1): 113-133) embryos are represented as plane sheets, cylinders and spheres. Analytical models are employed to describe oxygen diffusion and consumption in these geometrically simple shapes. A distinction was made between a situation where the water around the embryo is continuously being refreshed (running water) and a situation with completely stagnant water. Maximum sizes could be predicted for the model embryos in both situations and these theoretical predictions were compared to literature data of actual vertebrate embryos. As expected all embryos are smaller than the maximum size allowed in running water. In stagnant water only two of the eight species considered have lack of oxygen. Apparently, oxygen is not directly limiting size of vertebrate embryos.

This conclusion gave rise to the idea that substances other than oxygen might diffuse less easily through tissue and thus set tighter limits on the size and shape of a

vertebrate embryo. In chapter 4 oxygen and nutrient diffusion was analyzed in a zebrafish embryo (*Danio rerio*) with a very early circulatory system, in a running water situation. The embryo was represented as a one-dimensional stack of half cylinders lying on top of a yolk mass. At the boundary between yolk and embryonic tissue, an axial vessel was modelled. Nutrients could diffuse from the blood vessel into the surrounding tissue, while oxygen could diffuse both from the surrounding water and from the blood vessel into the surrounding tissue. This model showed oxygen not to be a limiting factor for either height or length of the embryo. Nutrient concentration, however, appeared to be much more constraining than oxygen concentration. In fact, the predicted maximum height of the zebrafish embryo based on nutrient diffusion was similar to the actual height of the animal.

So nutrient diffusion was predicted to constrain the size of a developing zebrafish embryo, while oxygen diffusion was not. But in the analysis so far, embryos were simplified to geometrically simple shapes and mainly running water situations were analyzed. The next step was to investigate the effect of intermediate flow velocities of the water around the embryo on the oxygen diffusion dynamics. Chapter 5 (published in the *Journal of Theoretical Biology* **212**(4), 521-533) gives an analysis of the effects of forced convection on the maximum size and shape of embryos. In high flow velocities (near running water, *cf.* chapter 3 and 4), a flattened shape appeared to be the most favorable for oxygen uptake. When flow velocities are very small, however (nearly stagnant water), a spherical shape appeared to be the most favorable for gas exchange. This was a rather remarkable find, stressing the positive effect of movement in the medium on oxygen supply to the non-spherical vertebrate embryos.

Chapter 6 (published in the *Bulletin of Mathematical Biology* **64**(1), 175-207) presents a general model of oxygen dynamics in small organism that includes the main features of the models described in the previous chapters. It further includes a more realistic concentration dependent oxygen consumption pattern of the embryo and the possibility to analyze different (though still geometrically simple) shapes. The main goal of this chapter was to give an overview of the analytical possibilities in the investigation of oxygen dynamics. The main conclusions from the previous chapters were supported by the more general model.

The main disadvantage of analytical diffusion models is the inaccurate representation of the embryo shape. This difficulty was solved in chapter 7, in which a numerical model of the oxygen dynamics in a realistically shaped zebrafish embryo was

developed. The model embryo consisted of yolk and respiring tissues. Oxygen diffusion and consumption were simulated with a computer program, which yielded the three-dimensional oxygen profile inside and around the embryo. The lowest oxygen partial pressure was predicted in the head with a gradient of posteriorly increasing pressure along the midline of the embryo. These predictions fit well with *in vivo* micro-electrode oxygen measurements, after adjustment of the values assigned to the model parameters. Furthermore, the oxygen permeability of embryonic tissues and yolk was found to be higher than expected. This is very advantageous to the embryo as oxygen can penetrate the respiring tissues relatively easily.

The expression of several endothelial growth factors (*e.g. vegf*) is known to be stimulated by hypoxia. In chapter 8 we compared the expression pattern of *vegf* in zebrafish embryos raised under normoxic and hypoxic conditions. Furthermore, we compared the expression pattern with a simulated three-dimensional oxygen partial pressure profile. No consistent differences in the *vegf* expression pattern were found between the hypoxic and normoxic group. This complies with the idea that early vessel formation in zebrafish is largely genetically determined. The apparent similarity between the *vegf* expression pattern and localization of low oxygen partial pressure has yet to be investigated in more detail. The available evidence suggests that diffusion constraints on early vascularization have been translated into genetic instructions and as such been trapped in the genome.

In between the chapters of this thesis, three *intermezzos* give some background information on a specific subject. Intermezzo I discusses briefly the history of the diffusion coefficient. Intermezzo II provides a mathematical analysis of mass transfer to a sphere in stokes flow and intermezzo III explains the difference between diffusivity and solubility.

Chapter 2

The Phylotypic Egg Timer¹

Von Baer and Haeckel provided the basis of what came to be known as the phylotypic egg timer: during their development vertebrate embryos pass through a period in which they show the archetype of the vertebrate body plan. During this period vertebrate embryos are similar, in both form and morphogenic processes taking place. The phylotypic egg timer has been explained using phylogenetic constraints on the mechanism of body plan formation. Physical laws also pose constraints on embryonic variability. Fathoming these physical and phylogenetic constraints gives us insight in the measure of freedom for variation at a specific stage of vertebrate embryonic development.

2.1 Introduction

In his *Entwicklungsgeschichte der Thiere*, Von Baer (1828) published four empirical laws of embryology: 1) common characters of a taxon develop earlier in ontogeny than specialized ones, 2) specialized forms develop from more general ones, 3) every embryo of a certain taxon diverges more and more from other taxa instead of going through those other forms, 4) an embryo of a higher taxon never resembles (the adult of) another taxon, though only its embryo. Von Baer argued that during ontogeny all animals diverge from one of the four embranchements (radiates, molluscs, articulates and vertebrates), defined in 1812 by Georges Cuvier. Although von Baer saw the similarity among vertebrate embryos, he never accepted the concept of evolution, not even after the publication of Darwin's *Origin of Species* in 1859 (Raff, 1996). It was Haeckel (1877) who combined the concept of evolution and the similarity among early vertebrate embryos, which culminated in his recapitulation theory or biogenetic law (Hall, 1992; Raff, 1996). With his four laws, von Baer already rejected the concept of

¹Kranenbarg, S. (2000). *Neth.J.Zool.* 50, 289-294. Reproduced with permission of Brill, Leiden.

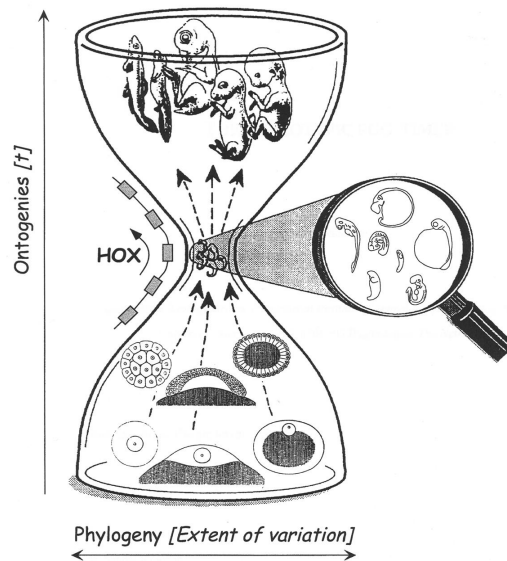


Figure 2.1: The phylotypic egg timer, modified after Duboule (1994b). Ontogeny progresses from bottom to top, while the width of the egg timer indicates the amount of variation present at each stage. The egg- and blastula-stages (lower half of the egg timer) are taken from Haeckel (1877). The embryos in the magnifying glass are redrawn from Richardson *et al.* (1997) and show some of the variation still present during the pharyngula period. Embryos in the upper half of the figure are taken from Duboule (1994b), though they are originally published by Haeckel (1877). The fish larva on the left was not correctly drawn by Haeckel.

recapitulation, which can be traced back until Aristotle’s (384 - 322 BC) Great Chain of Being (Raff, 1996). In his *Anthropogenie*, Haeckel (1877) published a series of comparative drawings which show different vertebrates to develop from a nearly identical “frühes Stadium mit Kiemenspalten, ohne Beine”. A citation from his *Natürliche Schöpfungs-Geschichte* (Haeckel, 1902) might serve to illustrate the implications on society of Haeckel’s theory and drawings: “Was sollen diese Edelleute noch von dem Vollblut, das in ihren privilegierten Adern rollt, denken, wenn sie erfahren, dass alle menschlichen Embryonen, adelige ebenso wie bürgerliche, während der ersten beiden Monate der Entwicklung von den geschwänzten Embryonen des Hundes und anderer Säugethiere kaum zu unterscheiden sind?” The developmental stage at which all vertebrates look rather similar is commonly called the pharyngula stage (Ballard, 1976) or phylotypic stage (Slack *et al.*, 1993). It is the stage at which all vertebrates express

the archetype of the vertebrate body plan (Duboule, 1994b).

2.2 The Phylotypic Egg Timer

Haeckel's recapitulation theory has largely been rejected and it is nowadays believed that phylogenetic divergence finds its origin in ontogenetic divergence. Early ontogenetic divergence is usually coupled to early common ancestors, while late ontogenetic divergence points to the close phylogenetic relationship of the species compared. The phylotypic stage of vertebrate development is not the earliest stage. In fact, stages prior to the pharyngula stage show quite some variation among vertebrates (Raff, 1996), of which Haeckel was well aware (Table II and III in Haeckel (1877); Fig. 2.1). This variation consists of, for example, differences in fertilization (Elinson, 1987), differences in the origin of cells constituting the extraembryonic membranes (resulting from cleavage or not), the existence of holoblastic and meroblastic cleavage in different groups of fish (Slack *et al.*, 1993) and differences in migration patterns and temporary structures among vertebrate classes (Ballard, 1976). This very early divergence followed by a more or less common stage is very interesting since we would expect a common early ontogeny followed by (relatively late) divergence. Apparently, stages prior to and after the phylotypic stage are more variable in an evolutionary sense than the phylotypic stage itself. This idea has been metaphorised as 'the phylotypic egg-timer' (Duboule, 1994b), 'the developmental hourglass' (Raff, 1996) or 'the evolutionary hourglass' (Richardson *et al.*, 1997). Recently, Richardson (1995) showed that heterochrony has shifted the developmental timing of structures in different vertebrates and that it would be more appropriate to speak of a phylotypic period instead of phylotypic stage (Fig. 2.1). The apparent variety in body size during the phylotypic period, led Richardson *et al.* (1997, 1998) to conclude that "differences between species become more apparent at late stages" (cf. Von Baer (1828)), though vertebrates are not virtually identical at earlier stages. Hox genes (homeobox genes that are organized in four vertebrate clusters of hox genes) play an important role in the proper organization of the vertebrate body plan, which takes place during the phylotypic period (Duboule, 1994b,a; Raff, 1996). There is a striking similarity in hox gene expression along the anterior-posterior axis among (and even beyond) all members of the subphylum. Hox genes are activated in a temporal sequence colinear with their position in the cluster (temporal colinearity; Fig. 2.1; Duboule (1994b)). The organisation of hox genes in clusters remains fairly constant among vertebrates.

This results in low flexibility of hox gene expression patterns, which might be coupled with the small window for variation in the phylotypic period (Duboule, 1994b). Besides hox genes, many other genes and induction sequences show striking similarities in all vertebrates. Examples are the growth factors involved in mesoderm induction, the genes of the organizer and the axial expressed genes involved in neurulation. Raff *et al.* (1991) argue that in early (i.e. pre-phylotypic) stages only few inductive processes take place and redundancy is omnipresent. During the phylotypic period, many global interactions take place and any real change in morphogenesis would be lethal. After the pharyngula period, there are many inductive interactions, but they are primarily local and changes are no longer necessarily lethal. This lack of evolutionary flexibility during a certain period of development may be an explanation for the existence of the phylotypic egg timer. Besides constraints on embryonic development that originated from mechanisms of gene expression or induction sequences during evolution (phylogenetic constraints), physical laws might also constrain embryonic development and consequently play a role in explaining the existence of the phylotypic egg-timer (Gilbert, 1991). All embryos are subject to a physical environment, which poses constraints on their development. The laws of hydrodynamics, for example, demand the developing heart to be attuned to the developing vessels for the blood to be pumped around properly. In addition, Fick's laws of diffusion might demand the development of a circulatory system at a certain size. Vertebrate embryos before the phylotypic period solely depend on diffusion for their internal oxygen distribution, since no circulatory system has developed yet. One can imagine that organisms that solely depend on diffusion for distributing oxygen inside their body cannot grow infinitely large. In fact, the constraints on size by the laws of diffusion are probably the reason why insects do not grow bigger and why flatworms are flat (McNeill Alexander, 1971; Krogh, 1941). We constructed a quantitative model (Kranenbarg *et al.*, 2000) describing diffusion of oxygen into embryos and with this model and literature values for the relevant input parameters, we were able to predict maximum allowed size of vertebrate embryos without a circulatory system. We found indeed that in two of the species considered (*Cyprinus carpio* (common carp) and *Clarias gariepinus* (African catfish)) the theoretical occurrence of oxygen shortage (when maximum size is reached) coincided with the first heart beat. In other species a circulatory system develops much earlier than the theoretical occurrence of oxygen shortage, so we hypothesized that other constraining factors (e.g. nutrient

distribution, removal of waste products) might demand the development of a circulatory system. Further modelling and experimentation should elucidate whether these other possible physical constraints play an important role in circulatory system development or whether phylogenetic constraints entirely rule the development of such a system. Unravelling physical and phylogenetic constraints will result in a lot of insight in the actual mechanisms of developmental processes and the measure of freedom involved and might eventually explain why all members of the subphylum Vertebrata go through a phylotypic period.

Acknowledgments

Dr. Henri Stroband and dr. Truus te Kronnie are greatly acknowledged for their comments on the manuscript.

Intermezzo I - A Brief History of the Diffusion Coefficient

In 1855, Fick was the first to quantitatively describe the process of diffusion. His description is based on the hypothesis that the rate of transfer of a diffusing substance through a unit area of section is proportional to the solute concentration gradient. Fick used the factor k as a proportionality factor, or “eine von der Natur der Substanzen abhängige Constante”. This relation came to be known as Fick’s first law of diffusion. With this hypothesis, Fick quantitatively described time-dependent changes in a solute concentration in what now is known as Fick’s second law of diffusion. Fick determined the value of k for diffusion of sodium chloride in water. The S.I. unit of this factor k is m^2/s .

In his 1897 publication on diffusion of gases in water, Hüffner used the term diffusion coefficient for the factor k and described it as “einen die spezifische Geschwindigkeit der betreffenden Gasmoleküle ausdrückenden Factor”. He defined the diffusion coefficient as the volume of gas diffusing through unit area and over unit thickness per unit time under unit pressure difference, divided by the absorption coefficient for the gas in question. As in Fick’s paper, the S.I. unit of the diffusion coefficient is m^2/s .

In 1919, Krogh realized that the absorption coefficients for gases in tissue are generally unknown and defined a diffusion constant as the volume of gas diffusing through unit area and over unit thickness per unit time under unit pressure difference. He did not use a symbol to describe the diffusion constant. Values for the Krogh diffusion constant are expressed in $\text{m}^2/(\text{Pa s})$ or its equivalent.

In his 1923 paper on oxygen diffusion into tissue slices, Warburg introduces the symbol D for the Krogh diffusion constant. Subsequently, in 1927, Fenn uses the same symbol for the diffusion constant in his work on oxygen diffusion into frog nerves. In 1928 however, in quoting Fenn’s 1927 paper, Harvey used the term diffusion coefficient instead of constant and erroneously omitted the factor time from its definition.

In 1931, Gerard was the first to apply Fick's diffusion theory including the 'true' diffusion coefficient D (in m^2/s) to oxygen diffusion into cells. Then, in contrast with his 1919 publication, Krogh also used the symbol D to describe the diffusion coefficient in his book on the comparative physiology of respiratory mechanisms, published in 1941. Yet he persisted in the unit $\text{m}^2/\text{Pa s}$ for his diffusion coefficient.

Up to and including the work of Krogh, diffusion of gases in tissue has experimentally been investigated only in equilibrium situations. In 1962, Grote and Thews acknowledged the essential dependency of time-dependent diffusion processes on the value of the 'true' diffusion coefficient D in m^2/s , defined in 1855 by Fick. They measured the value of the 'true' diffusion coefficient for the first time in heart tissue, thereby enabling the application of Fick's second law to the diffusion of gases in animal tissue.

In accordance with Millington (1955) and to prevent further confusion, it would seem clear to define a 'true' diffusion coefficient D with dimensions m^2/s to describe time-dependent diffusion processes.

$$\frac{\partial c}{\partial t} = D \left(\frac{\partial^2 c}{\partial x^2} + \frac{\partial^2 c}{\partial y^2} + \frac{\partial^2 c}{\partial z^2} \right) \quad (\text{I.1})$$

in which c is the local solute concentration, t is time and x , y and z are the 3 dimensions in which diffusion takes place.

In describing diffusive equilibrium situations in only one dimension, the 'true' diffusion coefficient D (in m^2/s) can be used in conjunction with concentration of the diffusing substance,

$$F_D = -D \frac{dc}{dx} \quad (\text{I.2})$$

where F_D is the rate of transfer in the x -direction through unit area of section (in $\text{kg}/(\text{m}^2 \text{ s})$), D is the 'true' diffusion coefficient and c is the concentration of the diffusing substance. Alternatively, the Krogh diffusion constant K , or permeability, in $\text{m}^2/(\text{Pa s})$ can be used in conjunction with partial pressure of the diffusing gas,

$$F_K = -K \frac{dp}{dx} \quad (\text{I.3})$$

where F_K is again the rate of transfer, though now in $\text{m}^3/(\text{m}^2 \text{ s})$, K is the Krogh diffusion constant and p is the partial pressure of the diffusing gas. The 'true' diffusion coefficient and the Krogh diffusion constant are interrelated by the Bunsen solubility coefficient:

$$K = \alpha_B D \quad (\text{I.4})$$

where α_B is the Bunsen solubility coefficient of the gas in question (in milliliters of gas at STPD dissolved per milliliter liquid at a partial pressure of one atmosphere, Altmann and Dittmer (1971)).

Chapter 3

Physical Constraints on Body Size in Teleost Embryos¹

All members of the subphylum ‘Vertebrata’ display the characteristics of the vertebrate body plan. These characteristics become apparent during the phylotypic period, in which all vertebrate embryos have a similar body shape and internal organization. Phylogenetic constraints probably limit the morphological variation during the phylotypic period. Physical laws, however, also limit growth and morphogenesis in embryos. We investigated to what extent oxygen availability - as a physical constraint - might limit morphological variation during embryonic development. This paper gives an analysis of time-dependent diffusion into spherical embryos without a circulatory system. Equilibrium appeared to settle in about 1.5 mins in running water and in about 10 mins in stagnant water. Hence, steady state conditions were assumed and expressions for maximum body size were obtained for spherical, cylindrical and sheet-like embryos in running water and spherical embryos in stagnant water. Predictions of the model based on literature data suggest that in running water – both for spherical, cylindrical and sheet-like embryos - diffusion alone suffices to cover the oxygen needs of a teleost embryo in its phylotypic period. The size of carp (*Cyprinus carpio*) and African catfish (*Clarias gariepinus*) embryos is very close to the predicted maximum. This suggests that in these species the development of a functional circulatory system is correlated with the onset of oxygen shortage. Oxygen availability is therefore a potentially important physical constraint on embryonic morphology, though in most species the circulatory system becomes functional well in advance of the onset of oxygen shortage and other demands than oxygen delivery (*e.g.* nutrient distribution, waste disposal, osmoregulation) might require the development of a circulatory system.

3.1 Introduction

McFarland *et al.* (1979) hypothesize the existence of an ancestral vertebrate and thus

¹Kranenbarg, S., Muller, M., Gielen, J.L.W. and Verhagen, J.H.G. (2000). *J. Theor. Biol.* 204(1), 113-133. Reproduced with permission of Academic Press.

the subphylum Vertebrata to be monophyletic. The body plan of this hypothetical ancestral vertebrate essentially is a bilateral symmetric, cephalized, tube-within-a-tube arrangement. Variations on this typically vertebrate body plan have led to the different taxa, found within the subphylum Vertebrata today.

Despite this variation, the basic body plan can still be recognized in all species, especially in embryonic and larval stages. Among all members of the subphylum a developmental stage is found which shows considerable similarity in morphology and anatomy (Duboule, 1994b; Elinson, 1987; Haeckel, 1877; Von Baer, 1828; Wolpert, 1991). It is commonly called the pharyngula stage (Ballard, 1976) or phylotypic stage (Slack *et al.*, 1993). Richardson (1995) and Richardson *et al.* (1997, 1998) showed that also during the phylotypic stage some morphological variation is present between members of the Vertebrata and argued that in this respect the phylotypic stage is better described as a phylotypic period, which we will adopt in this paper.

The genetic and molecular mechanisms acting at developmental stages prior to and during the phylotypic period are highly comparable among different vertebrates (*e.g.* Harvey (1996)). The pre-phylotypic stages, however, show considerable morphological variation (*cf.* different types of cleavage and gastrulation among different vertebrate classes) (Gilbert, 1994). Different selection pressures from the completely different environments in which vertebrate eggs develop (*e.g.* water versus land), have probably been instrumental in the evolution of very diverse ways of pre-phylotypic embryonic development.

Realization of the vertebrate body plan requires many inductive interactions which take place throughout the embryonic soma. This may have limited the morphological variation of the phylotypic period, during which organogenesis takes place. After the pharyngula period there are many, though primarily local, inductive interactions, posing no large constraints on variation in general morphology (Gilbert, 1994).

Besides these phylogenetic constraints, physical laws might also directly limit the amount of morphological variation in developing organisms (Gilbert, 1994). Early embryonic stages can only be provided with oxygen by means of diffusion. The process of diffusion, described by Fick's laws, limits the maximum body size of these embryonic stages. The development of a circulatory system can overcome these constraints. In this paper we intend to test the hypothesis that oxygen is a limiting factor in early embryonic development and that a circulatory system develops to overcome these limitations.

Models of diffusion into sheet-like, cylindrical and spherical tissue or cells date back to Warburg (1923; liver slices), Fenn (1927; frog nerves) and Harvey (1928; bacteria), respectively. All these authors modelled oxygen diffusion independent of time (Fick's first law of diffusion). The biological implications of the equations were reviewed by Krogh (1941), McNeill Alexander (1971) and Graham (1988). Fick's first law of diffusion was also used by *e.g.* Daykin (1965), Lee and Strathmann (1998), Seymour (1994), Seymour and Bradford (1995), Strathmann and Chaffee (1984), and Woods (1999) to describe oxygen diffusion into spherical organisms. Fick's first law of diffusion, however, does not take into account any changes in oxygen concentration over time and therefore implies an equilibrium situation. In the present paper we give an analysis of diffusion into spheres based on Fick's second law of diffusion, thus allowing changes in oxygen concentration over time. By analyzing the transient effects (time-dependent changes in oxygen concentration), we try to estimate their relative importance in models of oxygen diffusion into spherical organisms.

Weihs (1980) also modelled time-dependent oxygen diffusion into embryos, though he assumed a vascular system to distribute oxygen inside the embryo. Since we are interested in the constraints posed on embryos without a circulatory system, we included internal diffusion of oxygen as part of our model.

After analyzing the transient effects of diffusion, we apply the model to oxygen diffusion into pharyngulae of teleosts. Literature data of embryos of different species are fed into the model. The calculations lead to theoretical constraints on body size of these embryos if they were to rely solely on passive diffusion for their oxygen supply. These predictions are compared with the actual dimensions of embryos and similarities as well as discrepancies between theory and reality are discussed.

3.2 Model

(for abbreviations, see Appendix A)

3.2.1 Assumptions

To reduce mathematical complexity a number of assumptions are made in our model: (1) In our model a teleost embryo is represented by a homogenous oxygen consuming sphere, cylinder or plane sheet of fixed size, surrounded by a watery fluid. The actual

shape of the embryo is likely to be somewhere in between. (2) We only consider radially directed diffusion. (3) The egg capsule surrounding the embryo is assumed to have neither a facilitating nor an impeding effect on diffusion of oxygen from the surrounding water to the embryonic tissues (Berezovsky *et al.*, 1979; Rombough, 1988), though see discussion. (4) The volume-specific oxygen consumption, *i.e.* oxygen consumption of the embryos per unit volume of respiring tissues, is assumed to be constant, both throughout the embryo and throughout ontogeny (Balinsky, 1975; Rombough, 1998). This simplification also implies that oxygen consumption is independent of oxygen concentration, as long as the concentration *gradient* is large enough to provide a sufficient diffusive flow to meet the consumption requirements. Below a certain value of the ambient oxygen concentration, a large enough concentration gradient cannot be maintained anymore and the embryo is said to be unable to survive below this ambient concentration.

3.2.2 Oxygen diffusion into embryos living in running water

In running water the oxygen concentration at the body surface of an organism is assumed to equal the free water concentration. The governing equation is a partial differential equation describing the change in oxygen concentration inside the embryo as a function of place and time (Fick's second law of diffusion, Appendix B). The total body surface of an organism without a circulatory system is involved in taking up oxygen. First, we will solve Fick's second law for a spherical organism.

According to Fick's first law of diffusion,

$$J = DA \frac{dc}{dr} = D4\pi r^2 \frac{dc}{dr} \quad (3.1)$$

[where J = oxygen flow, D = diffusion coefficient, A = surface area; $4\pi r^2$ for a sphere, c = oxygen concentration, r = distance from the center of the sphere (co-ordinate)], oxygen flows from high to low concentrations with a rate proportional to the existing concentration difference. A net flow of oxygen leads to a proportional increase in oxygen concentration. Therefore, differentiating equation 3.1 with respect to r gives the rise in oxygen concentration at distance r from the center of the sphere due to the net inflow of oxygen at the concentric shell with radius r . Dividing by the surface area of this concentric shell ($4\pi r^2$) gives the rise in oxygen concentration in a point with radius r . In the following equation, we subtracted the term m , to account for consumption of oxygen by the sphere and Fick's second law of diffusion for a sphere

becomes:

$$\frac{\partial c}{\partial t} = \frac{D}{r^2} \frac{\partial}{\partial r} \left(r^2 \frac{\partial c}{\partial r} \right) - m \quad (3.2)$$

(where t = time, m = volume-specific oxygen consumption).

In order to solve this general partial differential equation, we specify it by the following boundary conditions (BC) and initial condition (IC): no oxygen is transported at the center of the sphere (BC₁; horizontal tangent to the oxygen concentration profile at $r = 0$ in Fig. 3.1), oxygen concentration at the body surface equals the free water concentration (BC₂; Figs. 3.1 A, C and E) and oxygen concentration outside the embryo equals the (constant) initial oxygen concentration (by definition C_∞) inside the embryo (IC). Appendix B gives a complete derivation of the solution to the partial differential equation and Figs. 3.1 A, C and E give a graphical representation.

Oxygen starvation will start at the center of the embryo. The oxygen concentration at the center can be described by the following equation:

$$c(0, t) = C_\infty - \frac{mR^2}{6D_e} + \frac{2mR^2}{D_e} \sum_{n=1}^{\infty} \frac{(-1)^{n+1}}{n^2\pi^2} e^{-n^2\pi^2 \frac{D_e t}{R^2}} \quad (3.3)$$

in which $c(0, t)$ = oxygen concentration at the center of the embryo as a function of time, C_∞ = free water oxygen concentration, R = radius of the embryo, D_e = oxygen diffusion coefficient of embryonic tissues, n = integer. In this equation a steady state part (first two terms of the right-hand side) and a transient part (last term of the right-hand side) are recognized. The transient part smoothly decreases to zero for time t approaches infinity. Therefore oxygen starvation will never occur in running water if $mR^2 \leq 6D_e C_\infty$, as is the case in Figs. 3.1 A and C. The maximum radius of a spherical embryo without a circulatory system and living in running water, can be written as:

$$R_{\max} = \sqrt{\frac{6D_e C_\infty}{m}} \quad \text{or} \quad \frac{V}{A} = \sqrt{\frac{2D_e C_\infty}{3m}} \quad (3.4)$$

where V = volume of the sphere and A = surface area of the sphere (*cf.* Harvey (1928)).

Thus the size of an embryo that solely depends on diffusion from the surrounding water for its oxygen supply will be limited by the oxygen concentration of the free water, the oxygen diffusion coefficient and its volume-specific oxygen consumption.

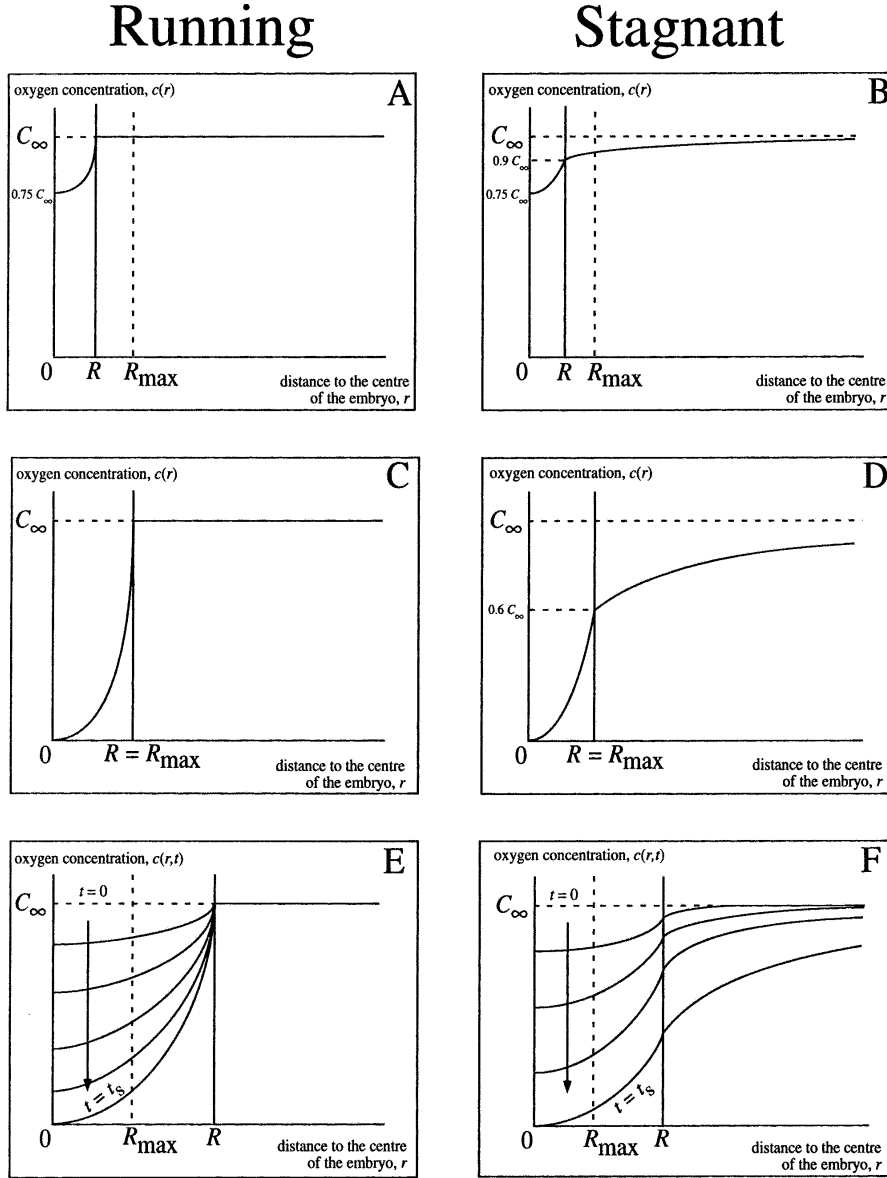


Figure 3.1: Schematic representation of the two models of a spherical embryo described in this paper. Oxygen concentration is plotted against distance from the center of the embryo in all six graphs. R_{\max} represents the maximum radius of the organism (*cf.* equations 3.4 and 3.9) and R represents the actual radius of the organism. The left row of graphs represents different situations in running water and the right row represents equivalent situations in stagnant water. Note that the maximum radius in running water is $1.29 (\sqrt{5/9})$ times as large as in stagnant water. A and B show the oxygen concentration profile in a steady state situation for running (A) and stagnant (B) water conditions, where $R = \frac{1}{2} R_{\max}$. In this example, the oxygen concentration at the center of the embryo will stabilize at $0.75 C_\infty$ in the stagnant water situation and at the body surface, the oxygen concentration stabilizes at $0.9 C_\infty$.

*caption continues on next page*¹

For embryos larger than this maximum volume, the moment of time after which oxygen starvation starts (t_s) is obtained by putting $c(0, t) = 0$ in equation 3.3 and iteratively evaluating different t -values with the help of a computer programme (Fig. 3.1 E and Fig. 3.4).

Further analysis of equation 3.3 shows that the time in which the first 90% of the drop in oxygen concentration from initial to equilibrium situation can be (over)estimated by (see Appendix B):

$$t = -\frac{R^2}{\pi^2 D_e} \ln \left(\frac{\pi^2}{120} \right) = \frac{0.25 R^2}{D_e} \quad (3.5)$$

For spherical embryos with a radius of about 0.5 mm and a diffusion coefficient of $6.55 \cdot 10^{-10} \text{ m}^2\text{s}^{-1}$ (equal to that of frog muscle; 20°C) this results in a time of about 1.5 mins. Since equilibrium appears to settle very quickly (*cf.* cell cycle in cleaving zebrafish embryo of 15 mins), the oxygen profile inside the embryo can be regarded as being in a steady state.

By extrapolating the steady state principle to cylindrical and sheet-like organisms, equivalent formulae for their maximum sizes are easily obtained by solving Fick's first law of diffusion. For a cylinder we obtain (*cf.* Fenn (1927)):

$$R_{\max} = \sqrt{\frac{4D_e C_\infty}{m}} \quad \text{or} \quad \frac{V}{A} = \sqrt{\frac{D_e C_\infty}{m}} \quad (3.6)$$

and for a plane sheet we obtain (*cf.* Warburg (1923)):

$$R_{\max} = \sqrt{\frac{2D_e C_\infty}{m}} \quad \text{or} \quad \frac{V}{A} = \sqrt{\frac{2D_e C_\infty}{m}} \quad (3.7)$$

It can be seen that when embryos are modelled as spheres, cylinders or plane sheets, maximum radii are in the proportion of $\sqrt{6} : \sqrt{4} : \sqrt{2}$, respectively. The result for the actual shape of an embryo is likely to be somewhere in between (Rappoldt, 1992).

¹In running water, the oxygen concentration outside the embryo remains constant (A, C and E), while a diffusion boundary layer will form outside the embryo in stagnant water (B, D and F). C and D show the steady-state oxygen distribution in running and stagnant water, respectively, where $R = R_{\max}$. The oxygen concentration at the center of the embryo stabilizes at 0. In stagnant water, the oxygen concentration at the skin surface stabilizes at $0.6C_\infty$. E and F show the decrease in oxygen concentration, indicated by the arrows, for running and stagnant water, respectively, where $R = 2R_{\max}$, until the concentration at the center of the embryo becomes zero (at $t = t_s$) and the embryo dies. Note the slight difference in inclination angle of the tangent to the inside and outside concentration profile at the body surface (B, D and F), caused by the different diffusion coefficients of oxygen in embryonic tissues and water.

3.2.3 Oxygen diffusion into embryos living in stagnant water

If an animal lives in stagnant water, the oxygen concentration at the body surface does not equal the free water concentration anymore, because a diffusion boundary layer will form. The governing equations now constitute a set of two partial differential equations; one describing the change in oxygen concentration inside the embryo and one describing the change in oxygen concentration outside the embryo, both as a function of place and time as described by Fick's second law of diffusion.

Again, in order to solve the two partial differential equations for a spherical organism, we specify and bind them together by the following boundary and initial conditions: no oxygen is transported at the center of the embryo (BC₁; horizontal tangent to the oxygen concentration profile at $r = 0$ in Fig. 3.1), oxygen concentration at the surface of the embryo is equal for both partial differential equations (BC₂), the same holds true for oxygen transport over the body surface (BC₃) and the oxygen concentration equals the free water concentration at infinite distance from the embryo (BC₄; Figs. 3.1 B, D and F). Furthermore, the (constant) initial oxygen concentration outside the embryo equals the (constant) initial oxygen concentration inside the embryo and both are equal to the free water oxygen concentration (IC). In Appendix B a complete derivation of the solution to this set of partial differential equations can be found. Figs. 3.1 B, D and F give a graphical representation of the solution.

As already mentioned before, oxygen starvation will start at the center of the embryo and for this case the oxygen concentration at the center of the organism can be described by the following equation:

$$c(0, t) = C_\infty - mR^2 \frac{2D_e + D_w}{6D_e D_w} + \frac{m}{\pi} \int_0^\infty \frac{e^{-xt}}{x} \times \frac{\sqrt{D_w D_e} R^2 \sin\left(\frac{R\sqrt{x}}{\sqrt{D_e}}\right) - \sqrt{D_w} R^3 \sqrt{x} \cos\left(\frac{R\sqrt{x}}{\sqrt{D_e}}\right)}{D_w R^2 x \sin^2\left(\frac{R\sqrt{x}}{\sqrt{D_e}}\right) + \left[(D_w - D_e) \sin\left(\frac{R\sqrt{x}}{\sqrt{D_e}}\right) + R\sqrt{D_e} \sqrt{x} \cos\left(\frac{R\sqrt{x}}{\sqrt{D_e}}\right)\right]^2} dx \quad (3.8)$$

in which x = integration variable.

In this equation again a steady state part (first two terms of the right-hand side) and a transient part (last term of the right-hand side) can be recognized. The transient part smoothly decreases to zero for time t approaches infinity. Therefore, oxygen starvation will never occur in stagnant water if $mR^2 \leq 6D_e D_w C_\infty / (2D_e + D_w)$, as is

the case in Figs. 3.1 B and D and

$$R_{max} = \sqrt{\frac{6D_e D_w C_\infty}{(2D_e + D_w)m}} \quad \text{or} \quad \frac{V}{A} = \sqrt{\frac{2D_e D_w C_\infty}{(2D_e + D_w)3m}} \quad (3.9)$$

cf. Lee and Strathmann (1998).

If this condition is not met, the moment of time t after which oxygen starvation starts (t_s) is obtained by putting $c(0, t) = 0$ in equation 3.8, analogous to the running water situation (Fig. 3.1 F).

For relatively large values of t (see Fig. 3.2), equation 3.8 can be approximated by:

$$c(0, \tau) = C_\infty - mR^2 \frac{2D_e + D_w}{6D_e D_w} + \frac{2mR^2 \sqrt{D_e D_w}}{3\pi D_w^2} \int_0^\infty e^{-y^2 \tau} dy \quad (3.10)$$

where $\tau = D_e t / R^2$ and $y = \sqrt{x R^2 / D_e}$.

Equation 3.10 can be solved to give the time in which the central oxygen concentration reaches a value 10% of the difference between initial and equilibrium concentration above its equilibrium value (see Appendix B; equation 3.55):

$$t = \frac{5.0R^2}{D_w} \quad (3.11)$$

cf. Byatt-Smith *et al.* (1991). Note that m and C_∞ disappeared from the equation [cf. equation 3.5], due to the fact that we calculate when the oxygen concentration reaches a value close to the equilibrium instead of calculating when an absolute value is reached (see Appendix B). For the same embryo used in the running water case ($D_w = 1.96 \times 10^{-9} \text{ m}^2 \text{ s}^{-1}$), equilibrium will have settled in about 10 mins (*cf.* 5-10 mins to electrode stabilization in oxygen diffusion boundary layer measurements by Rombough (1998)). The time of 10 mins is in the order of two thirds of a cell cycle (Kimmel *et al.*, 1995). The oxygen profile in stagnant water can therefore also be considered to be in equilibrium.

Rewriting Fick's first law of diffusion for a cylinder shows that the concentration profile outside the embryo is described by a ln-function ($du/dr = R^2 m / 2D_w r$) and for a sheet, the profile is described by a straight line ($du/dr = Rm / D_w$). Both these functions never reach a maximum value for $r \rightarrow \infty$ and therefore, no steady state can be calculated for a cylinder or a sheet (integration constants become infinitely large, *cf.* Lee and Strathmann (1998)).

The thickness of the diffusion boundary layer (Berezovsky *et al.*, 1979; Pinder and Friet, 1994; Rombough, 1998) is defined as the distance from the skin surface to the

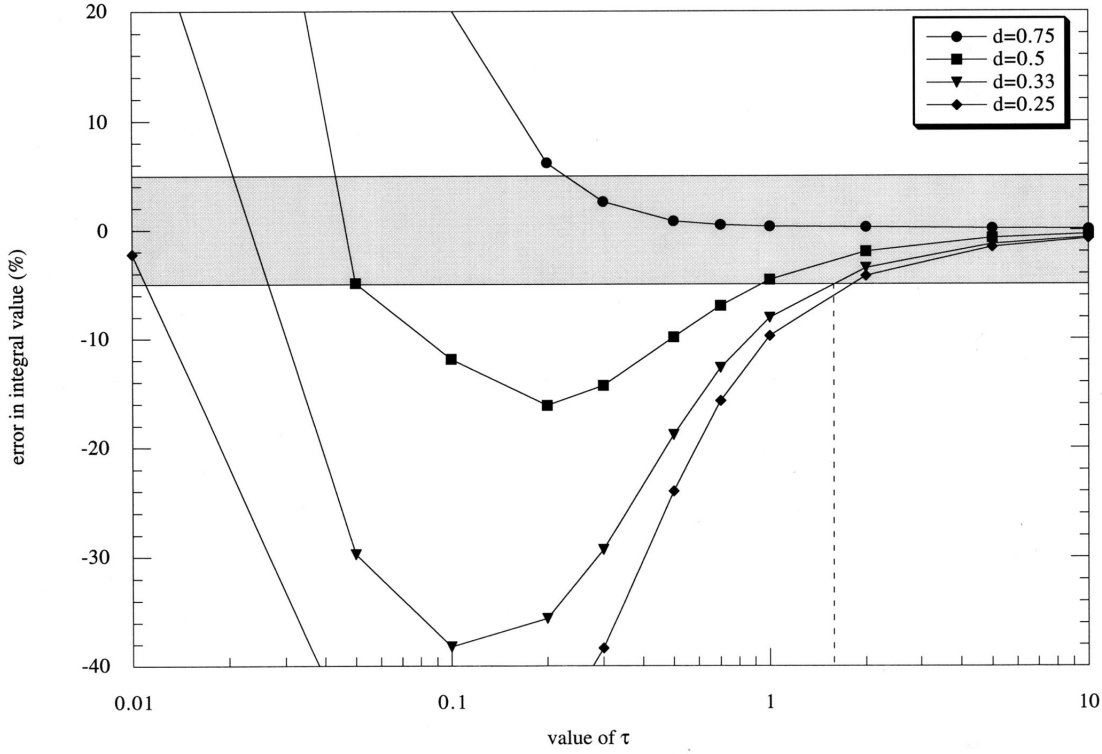


Figure 3.2: Graphical representation of the validation for simplifying equation 3.50. Each line represents the percentual difference between values of the actual and simplified integrals for a range of tau (τ) values. The value of the actual integral (I) was calculated using the Rhomberg method, while the simplified integral (II) was calculated analytically. The difference between the two values was converted to a percentage of the actual value (I). A diffusion coefficient of 10^{-9} m s^{-2} was assumed in the calculations. The four different lines represent different values of d , where $D_e = dD_w$. It can be seen that for the value of d we use (0.33), the error of the simplified integral is less than 5% (grey area) if approximately, $\tau \geq 1$, i.e. $t \geq R^2/D_e$.

$$I = 3D_w^2 \int_0^\infty \frac{e^{-y^2\tau}}{y} \frac{\sin y - y \cos y}{D_e D_w y^2 \sin^2 y + [(D_w - D_e) \sin y + D_e y \cos y]^2} dy$$

$$II = \int_0^\infty e^{-y^2\tau} dy.$$

point where the oxygen concentration has reached $p_\delta\%$ of the free water concentration. For the ratio of theoretical diffusion boundary layer thickness and theoretical maximum radius of a spherical organism, we can write (see Appendix B):

$$\frac{\delta}{R_{max}} = -\frac{0.4}{1 - 0.01p_\delta} - 1 \quad (3.12)$$

in which δ = diffusion boundary layer thickness. If we define p_δ to be 95% of the free water oxygen concentration, it can be calculated from equation 3.12 that the diffusion boundary layer thickness is seven times the maximum radius of the animal.

3.3 Parameter Values and Predictions on Morphogenesis

Values of the input parameters are based on literature data. Diffusion coefficients for oxygen in water were calculated according to equation 3.13 (Van Stroe and Janssen, 1993), where salinity was not taken into account:

$$D_w = 3.051 \times 10^{-6} e^{-17900/8.314T_k} \quad (3.13)$$

in which T_k = temperature in K; see Appendix A. According to Graham (1988), the diffusion coefficient of oxygen in sea water is about 8% smaller than in fresh water at 20°C. The diffusion coefficient of oxygen in embryonic tissue is likely to be close to that of other soft animal tissue (McNeill Alexander, 1971; Krogh, 1941). Values for frog muscle, frog and dog connective tissue are all about one third of that for the diffusion of oxygen in pure water. Therefore, D_e is taken to be 33% of that in water.

Free water oxygen concentration at different temperatures was determined after a polynomial regression of data from Golterman *et al.* (1978), who gave solubility of oxygen in water in equilibrium with air at 760 mm Hg and 100% relative humidity:

$$C_\infty = 2.1753 - 0.020796T_k + 6.686 \times 10^{-5}T_k^2 - 7.2074 \times 10^{-8}T_k^3 \quad (3.14)$$

Graham (1988) gives a value for the oxygen content of sea water about 20% lower than that for fresh water at 20°C.

Table 3.1 gives literature values of the input parameters of the model, calculated values for diffusion coefficients and oxygen concentration and predictions on body size of 8 different teleost species. The predictions in Table 3.1 are in part based on equations 3.13 and 3.14, thus neglecting the effects of salinity. The effects of salinity on predicted body size are evaluated in the discussion.

Oxygen consumption of common carp (*Cyprinus carpio*) and zebrafish (*Danio rerio*) was measured per animal only (Kaushik *et al.*, 1982; Skidmore, 1967). In order to calculate the volume-specific oxygen consumption of these species, the volume of

Table 3.1: Values of oxygen concentration (C_∞), temperature (T), diffusion coefficients of oxygen in embryonic tissue (D_e) and water (D_w), oxygen consumption (m), weight (W , either dry weight, DW or wet weight WW), volume (V), surface area (A), actual volume-to-surface ratios and predicted volume-to-surface ratios (V/A) for a sheet, cylinder and sphere.

Species	stage	C_∞ $\times 10^{-3}$	T $^\circ\text{C}$	D_e $\times 10^{-10}$	D_w $\times 10^{-9}$	m original value	
Winter flounder <i>Pseudopleuronectes americanus</i> ^a	hatch	12.2	6.5	4.59	1.38	0.016 ^j	$\mu\text{l (egg h)}^{-1}$
Plaice <i>Pleuronectes platessa</i> ^b	hatch	11.2	10	5.05	1.52	0.2 ^k	$\mu\text{l (egg h)}^{-1}$
Herring <i>Clupea harengus</i> ^c	hatch	10.5	13	5.47	1.64	3 ^k	$\mu\text{l (24 h org)}^{-1}$
Largemouth bass <i>Micropterus salmoides</i> ^d	hatch	9.00	20	6.55	1.96	0.022 ^l	$\mu\text{g (mg min)}^{-1}$
Common carp <i>Cyprinus carpio</i> ^e	first circ.	9.00	20	6.55	1.96	0.685 ^k	$\text{mg(1000 fish h)}^{-1}$
African catfish <i>Clarias gariepinus</i> ^f	hatch*	8.66	22	6.88	2.06	0.53 ^k	$\text{mm}^3 (\text{ind h})^{-1}$
African catfish <i>Clarias gariepinus</i> ^f	hatch*	8.19	25	7.41	2.22	0.43 ^k	$\text{mm}^3 (\text{ind h})^{-1}$
Zebrafish <i>Danio rerio</i> ^g	first circ.	8.19	25	7.41	2.22	0.072 ^m	$\mu\text{l (fish h)}^{-1}$
African catfish <i>Clarias gariepinus</i> ^h	hatch*	7.76	28	7.96	2.39	917.2 ^m	$\text{nmol(mg DW h)}^{-1}$
African catfish <i>Clarias gariepinus</i> ^f	hatch*	7.76	28	7.96	2.39	0.33 ^k	$\text{mm}^3 (\text{ind h})^{-1}$
Rabbitfish <i>Siganus randalli</i> ⁱ	hatch	7.76	28	7.96	2.39	0.0805 ^k	$\mu\text{g (ind h)}^{-1}$

^a Cetta and Capuzzo (1982).

^b deSilva and Tytler (1973).

^c Eldridge *et al.* (1977).

^d Spoor (1977).

^e Kaushik *et al.* (1982).

^f Kamler *et al.* (1994).

^g Skidmore (1967).

^h Conceição (unpubl. data).

ⁱ Nelson and Wilkins (1994).

^j Extrapolated from values in text.

W		V	m	A	V/A			V/A sphere	
original value		mm ³	kg m ⁻³ s ⁻¹	mm ²	act.	sheet	cyl.	runn.	stagn.
13.1 ^m	μg DW	0.13	4.8×10 ⁻⁵	2.3	0.056	0.48	0.34	0.28	0.22
0.047 ⁿ	mg DW	0.47	1.7×10 ⁻⁴	5.4	0.087	0.26	0.18	0.15	0.12
116 ^k	μg DW	1.16	4.3×10 ⁻⁵	9.9	0.12	0.52	0.37	0.30	0.23
0.76 ^l	mg WW	0.76	3.7×10 ⁻⁴	7.5	0.10	0.18	0.12	0.10	0.078 ^r
		0.17 ^p	1.1×10 ⁻³	2.8	0.062	0.10	0.073	0.060 ^r	0.038 ^r
47.4 ^m	μg DW	0.47	4.4×10 ⁻⁴	5.4	0.087	0.16	0.12	0.10	0.073 ^r
45.2 ^m	μg DW	0.45	3.8×10 ⁻⁴	5.3	0.085	0.18	0.13	0.10	0.080
		0.07 ^q	4.1×10 ⁻⁴	1.5	0.046	0.17	0.12	0.10	0.078
0.041 ^m	mg DW	0.41	8.2×10 ⁻⁴	5.0	0.082	0.12	0.087	0.071 ^r	0.055 ^r
32.9 ^m	μg DW	0.33	4.0×10 ⁻⁴	4.3	0.077	0.18	0.13	0.10	0.080
0.008 ^o	mgDW	0.08	2.8×10 ⁻⁴	1.7	0.048	0.21	0.15	0.12	0.094

^k Read from graph.

^l Extrapolated from table.

^m Read from table.

ⁿ Calculated from data on egg-specific and mass-specific m .

^o Read from graph and calculated by subtracting yolk volume.

^p Volume estimated from scaled drawings in Neudecker (1976).

^q Volume estimated from scaled drawings in Kimmel *et al.* (1995).

^r Indicates predicted maximum body sizes smaller than the actual ones.

* Hatching coincides with appearance of fully functional circulatory system (Zaki and Abdula, 1983).

the embryonic tissues was estimated from scaled drawings in Neudecker (1976) and Kimmel *et al.* (1995), respectively. Subsequently, oxygen consumption per animal was divided by the volume of respiring tissues. Whenever literature data on oxygen consumption was given on a dry weight basis, a dry weight percentage of 10 was assumed to convert dry weight to wet weight (Finn *et al.*, 1991). A density of embryonic tissues of 10^3 kg m^{-3} was assumed to convert mass to volume.

The values of the volume-specific oxygen consumption are based on the volume of respiring tissue only (so excluding yolk, perivitelline fluid and egg-capsule). In order to be able to convert embryonic size and shape to a volume to surface ratio, we needed to obtain both volume and surface area of the respiring tissues. The volume was obtained as mentioned in the previous paragraph. To our knowledge, the only references that give surface area of early teleost larvae in some detail, are Rombough and Moroz (1990) and Rombough (1998). Rombough (1998) gives head and trunk area of newly hatched rainbow trout (*Oncorhynchus mykiss*). In order to be able to calculate volume to surface ratios for the species in Table 3.1, we assumed area to relate to volume to the power 0.67 (and thus we assumed the species in Table 3.1 to be isomorphic to the newly hatched *Oncorhynchus* larvae). This resulted in the following relation to calculate surface area from volume for embryos in their pharyngula period:

$$A = 9.0V^{0.67} \quad (3.15)$$

To give a preliminary validation of this model, we measured the volume to surface ratio of a zebrafish embryo in its pharyngula period (33 hpf), using the ellipse method as described by Drost and Van den Boogaart (1986). Using a digitizer tablet and a computer program, the embryo, as defined by a lateral and dorsal view (from Kimmel *et al.* (1995)) is converted to a series of ellipses describing its contour. The volume of the embryo is the integral of the area of the ellipses over the length of the embryo. The mean area of the ellipses was used as the base of a cylinder with a length equal to that of the embryo and the total surface area was taken as the surface area of the embryo. This approximate method yielded the relation $A = 8.65V^{0.67}$, which was interpreted as a confirmation of equation 3.15.

As we are interested in the possible physical needs for an active oxygen transport system, data were taken - when available - at the stage where blood could first be seen to circulate through the vessels ('first circulation'). In species indicated by an asterisk (*) in Table 3.1, hatching coincides with 'first circulation'. If data of the 'first circulation' stage were not available, data of the hatching stage were taken.

Since blood typically begins to circulate by about 40% of the way through embryonic development (Rombough, *pers. comm.*), the actual volume to surface ratios at the ‘first circulation’ stage of winter flounder (*Pseudopleuronectes americanus*), plaice (*Pleuronectes platessa*), herring (*Clupea harengus*), largemouth bass (*Micropterus salmoides*) and rabbitfish (*Siganus randalli*) are probably smaller, though certainly not larger than the ones listed in Table 3.1 (see discussion).

Metabolic rate depends on temperature (Rombough, 1988). By using the regression line given in Rombough (1988) for metabolic rate on temperature together with

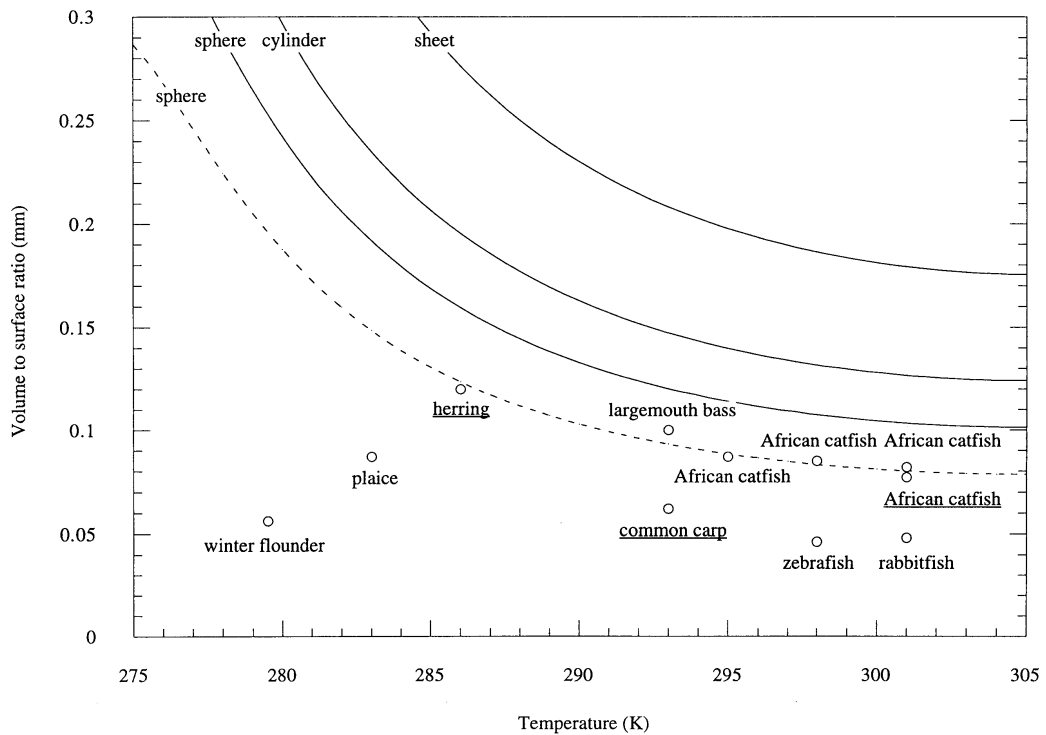


Figure 3.3: Graphical representation of the predicted survival time as a function of temperature. Using the regression line of metabolic rate on temperature in Rombough (1988) together with equations 3.13 and 3.14, maximum size can be expressed as a function of temperature. Solid lines represent maximum volume-to-surface ratio of a sphere, cylinder and sheet in running water, while the dotted line represents the maximum volume-to-surface ratio of a sphere in stagnant water. Actual volume-to-surface ratios (Table 3.1) are also plotted. Metabolic rate of underlined species (as given in Table 3.1) deviates considerably from the regression line in citetrombough88(*cf.* Fig. 3.5) and the results for these species should therefore be interpreted with caution (see text).

equations 3.13 and 3.14, theoretical maximum volume to surface ratios can be calculated as a function of temperature [equations 3.4, 3.6, 3.7, 3.9, see Fig. 3.3]. It can be seen in Fig. 3.3 that most species are smaller than their predicted maximum size (though see discussion).

3.4 Discussion

Our analysis of the time-dependent effects of oxygen consumption in small organisms shows that an equilibrium situation is reached very quickly (about 1.5 mins in running water and about 10 mins in stagnant water), provided that the animal is smaller than its maximum size. If animals are larger than their maximum size, oxygen concentration in the center will generally drop to zero within a very limited amount of time, as survival time sharply decreases with size (Fig. 3.4). Therefore, using Fick's first law for modelling diffusion into small embryos is a valid simplification (*e.g.* models by McNeill Alexander (1971); Fenn (1927); Harvey (1928); Krogh (1941); Warburg (1923)). Byatt-Smith *et al.* (1991) reached the same conclusion for oxygen diffusion into mouse and human preimplantation embryos.

Based on Fick's first law of diffusion, Fenn (1927) predicts the maximum radius of nerves to be 0.213 cm, which is about the size of the largest dogfish nerves. Seymour and Bradford (1995) predicted maximum radius of a globular egg mass of the frog *Limnodynastes tasmaniensis* to be about 2 cm, while the actual limit is 1.3 cm. Egg-masses of 7 gastropod species appear to obtain a size (radius varying from 0.4 to 3.5 mm) which corresponds to the predicted maximum radius (0.71 to 3.4 mm; Lee and Strathmann (1998)). Warburg (1923) predicted liver slices to be thinner than 0.047 cm to survive in water saturated with pure oxygen. Experiments were in agreement with the theory (Minami, 1923). McNeill Alexander (1971) used the same law to predict that flatworms can attain a maximum thickness of about 0.06 cm, which generally is conform observation in nature. Krogh (1941) draws the general conclusion that 'when metabolism is fairly high, diffusion alone can provide sufficient oxygen only to organisms of 1 mm diameter or less, while larger forms depending on diffusion must have a low metabolism'.

Predictions on maximum size of solid biological structures appear to vary from about 0.5 to about 2 mm (egg masses include a lot of non-respiring jelly). Table 3.1 shows that predictions on maximum body size of teleost embryos range from 0.18 mm to 0.90 mm when modelled as spheres in running water (where $R_{max} = 3V/A$)

and from 0.11 to 0.69 when modelled as spheres in stagnant water. The biological structures investigated in this paper (*i.e.* teleost embryos) apparently lead to relatively small predicted maximum sizes. Actual radii (when converted volume-to-surface-ratio to the radius of an equivalent sphere), however, range from 0.14 mm (zebrafish) to 0.36 mm (herring) and fall well within the range of predicted maximum sizes.

When looking at Table 3.1 in more detail, the actual volume-to-surface-ratio of all species (except common carp and African catfish) is smaller than the predicted maximum radius in running water, regardless of the shape of the model embryo. Since the actual shape of the embryo will be somewhere intermediate between a plane sheet, cylinder and sphere (*cf.* Rappoldt (1992)), none of the actual embryos will experience oxygen shortage in running water.

In stagnant water, no general rule is applicable according to the predictions in Table 3.1. Winter flounder, plaice, herring, zebrafish and rabbitfish will not experience oxygen shortage in stagnant water. Actual volume to surface ratios of common carp and African catfish embryos are relatively close to the predicted maximum values of spheres in stagnant water [4-39% difference *versus* 70-380% difference in other species (excluding the largemouth bass)], suggesting a correlation between the onset of oxygen shortage and the appearance of a functional circulatory system. According to Table 3.1, largemouth bass will also experience oxygen shortage, though for this species data of the hatching stage were taken while circulation probably starts earlier. The embryo will therefore be smaller at the onset of circulation and actual size might be smaller than predicted maximum size.

It is unclear however, whether the conditions actually experienced by the embryos resemble the stagnant water situation or the running water situation. Several ways have been proposed in which the oxygen-poor diffusion boundary layer is refreshed, either by the embryo itself or by the parents. Parental ‘fin-fanning’ to create a current of oxygen-rich water over the eggs (*e.g.* Cichlidae, Gasterosteidae) probably increases the amount of oxygen available to the embryo. Muscle contractions, which can be recognized 19 hours post fertilization in case of the zebrafish (first circulation occurs 31 hours post fertilization at 25°C; Kimmel *et al.* (1995)), might also serve such a goal (Kamler, 1992; Osse and Van den Boogaart, 1994). Since the diffusion boundary layer thickness (equation 3.12) can be calculated to measure several millimeters to even centimeters in a steady state situation in stagnant water, it well extends outside the egg capsule of the fishes and flow of the water surrounding the egg capsule might be

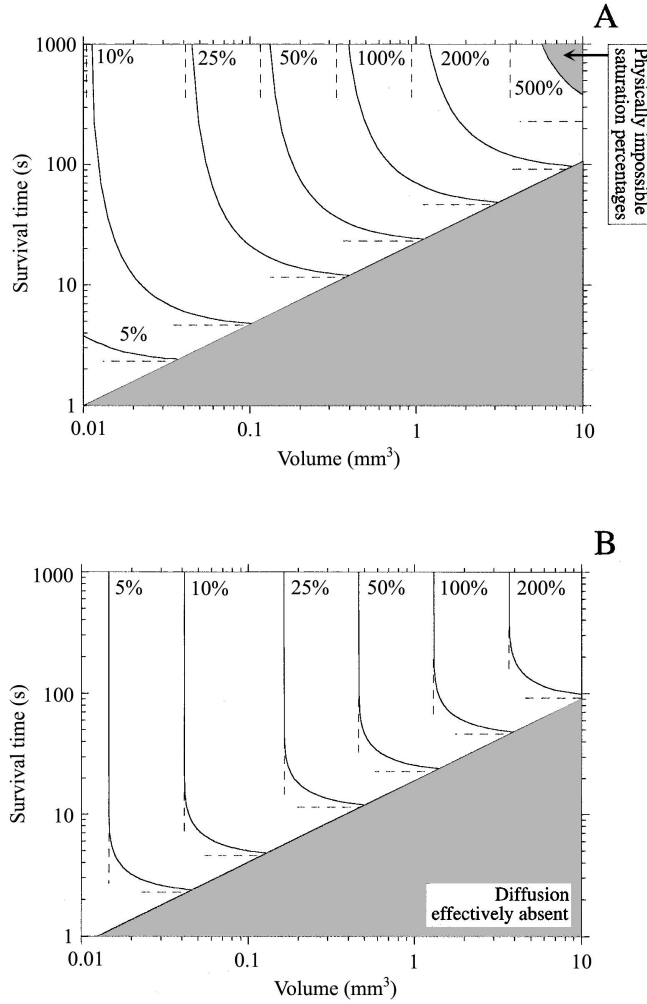


Figure 3.4: (A) Predicted survival times (s) in *running water* as a function of volume (mm³) of the zebrafish (*Danio rerio*) embryo for different oxygen saturation percentages. Each line represents the effect of volume on survival time for one specified oxygen saturation percentage. It can be seen that survival time decreases with increasing volume of the embryo, while survival time increases with increasing oxygen saturation value. The line with a saturation percentage of 100% represents water in equilibrium with air (approximately 20% oxygen) at 1 atm and 100% relative humidity. Dashed lines indicate vertical and horizontal asymptotes of each line. The vertical asymptote indicates the maximum volume V_{\max} ($= \frac{4}{3}\pi R_{\max}^3$) at that particular oxygen saturation percentage and therefore the embryo can survive indefinitely if smaller than V_{\max} (left of the asymptote). The horizontal asymptote illustrates the fact that even if the embryo is very large and diffusion is effectively absent, the embryo can survive a certain amount of time on the oxygen initially present in its body. This amount of time is given by C_{∞}/m ; the solution of equation 3.30 without the diffusion term. The shaded area includes the area where diffusion is effectively absent, *i.e.* the survival time differs less than 5% from its limiting value of C_{∞}/m .

*caption continues on next page*¹

a supplier of oxygen to the developing eggs. Furthermore, the embryonic metabolism causes higher concentrations of excretory products in the diffusion boundary layer thus increasing the density of water around the embryo. This ‘heavy’ water drops downward due to gravity, thereby creating a flow of water around the embryo in stagnant water. Theoretically this can provide a supply of oxygen to developing eggs (O’Brien *et al.*, 1978). Alderdice *et al.* (1984) suggested that a pumping mechanism of the egg capsule might also serve to facilitate respiratory gas exchange. Metabolic heat production possibly creates a convective water flow in a similar fashion.

Regarding all these ways of boundary layer refreshment, it is highly unlikely that any embryo will be surrounded by completely stagnant water. Therefore, just as the actual shape of the embryo is intermediate between a sheet, cylinder and sphere, the physical environment will be intermediate between completely stagnant water and a continuously refreshed diffusion boundary layer. This suggests that only in common carp and African catfish embryos the development of a circulatory system coincides with the onset of oxygen shortage (Table 3.1).

As explained in section 3.3, the effects of salinity on predicted maximum body size are neglected so far. When assuming the 20% decrease in oxygen content of sea water and 8% decrease in diffusion coefficient of oxygen in sea water to be valid for a large temperature range, the predicted volume to surface ratios will decrease by about 14% (*cf. e.g.* equation 3.4). In Table 3.1, we present four sea water species: winter flounder, plaice, herring and rabbitfish. All four of these species are substantially smaller than the predicted maximum sizes (Table 3.1). This situation does not change when decreasing the predicted body size by 14%, even when the embryos are modelled as spheres in stagnant water.

The predictions in Table 3.1 are based on our model in which several assumptions were made (section 3.2.1). The assumption of modelling an embryo as either a plane sheet, cylinder or sphere, has been accounted for by interpreting the actual embryo

¹(B) Predicted survival times (s) in *stagnant water* as a function of the volume (mm³) of the zebrafish (*Danio rerio*) embryo for different oxygen saturation percentages (*cf.* Fig 3.4 A). Note that the minimum survival time in this graph is the same as that Fig. 3.4 A (horizontal asymptote), while the maximum volume (vertical asymptote) is 2 times as small as in Fig. 3.4 A. As water in equilibrium with air (approximately 20% oxygen) is said to be 100% saturated, the line with a saturation percentage of 500% represents the theoretically maximum oxygen saturation percentage (water in equilibrium with pure oxygen; five times as much as water in equilibrium with air). The shaded area in the upper right corner indicates the physical impossibility to have oxygen saturation percentages above 500%. In Fig. 3.4 A this area is invisible.

as being intermediate between these geometric forms.

There is no consensus about the effects of the egg capsule on oxygen diffusion (Rombough, 1988) and these effects have been neglected so far. The following analysis, however, is useful if the capsule does constrain oxygen diffusion indeed. Gerard (1931) gives the solution of Fick's first law of diffusion for a sphere in which the diffusion coefficient is different in the central and cortical part of the sphere (where the oxygen concentration at the surface is constant, *cf.* running water condition). To give an indication of the possible impeding effects of the egg capsule on oxygen diffusion, we slightly modified Gerard's equation to account for the lack of oxygen consumption in the cortical part. Modified after Gerard (1931), we obtain:

$$R_{max} = \sqrt{\frac{q}{p^2 + q - 1}} \sqrt{\frac{6D_e C_\infty}{m}} \quad (3.16)$$

where q = ratio of diffusion coefficients of oxygen in capsule and embryonic tissue respectively, p = ratio of radius of embryo + capsule and radius of the embryo, respectively.

For a cylindrical and sheet-like embryo, we obtain respectively:

$$R_{max} = \sqrt{\frac{q}{q + 2 \ln p}} \sqrt{\frac{4D_e C_\infty}{m}} \quad (3.17)$$

$$R_{max} = \sqrt{\frac{q}{2p + q - 2}} \sqrt{\frac{2D_e C_\infty}{m}} \quad (3.18)$$

If we model the capsule as a spherical shell against a spherical embryo and if we take $q = 0.3$ (Rombough, 1988) and $p = 1.05$ (Daykin, 1965), the maximum radius of the embryo is about 86% of the value without a capsule. For a cylindrical and sheet-like embryo, the effects are virtually identical for the same values of p and q . This is a very crude approximation of the actual effects of the capsule, since (1) capsule diffusion coefficients and thicknesses may vary amongst species (Rombough, 1988) and (2) we did not take into account the varying amount of perivitelline fluid between embryo and capsule. Special caution should be used when extrapolating these results to other vertebrate classes. Amphibian embryos, for instance, have much thicker egg capsules that can have large effects on the oxygenation of the embryos (Seymour, 1994). Nevertheless, our crude analysis gives an idea of the possible impeding effects of an egg capsule on oxygen diffusion in teleost embryos. A decrease in the predicted maximum radius of the organisms of 14% does not change the interpretation of the

results in Table 3.1 as outlined above, and neither does a combination of salinity and capsule effects.

The assumption of a constant volume-specific oxygen consumption is shortly explained in section 3.2.1. In our model, embryos are unable to grow bigger if diffusion cannot maintain a large enough gradient to enable constant respiration anymore. However, when subjected to extremely low oxygen concentrations, embryos lower their consumption rate. In this way they are able to survive oxygen-poor conditions. We consider it unlikely, however, that such an oxygen limited period has been incorporated as part of a life history strategy during evolution. Thus predicting an impossibility to survive should be interpreted from an evolutionary viewpoint.

We checked the reliability of the oxygen consumption data by superimposing our (literature) data on a graph from Rombough (1988) (Fig. 3.5). Considering the amount of variation in the original figure, our data agree very well with the general trend. However, the oxygen consumption of common carp (Kaushik *et al.*, 1982) and African catfish (Conceição, unpub. data) are relatively high, while the value for herring (Eldridge *et al.*, 1977) is relatively low. Decreasing the oxygen consumption of the African catfish to a value close to the regression line in Fig. 3.5 (thus with a factor 2), would yield predicted volume to surface ratios similar to those based on the data from Kamler *et al.* (1994). Increasing the oxygen consumption of herring to a value close to the regression line (factor 3) would still leave the herring embryo smaller than the predicted maximum (volume to surface ratio 0.12 versus 0.13, respectively, for a spherical embryo in stagnant water). Decreasing the value for common carp with a factor 4 would make the predicted maximum body size larger than the actual body size (Table 3.1). Thus, a value for the oxygen consumption of common carp closer to the regression line in Fig. 3.5 would predict no oxygen shortage to occur in common carp, while predictions based on the original value would. Although we have no reason to question the data from Kaushik *et al.* (1982), the predictions on maximum body size of common carp should be interpreted with caution and certainly not as a general trend.

The deviations from the regression line mentioned in the previous paragraph also have consequences for the results in Fig. 3.3. Since the regression line in Rombough (1988) underestimates the metabolic rate of common carp and African catfish (underlined) as compared to the data in Table 3.1 (Fig. 3.5), the predicted maximum sizes for these species are overestimated and these species actually are closer to their

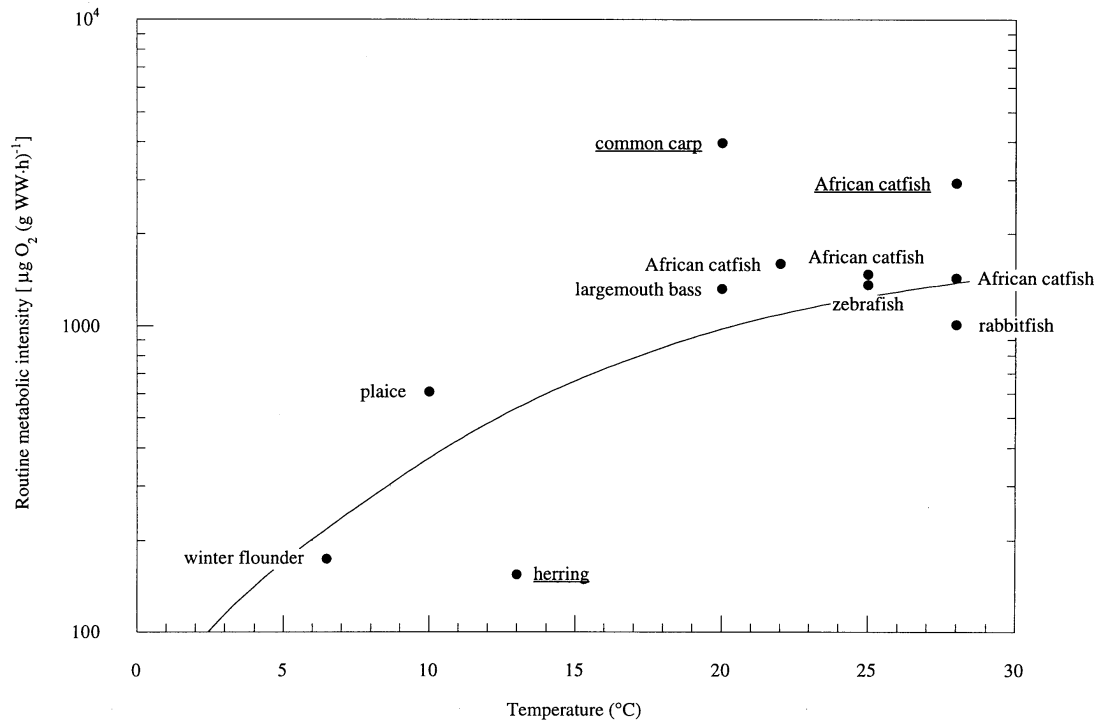


Figure 3.5: Graph of oxygen consumption as a function of temperature. The line represents the regression line of Rombough (1988). The black dots represent the oxygen consumption data from Table 3.1. Herring (*Clupea harengus*), common carp (*Cyprinus carpio*) and African catfish (*Clarias gariepinus*) are underlined and discussed separately because of their apparent deviation from the regression line.

maximum size than suggested in Fig. 3.3 (*cf.* Table 3.1). The reverse is true for herring (*cf.* Fig. 3.5 and Table 3.1).

By making the assumptions as mentioned earlier, we simplified the real situation, though the resulting model appears to give an adequate description of the diffusion process taking place. Including more realistic features in the model (*e.g.* actual shape of the embryo, egg capsule) will slightly change our predictions, though not the general picture emerging from Table 3.1. The general picture will still be that diffusion across the body surface of teleost embryos is adequate for their oxygen supply even beyond the time a circulatory system is functional. The circulatory system, therefore, does not develop primarily to increase oxygen availability to the embryo. And oxygen availability does not seem to be a direct driving factor for the development of a

circulatory system. We thus have to reject our hypothesis.

Of the eight species in Table 3.1, only two (common carp and African catfish) are bred for commercial (*i.e.* consumption) purposes. It is in these two species that the actual size is very close to the predicted maximum size (and even larger than the predicted maximum size for completely stagnant water). This might indicate that these species are artificially selected to grow as fast as possible and therefore obtain the maximum possible size as predicted by our model. In the not commercially bred species, the circulatory system develops and becomes functional before the onset of oxygen shortage as a built-in safety factor (prosynchronotropy; Burggren and Territo (1995)). These findings are in agreement with the results of Pelster and Burggren (1996), who found that functional ablation of haemoglobin did not affect oxygen-dependent physiological processes in zebrafish (*Danio rerio*) larvae of 4 days old. They concluded that diffusion of oxygen over the body surface was still adequate, though oxygen carriage in the blood plasma was not impaired and might still have played a role. Other possible driving factors for circulatory system development include transport of nutrients and waste products and demands on blood flow for remodelling and further development of the embryonic vascular system (Risau and Flamme, 1995).

Acknowledgements

Dr. Henri Stroband, dr. Truus te Kronnie, Jos van den Boogaart, dr. Igor Spierts, dr. Jan Osse and dr. Johan van Leeuwen are greatly acknowledged for their stimulating interest, useful discussions and valuable comments on the manuscript. Dr. R. S. Seymour and an anonymous referee are also acknowledged for their detailed comments, which greatly helped to improve the manuscript.

Appendix A - Abbreviations and units of the parameters used in the diffusion models

Par.	Description	Unit
A	surface area	m^2
b	percentage of the difference between initial and equilibrium concentration	%
c	oxygen concentration inside the embryo	kg m^{-3}
$c(r, t)$	oxygen concentration as a function of place and time	kg m^{-3}
$c(0, t)$	oxygen concentration at the center as a function of time	kg m^{-3}
$c(R, t)$	oxygen concentration at the body surface as a function of time	kg m^{-3}
$c(r, 0)$	oxygen concentration as a function of place at $t = 0$	kg m^{-3}
$C(r, s)$	Laplace transformed $c(r, t)$	kg m^{-3}
C_∞	oxygen concentration of free water in equilibrium with air at 1 atmosphere and 100% relative humidity	kg m^{-3}
d	ratio of D_e and D_w	—
D_e	oxygen diffusion coefficient of embryonic tissues	$\text{m}^2 \text{s}^{-1}$
D_w	oxygen diffusion coefficient of water	$\text{m}^2 \text{s}^{-1}$
$F(s)$	$F(s) = C(r, s)e^{st}$	kg s m^{-3}
G	integration constant	kg s m^{-2}
H	integration constant	kg s m^{-2}
J	oxygen flow	kg s^{-1}
m	volume-specific oxygen consumption of respiring tissues	$\text{kg m}^{-3} \text{s}^{-1}$
n	integer denoting the summations of subsequent contributions of the unsteady part. These contributions becomes smaller when n increases.	—
p_δ	percentage of free water oxygen concentration at end of diffusion boundary layer	%
p	ratio of radius of embryo + capsule and radius of the embryo	—
q	ratio of diffusion coefficients of oxygen in capsule and embryonic tissue	—

r	distance from center of organism	m
R	radius of organism	m
R_{max}	maximum radius of the organism	m
s	Laplace transform variable	s^{-1}
T_c	temperature	$^{\circ}\text{C}$
T_k	temperature	K
t_s	survival time	s
$u(r, t)$	oxygen concentration outside the embryo	kg m^{-3}
$u(\infty, t)$	oxygen concentration at the end of the diffusion boundary layer	kg m^{-3}
$u(R, t)$	oxygen concentration at the body surface as a function of time	kg m^{-3}
$u(r, 0)$	oxygen concentration outside the embryo as a function of place at $t = 0$	kg m^{-3}
$U(r, s)$	Laplace transformed $u(r, t)$	kg m^{-3}
x	integration variable	—
V	volume of the organism	m^3
V_{max}	maximum volume of the organism	m^3
$w(r, t)$	transformed oxygen concentration (Appendix B.4)	kg m^{-2}
$w(0, t)$	transformed oxygen concentration at the center as a function of time	kg m^{-2}
$w(R, t)$	transformed oxygen concentration at the body surface as a function of time	kg m^{-2}
$w(r, 0)$	transformed oxygen concentration as a function of place at $t = 0$	kg m^{-2}
δ	diffusion boundary layer thickness	m
γ	complex number	—
Ω	contour used to invert $C(r, s)$	—
\mathcal{L}	Laplace transform operator	—

Appendix B

Diffusion of oxygen into embryos living in running water

The origin of a spherical co-ordinate system is placed at the center of the spherical embryo. The oxygen concentration at place r and time t ($0 \leq r < R$, $t > 0$) inside the embryo is denoted by $c(r, t)$. The oxygen concentration outside the embryo and the (constant) initial oxygen concentration inside the embryo are supposed to be equal and are denoted by C_∞ . With m the volume-specific oxygen consumption and D_e the oxygen diffusion coefficient of embryonic tissue, the governing equations are:

$$\frac{\partial c(r, t)}{\partial t} = \frac{D_e}{r^2} \frac{\partial}{\partial r} \left(r^2 \frac{\partial c(r, t)}{\partial r} \right) - m \quad (3.19)$$

with boundary (BC) and initial (IC) conditions:

$$\text{IC: } c(r, 0) = C_\infty, \quad \text{BC}_1: \frac{\partial c(0, t)}{\partial r} = 0, \quad \text{BC}_2: c(R, t) = C_\infty$$

With the help of the transformation (Carslaw and Jaeger, 1959)

$$w(r, t) = rc(r, t) - rC_\infty \quad (3.20)$$

equation set 3.19 reduces to:

$$\frac{\partial w(r, t)}{\partial t} = D_e \frac{\partial^2 w(r, t)}{\partial r^2} - mr \quad (3.21)$$

with boundary (BC) and initial (IC) conditions:

$$\text{IC: } w(r, 0) = 0, \quad \text{BC}_1: w(0, t) = 0, \quad \text{BC}_2: w(R, t) = 0$$

Separation of variables yields for equation set 3.21 the solution:

$$w(r, t) = \frac{m}{6D_e} (r^3 - R^2 r) + \frac{2mR^3}{D_e} \sum_{n=1}^{\infty} \frac{(-1)^{n+1}}{n^3 \pi^3} \sin \left(n\pi \frac{r}{R} \right) e^{-n^2 \pi^2 \frac{D_e t}{R^2}} \quad (3.22)$$

With the help of equation 3.20 it follows that

$$c(r, t) = C_\infty + \frac{m}{6D_e} (r^2 - R^2) + \frac{2mR^3}{D_e} \sum_{n=1}^{\infty} \frac{(-1)^{n+1}}{n^3 \pi^3} \frac{1}{r} \sin \left(n\pi \frac{r}{R} \right) e^{-n^2 \pi^2 \frac{D_e t}{R^2}} \quad (3.23)$$

in which easily a steady state part and a transient part is recognized. Oxygen starvation will start at the center of the embryo. From equation 3.23 it follows that

$$c(0, t) = \lim_{r \downarrow 0} c(r, t) = C_\infty - \frac{mR^2}{6D_e} + \frac{2mR^2}{D_e} \sum_{n=1}^{\infty} \frac{(-1)^{n+1}}{n^2\pi^2} e^{-n^2\pi^2 \frac{D_e t}{R^2}} \quad (3.24)$$

Equation 3.24 can be written as:

$$c(0, t) = C_\infty - \frac{mR^2}{6D_e} + \frac{2mR^2}{D_e} \left(\frac{1}{\pi^2} e^{\frac{-\pi^2 D_e t}{R^2}} - \frac{1}{4\pi^2} e^{\frac{-4\pi^2 D_e t}{R^2}} + \frac{1}{9\pi^2} e^{\frac{-9\pi^2 D_e t}{R^2}} - \dots \right) \quad (3.25)$$

By using only the first term to approximate equation 3.24, we obtain:

$$c(0, t) = C_\infty - \frac{mR^2}{6D_e} + \frac{2mR^2}{\pi^2 D_e} e^{\frac{-\pi^2 D_e t}{R^2}} \quad (3.26)$$

Now suppose we want to calculate when the central oxygen concentration reaches a value $b\%$ of the difference between initial and equilibrium concentration above its equilibrium value:

$$\frac{b}{100} \frac{mR^2}{6D_e} = \frac{2mR^2}{\pi^2 D_e} e^{\frac{-\pi^2 D_e t}{R^2}} \quad (3.27)$$

and thus

$$t = -\frac{R^2}{\pi^2 D_e} \ln \left(\frac{b\pi^2}{1200} \right) \quad (3.28)$$

Note that this is an overestimation of the time until equilibrium as including subsequent terms of equation 3.24 leads to still smaller values of t [including three terms in equation 3.26 leads to a time 0.2% smaller than resulting from equation 3.28]. If $p = 10\%$ then equation 3.28 reduces to:

$$t = \frac{0.25R^2}{D_e} \quad (3.29)$$

Diffusion of oxygen into embryos living in stagnant water

Again, the center of the embryo is used as the origin of a spherical co-ordinate system. As before, the oxygen concentration at place r and time t ($0 \leq r < R, t > 0$) inside the embryo is denoted by $c(r, t)$. The oxygen concentration in the surrounding water is denoted by $u(r, t)$, ($r > R, t > 0$). The initial oxygen concentrations inside the

embryo and in the surrounding water are supposed to be equal and are denoted by C_∞ . With m and D_e as before, and with D_w the oxygen diffusion coefficient of water, the governing equations are:

$$\frac{\partial c(r, t)}{\partial t} = \frac{D_e}{r^2} \frac{\partial}{\partial r} \left(r^2 \frac{\partial c(r, t)}{\partial r} \right) - m \quad (3.30)$$

with boundary (BC) and initial (IC) conditions:

$$\text{IC: } c(r, 0) = C_\infty, \quad \text{BC}_1: \frac{\partial c(0, t)}{\partial r} = 0 \quad (3.31)$$

$$\text{BC}_2: c(R, t) = u(R, t), \quad \text{BC}_3: D_e \frac{\partial c(R, t)}{\partial r} = D_w \frac{\partial u(R, t)}{\partial r} \quad (3.32)$$

$$\frac{\partial u(r, t)}{\partial t} = \frac{D_w}{r^2} \frac{\partial}{\partial r} \left(r^2 \frac{\partial u(r, t)}{\partial r} \right) \quad (3.33)$$

with boundary (BC) and initial (IC) conditions:

$$\text{IC: } u(r, 0) = C_\infty, \quad \text{BC}_4: u(\infty, t) = C_\infty \quad (3.34)$$

The transfer of oxygen between embryo and surrounding water is described by equation set 3.32.

Next the Laplace transform \mathcal{L} with respect to time is applied (Duffy, 1994). With

$$\mathcal{L} : c(r, t) \Rightarrow C(r, s) \quad \text{and} \quad \mathcal{L} : u(r, t) \Rightarrow U(r, s) \quad (3.35)$$

equations 3.30 and 3.33 change into simple second order differential equations for $C(r, s)$ and $U(r, s)$. It follows that

$$C(r, s) = \frac{C_\infty}{s} - \frac{m}{s^2} + \frac{G}{r} \sinh \left(\frac{r\sqrt{s}}{\sqrt{D_e}} \right) \quad (3.36)$$

and

$$U(r, s) = \frac{C_\infty}{s} + \frac{H}{r} e^{-\frac{r\sqrt{s}}{\sqrt{D_w}}} \quad (3.37)$$

The values of the integration constants G and H are easily found with the help of (the transformed) equation 3.32. For the inner region this leads to

$$\begin{aligned} C(r, s) = & \frac{C_\infty}{s} - \frac{m}{s^2} + \\ & + \frac{m}{s^2} \frac{(D_w + R\sqrt{D_w}\sqrt{s}) \frac{R}{r} \sinh \left(\frac{r\sqrt{s}}{\sqrt{D_e}} \right)}{(D_w - D_e + R\sqrt{D_w}\sqrt{s}) \sinh \left(\frac{R\sqrt{s}}{\sqrt{D_e}} \right) + R\sqrt{D_e}\sqrt{s} \cosh \left(\frac{R\sqrt{s}}{\sqrt{D_e}} \right)} \end{aligned} \quad (3.38)$$

And for the outer region this leads to

$$U(r, s) = \frac{C_\infty}{s} - \frac{m}{s^2} \frac{\left(-D_e \sinh\left(\frac{R\sqrt{s}}{\sqrt{D_e}}\right) + R\sqrt{D_e}\sqrt{s} \cosh\left(\frac{R\sqrt{s}}{\sqrt{D_e}}\right)\right) \frac{R}{r} e^{\frac{-(r-R)\sqrt{s}}{\sqrt{D_w}}}}{\left(D_w - D_e\right) \sinh\left(\frac{R\sqrt{s}}{\sqrt{D_e}}\right) + R\sqrt{D_w}\sqrt{s} \sinh\left(\frac{R\sqrt{s}}{\sqrt{D_e}}\right) + R\sqrt{D_e}\sqrt{s} \cosh\left(\frac{R\sqrt{s}}{\sqrt{D_e}}\right)} \quad (3.39)$$

Observe that equations 3.38 and 3.39 already furnish the steady state for $c(r, t)$ and $u(r, t)$, respectively:

$$c(r, \infty) = \lim_{t \uparrow \infty} c(r, t) = \lim_{s \downarrow 0} sC(r, s) = C_\infty + \frac{m}{6D_e} (r^2 - R^2) - \frac{m}{3D_w} R^2 \quad (3.40)$$

$$u(r, \infty) = \lim_{t \uparrow \infty} u(r, t) = \lim_{s \downarrow 0} sU(r, s) = C_\infty - \frac{mR^3}{3D_w r} \quad (3.41)$$

By defining diffusion boundary layer thickness δ as the distance from the skin surface to the point where the oxygen concentration will eventually reach $p_\delta\%$ of the free water concentration, we can write:

$$0.01p_\delta C_\infty = C_\infty - \frac{mR^3}{3D_w(\delta + R)} \quad (3.42)$$

By assuming $c(0, \infty) = 0$ and $D_e = 0.33D_w$, and using equation 3.9, 3.42 can be rewritten as:

$$\frac{\delta}{R_{max}} = \frac{0.4}{1 - 0.01p_\delta} - 1 \quad (3.43)$$

The complex function $C(r, s)$ possesses a branch point at $s = 0$. If we cut the complex s -plane along the real axis from $s = 0$ to $s = -\infty$, then the transform $C(r, s)$ is analytic on the remaining part of the s -plane. To retrieve the Laplace-original $c(r, t)$ we have to evaluate the following contour integral in the complex s -plane.

$$c(r, t) = \frac{1}{2\pi i} \int_{\gamma - i\infty}^{\gamma + i\infty} F(s) ds \quad (3.44)$$

with $F(s) = C(r, s)e^{st}$ and $\text{Re}(\gamma) > 0$. This integral is simplified with the help of the contour Ω given in Fig. 3.6, on account of the equality

$$\frac{1}{2\pi i} \int_{ABC} F(s) ds = \frac{1}{2\pi i} \int_{ADEF C} F(s) ds \quad (3.45)$$

The contribution of the large semicircle around $s = 0$ disappears if we take its radius to infinity. And if we let the radius of the small circle around $s = 0$ approach

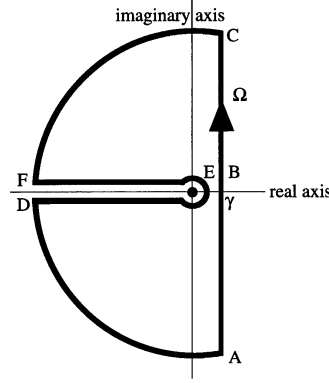


Figure 3.6: Contour used to invert $C(r, s)$. During the inverse Laplace transformation of $C(r, s)$, integration in the complex s -plane along ABC is simplified by substituting it with integration along ADEFC.

zero, its contribution yields once more the steady state $c(r, \infty)$ of our problem, as given by equation 3.40.

Hence, the transient part of the solution is determined by the contributions of the two straight lines between $s = 0$ and $s = -\infty$:

$$c_{trans}(r, t) = \frac{1}{2\pi i} \int_{-\infty}^0 F_{-}(s) ds + \frac{1}{2\pi i} \int_0^{-\infty} F_{+}(s) ds \quad (3.46)$$

where $F_{-}(s)$ and $F_{+}(s)$ denote the limit of $F(s)$ as we approach the branch cut from below or from above. With the substitution $s = -x$ it follows that

$$c_{trans}(r, t) = \frac{m}{\pi} \int_0^{\infty} \frac{e^{-xt}}{x^2} \frac{R}{r} \sin\left(\frac{r\sqrt{x}}{\sqrt{D_e}}\right) \times \frac{\sqrt{D_w} D_e R \sqrt{x} \sin\left(\frac{R\sqrt{x}}{\sqrt{D_e}}\right) - \sqrt{D_e} D_w R^2 x \cos\left(\frac{R\sqrt{x}}{\sqrt{D_e}}\right)}{D_w R^2 x \sin^2\left(\frac{R\sqrt{x}}{\sqrt{D_e}}\right) + \left((D_w - D_e) \sin\left(\frac{R\sqrt{x}}{\sqrt{D_e}}\right) + R\sqrt{D_e} \sqrt{x} \cos\left(\frac{R\sqrt{x}}{\sqrt{D_e}}\right)\right)^2} dx \quad (3.47)$$

Thus, with the help of equations 3.40 and 3.47, it follows that

$$c(r, t) = C_{\infty} + \frac{m}{6D_e} (r^2 - R^2) - \frac{m}{3D_w} R^2 + c_{trans}(r, t) \quad (3.48)$$

As already said before, oxygen starvation will start at the center of the embryo.

From equations 3.48 and 3.47 it follows that

$$c(0, t) = \lim_{r \downarrow 0} c(r, t) = C_\infty - mR^2 \frac{2D_e + D_w}{6D_e D_w} + \frac{m}{\pi} \int_0^\infty \frac{e^{-xt}}{x} \times \frac{\sqrt{D_w D_e} R^2 \sin\left(\frac{R\sqrt{x}}{\sqrt{D_e}}\right) - \sqrt{D_w} R^3 \sqrt{x} \cos\left(\frac{R\sqrt{x}}{\sqrt{D_e}}\right)}{D_w R^2 x \sin^2\left(\frac{R\sqrt{x}}{\sqrt{D_e}}\right) + \left((D_w - D_e) \sin\left(\frac{R\sqrt{x}}{\sqrt{D_e}}\right) + R\sqrt{D_e} \sqrt{x} \cos\left(\frac{R\sqrt{x}}{\sqrt{D_e}}\right)\right)^2} dx \quad (3.49)$$

By taking $\tau = D_e t / R^2$ and $y = \sqrt{x R^2 / D_e}$, equation 3.48 reduces to:

$$c(0, \tau) = C_\infty - mR^2 \frac{2D_e + D_w}{6D_e D_w} + \frac{2mR^2 \sqrt{D_w D_e}}{\pi} \times \int_0^\infty \frac{e^{-y^2 \tau}}{y} \frac{\sin y - y \cos y}{D_e D_w y^2 \sin^2 y + ((D_w - D_e) \sin y + D_e y \cos y)^2} dy \quad (3.50)$$

For large values of t (typically $t > R^2 / D_e$, see Fig. 3.2), equation 3.50 can be approximated by:

$$c(0, \tau) = C_\infty - mR^2 \frac{2D_e + D_w}{6D_e D_w} + \frac{2mR^2 \sqrt{D_e D_w}}{3\pi D_w^2} \int_0^\infty e^{-y^2 \tau} dy \quad (3.51)$$

Equation 3.51 can be solved as:

$$c(0, \tau) = C_\infty - mR^2 \frac{2D_e + D_w}{6D_e D_w} + \frac{mR^2 \sqrt{D_e D_w}}{3\pi D_w^2} \sqrt{\frac{\pi}{\tau}} \quad (3.52)$$

Now suppose we want to calculate when the central oxygen concentration reaches a value $b\%$ of the difference between initial and equilibrium concentration above its equilibrium value:

$$\frac{b}{100} mR^2 \frac{2D_e + D_w}{6D_e D_w} = \frac{mR^2 \sqrt{D_e D_w}}{3\pi D_w^2} \sqrt{\frac{\pi}{\tau}} \quad (3.53)$$

which can be rewritten as:

$$t = \frac{40000 D_e^2 R^2}{\pi b^2 D_w (2D_e + D_w)^2} \quad (3.54)$$

If $D_e = 0.33 D_w$ and $b = 10\%$ then equation 3.54 reduces to:

$$t = \frac{5.0 R^2}{D_w} \quad (3.55)$$

Chapter 4

Metabolic Constraints on Morphology of the Zebrafish Embryo (*Danio rerio*)¹

Metabolic requirements pose restrictions upon the morphology of organisms. Their size and shape should be kept within certain limits in order to maintain adequate supply and removal of molecules involved in metabolism. We investigated the restricting role of oxygen and nutrient supply on the development of zebrafish embryos shortly after the initiation of circulation, and the importance of this circulation for the distribution of these molecules. For that purpose we developed a model calculating the maximum dimensions of such embryos, based on the requirement of a sufficient supply of oxygen and nutrients. The model shows that in oxygen-saturated water oxygen allows for embryos to grow considerably larger than actual ones, and therefore does probably not directly limit development. The dimensions calculated on the basis of nutrient demand lie close to the actual ones, indicating nutrients, contrary to oxygen, to be a limiting factor for growth of the zebrafish embryo. The calculations also imply that in this stage adequate nutrient transport requires the presence of a primitive circulatory system, while oxygen transport does not.

4.1 Introduction

The development of a functioning vertebrate body from a fertilized egg involves both genetic determination of cells and imposition of cell fate by adjacent tissue (Browder, 1984). Although the ultimate result of these processes is formation of the adult body, they also at least partially determine the shape of the developing embryo. Especially the latter of the two processes (called induction) poses restrictions upon embryo morphology, since it requires a specific arrangement of tissues. While acknowledging the

¹In preparation: Brascamp, J.W., Kranenbarg, S. and Muller, M.

importance of these phylogenetic factors, the present paper focuses on the influence of physical factors on embryo morphology.

Particularly important physical factors for development are the availability of oxygen and nutrients, the molecules fuelling metabolism. We studied these factors and their potentially limiting effects on development of the zebrafish embryo (*Danio rerio*). Kranenbarg *et al.* (2000) showed oxygen availability not to be directly limiting for growth in the early, pre-circulation, teleost embryo. During this early developmental period yolk cell degradation in most teleosts is slow (Heming and Buddington, 1988), and nutrients are probably provided by scattered intracellular yolk particles (Sire *et al.*, 1994). This study addresses the role of oxygen and nutrient availability in the development of somewhat older zebrafish embryos, in which nutrients from the yolk cell and oxygen from surrounding water are distributed through the body by a primitive circulatory system. For that purpose, the dynamics of oxygen and nutrients inside the zebrafish embryo during this period were simulated using a mathematical model. The model predicts size and shape of the embryo and investigates the importance of the vascular system, based on metabolic requirements of body tissues.

4.2 Materials and Methods

4.2.1 Model

Biological background

The initial circulatory system of the zebrafish has a fairly simple architecture (Fig. 4.1). Blood is carried from the heart towards the tail by the dorsal aorta, and is transported back through the trunk by the cardinal vein, eventually returning to the heart after passage over the yolk cell. No lower level branches are present at this stage.

Both the artery and the vein are paired in the most rostral region, but merge to single ducts dorsal of the yolk cell (Rieb, 1973; Isogai *et al.*, 2001). Both oxygen and nutrients are supposed to diffuse into the blood as it flows over the yolk cell, then be transported into the body by the blood stream, and subsequently into (other) tissues by diffusion. Since fish yolk is a highly diverse substance, nutrients diffusing into the blood can be of various types. However, the most abundant yolk components are proteins and fat (Heming and Buddington, 1988; Suzuki and Suyami, 1983), which move into the blood as free amino acids and very low density lipoproteins (VLDL), respectively (Sire *et al.*, 1994). Contrary to nutrients, oxygen can reach the embryonic

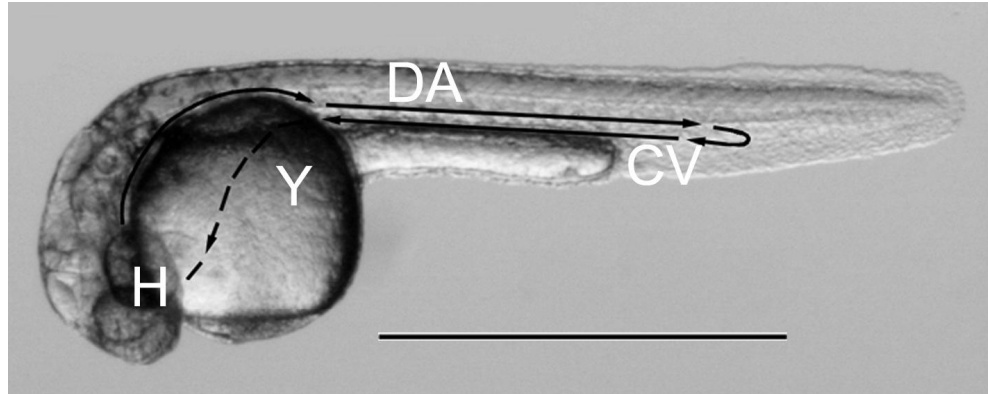


Figure 4.1: Overview of the circulatory system of the zebrafish at 30 hours post fertilization. The position of the dorsal aorta, the cardinal vein, the heart and the yolk cell are indicated by DA, CV, H and Y, respectively. The vascular bed of the yolk cell is represented by a dashed line.

tissue by diffusion through the skin as well. As soon as either nutrients or oxygen molecules reach respiring tissue, they can be taken up by cells and be metabolized.

Simplifying assumptions

The following simplifying assumptions were made in order to model the situation described in the previous section. See also Fig. 4.2.

- The approximately conical embryo body is represented as a series of aligned half cylinders of decreasing radius, neglecting the curvature of the embryo.
- The initially paired artery running from the heart towards the tail is represented as a single tube along the central axis of these half cylinders.
- Amino acids and very low density lipoproteins are the only nutrients considered in this model.
- The rate of oxygen uptake into cells is supposed to be independent of extracellular concentrations (Longmuir, 1957), as is that of nutrient uptake.
- Diffusion of molecules within the body in any other than radial direction (*i.e.* perpendicular to the longitudinal axis) is neglected.

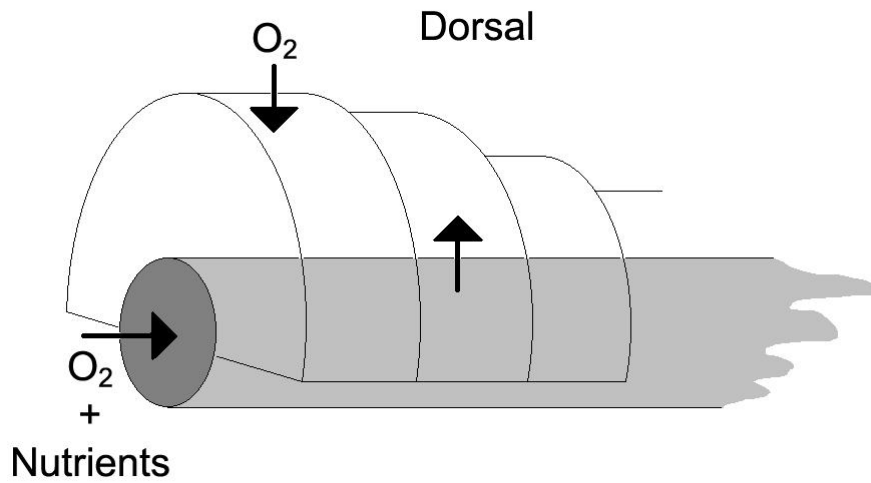


Figure 4.2: Approximation of the embryo body using half cylinders. The central cylinder, depicted in grey, represents the dorsal aorta. The larger half cylinders represent the embryonic tissue. The arrows indicate net molecule movement via the blood vessel (nutrients and oxygen) and through the skin (only oxygen)

- Tissue can survive any low oxygen (Padilla and Roth, 2001) or nutrient concentration higher than zero.
- The system is in equilibrium.

Modelling nutrient dynamics

In the model nutrients move through a central cylinder representing the blood vessel, along a longitudinal axis. Diffusion in radial direction leads them out of the central cylinder into a concentric larger half cylinder element, representing tissue (Fig. 4.2). Within this tissue the nutrient concentration declines from the blood vessel outward, due to consumption and radial diffusion. The maximum supportable radius of one specific half cylinder of tissue is calculated as the radius at which the nutrient concentration reaches zero. By repeating this procedure for subsequent tissue slices until no nutrients are left in the vessel, the maximum length and length dependent radius of the model embryo are calculated.

The calculations essentially consist of two steps. First the maximum radius of a

half cylinder I is calculated numerically from

$$c_{n,I} = \frac{m_n}{4D_n} \left(-2r_{n,I}^2 \ln \left(\frac{r_b}{r_{n,I}} \right) + r_b^2 - r_{n,I}^2 \right) \quad (4.1)$$

(*cf.* Currie (1961)). In this equation $c_{n,I}$ is blood nutrient concentration at level I [kg m^{-3}], m_n is nutrient consumption rate [$\text{kg m}^{-3} \text{s}^{-1}$], D_n is nutrient diffusion coefficient [$\text{m}^2 \text{s}^{-1}$], $r_{n,I}$ is calculated embryo (or half cylinder) radius [m], and r_b is blood vessel radius [m]. Next, the nutrient concentration in the blood vessel running through the subsequent half cylinder $I+1$ is calculated:

$$c_{n,I+1} = c_{n,I} - \frac{m_n \pi (r_{n,I}^2 - r_b^2) l}{2\Phi} \quad (4.2)$$

in which Φ is the blood flux [$\text{m}^3 \text{s}^{-1}$], and l is the half cylinder height [m]. Equation 4.1 can now be repeated for the next slice, *et cetera* until no nutrients are left in the vessel.

Modelling oxygen dynamics

For oxygen, model geometry is essentially the same as for nutrients, the only difference being that diffusion into the tissue now takes place from the outside as well as from the inside (Fig. 4.2). Therefore, the radii are obtained using an extended version of the calculations for nutrients. First the radius is calculated that a given slice can reach using oxygen originating from the blood alone, exactly like it was done for nutrients. Then, the extra radius is calculated that can be supported by oxygen coming from the surrounding water. No concentration gradient develops outside of the embryo, which corresponds to a running water situation.

The radius supported by oxygen from the blood at level I is calculated from

$$c_{O,I} = \frac{m_O}{4D_O} \left(-2r_{O,I}^2 \ln \left(\frac{r_b}{r_{O,I}} \right) + r_b^2 - r_{O,I}^2 \right) \quad (4.3)$$

in which $r_{O,I}$ is the radius supported by blood oxygen. See equation 4.1 for the meanings of the remaining parameters, subscript O indicating ‘oxygen’. Subsequently the total tissue radius supported by oxygen is calculated using

$$c_{O,\infty} = \frac{m_O}{4D_O} \left(-2r_{O,I}^2 \ln \left(\frac{r_{O,I}^{tot}}{r_{O,I}} \right) + r_{O,I}^{tot\,2} - r_{O,I}^2 \right) \quad (4.4)$$

in which $c_{O,\infty}$ is ambient oxygen concentration and $r_{O,I}^{tot}$ is total embryo radius. Analogous to the situation concerning nutrients, the next step is calculating the oxygen concentration in the first downstream slice. Due to the binding of oxygen to hemoglobin,

equation 4.2 is extended to:

$$c_{O,I+1} = c_{O,I} + bS_I - \frac{m_O\pi(r_{O,I}^2 - r_b^2)l}{2\Phi} - bS_{I+1} \quad (4.5)$$

In this equation b is oxygen carrying capacity of hemoglobin and S_I and S_{I+1} are the fractions of oxygen-saturated hemoglobin for I and $I + 1$, respectively. Equation 4.5 is solved numerically, using a sigmoidal relation between oxygen concentration c_O and hemoglobin saturation fraction S : $S = \frac{\alpha c_O^\beta}{1 + \alpha c_O^\beta}$, where α and β are constants.

4.2.2 Experimental procedures

Newly fertilized zebrafish eggs were collected and kept in a water filled petri dish at 28°C. We measured the cross sectional area of the yolk cell (n=10) from microscopic images taken every hour from 25 to 30 hours post fertilization (hpf), in order to estimate the yolk volume, assuming a spherical yolk cell. The derivative of the resulting volume-to-time-curve was determined to estimate the rate of yolk volume loss dV/dt . Blood flow velocity u through the dorsal aorta was estimated by measuring the velocity of red blood cells in the aorta of 30 hpf embryos (n=2), filmed using a high speed camera (Speed Cam). We measured the radius r_b of the dorsal aorta, over the vessel section (of almost uniform width) lying caudal from the anus (n=4). For this purpose we visualized the vasculature from microscopic images, using ‘digital motion analysis’ as described by Schwerte and Pelster (2000). To be able to compare the model predictions to the actual embryo dimensions, we measured the height of 30 hpf embryos (n=2) along their longitudinal axis from microscopic images. For a relevant comparison to our model, we only measured tissue dorsal from the aorta, and we excluded the finfold.

4.3 Results

4.3.1 Parameter values

The used parameters are listed in Table 4.1, along with their estimated values, which are explained in the text.

Parameter b represents the oxygen carrying capacity of hemoglobin. Willmer (1933) gives this value for various tropical fresh-water fishes. He finds considerable differences between species, apparently correlated mainly with habitat, but for all

Table 4.1: The parameters used in our model, and their respective values. Details are given in the text.

Par.	Description	Value	Unit
b	Hemoglobin O ₂ carrying capacity	1.5×10^{-1}	kg m ⁻³
$c_{n,1}$	Blood nutrient concentration in first half cylinder	2.4×10^{-2}	kg m ⁻³
$c_{O,1}$	Blood O ₂ concentration in first half cylinder	8.3×10^{-3}	kg m ⁻³
C_∞	Ambient O ₂ concentration	8.3×10^{-3}	kg m ⁻³
D_n	Nutrient diffusion coefficient	3.5×10^{-10}	m ² s ⁻¹
D_O	O ₂ diffusion coefficient	2.2×10^{-9}	m ² s ⁻¹
m_n	Nutrient consumption rate	3.3×10^{-4}	kg m ⁻³ s ⁻¹
m_O	O ₂ consumption rate	4.1×10^{-4}	kg m ⁻³ s ⁻¹
r_b	Aorta radius	2.4×10^{-5}	m
α	Constant defining hemoglobin O ₂ saturation curve	5.8×10^4	-
β	Constant defining hemoglobin O ₂ saturation curve	1.5	-
Φ	Blood flux	3.3×10^{-12}	m ³ s ⁻¹

three species living in rivers (like zebrafish does), the carrying capacities are remarkably similar. The average value for these species (*Mylosetiger*, *Hydrolycus scomberoides* and *Pterodoras granulosus*) is 1.5×10^{-1} kg m⁻³ (SD 4.1×10^{-3}). This value is used in our model, based on the fact that these three species live in water of similar temperature and oxygen content as the zebrafish.

The nutrient concentration in blood entering the first section, $c_{n,1}$, is calculated by dividing rate of mass loss of the yolk cell by blood flux: $c_{n,1} = \frac{(dV/dt)\rho\gamma}{\Phi}$. The value of ρ (the specific wet weight of yolk) is estimated as 10^3 kg m⁻³, and for the wet weight to dry weight conversion factor γ we use a value of 0.1 (Finn *et al.*, 1991). Together with the experimentally found value of 8.1×10^{-14} kg s⁻¹ for dV/dt , and the value for Φ mentioned in Table 4.1, this results in a $c_{n,1}$ value of 2.4×10^{-2} kg m⁻³.

The oxygen concentration $c_{O,1}$ in blood entering the first cylinder is estimated by assuming that blood flowing over the yolk sac obtains the same oxygen concentration as the surrounding water: C_∞ . If the embryos are surrounded by oxygen saturated water of 28°C, C_∞ equals 8.3×10^{-3} kg m⁻³ (Golterman *et al.*, 1978).

D is the diffusion coefficient at 28°C of either oxygen or nutrients through tissue.

For oxygen a value of $2.2 \times 10^{-9} \text{ m}^2 \text{ s}^{-1}$ is taken from Kranenbarg *et al.* (2000). One of the parameters defining a molecule's diffusion coefficient is its size, as shown by the Stokes-Einstein equation: $D = \frac{k_B T}{6\pi\mu r}$ (Cussler, 1997), in which k_B is Boltzman's constant, T is temperature, μ is solvent dynamic viscosity and r is solute molecule radius. In this study, the diffusion coefficient of the smallest, and therefore fastest, amino acid (glycine) is used. The diffusion coefficients of all other amino acids as well as that of VLDL, which have a radius around 100 times that of amino acids, are bound to be smaller than the one used, so that we calculate the upper possible limit of nutrient movement by diffusion. Various authors (Mahler *et al.*, 1985; Desaulniers *et al.*, 1996; Dowse *et al.*, 2000) find that the diffusion coefficient of oxygen is around 3 times larger in water than in a range of tissues. Considering the Stokes-Einstein equation, it is probable that this relation also applies to glycine. The diffusion coefficient of glycine in water is taken from Cussler (1997) and divided by 3, yielding a value for D_n of $3.5 \times 10^{-10} \text{ m}^2 \text{ s}^{-1}$.

The parameter α , together with β , defines the sigmoidal curve indicating the relationship between blood plasma oxygen concentration and percentage hemoglobin saturation. The paper by Willmer (1933) from which b is estimated, also gives relationships between oxygen pressure and percentage blood saturation for the same fishes. By fitting a sigmoidal curve to the graph for *Myleus setiger* at 10 mm Hg CO_2 , a value for α of 5.8×10^4 is found.

m_O is the volume specific consumption rate of oxygen. Kranenbarg *et al.* (2000) give a value of $4.1 \times 10^{-4} \text{ kg m}^{-3} \text{ s}^{-1}$, which is adopted in this study. The corresponding consumption rate for nutrients m_n is calculated from this value, using the amount of oxygen needed to utilize a given amount of yolk. Consumption of 1 kg of oxygen corresponds to metabolizing $7.3 \times 10^{-1} \text{ kg}$ protein or 1.5 kg fat (Blaxter, 1988). The protein to lipid weight ratio in fish yolk, calculated from data on eleven different species (Heming and Buddington, 1988), is 3.9 (SD 2.6). Combining these values, a value for m_n of $3.3 \times 10^{-4} \text{ kg m}^{-3} \text{ s}^{-1}$ (SD 2.7×10^{-5}) is calculated.

Along with α , parameter β is estimated from Willmer (1933), yielding a value of 1.5. The blood vessel radius r_b is experimentally determined to be $2.4 \times 10^{-5} \text{ m}$ (SD 2.4×10^{-6} , $n=4$). The blood flux Φ is calculated by multiplying blood flow speed u , experimentally determined at $1.8 \times 10^{-3} \text{ m s}^{-1}$ (SD 1.5×10^{-4} , $n=2$) with the aorta cross-sectional area, calculated from r_b assuming a cylindrical aorta. This results in a value for Φ of $3.3 \times 10^{-12} \text{ m}^3 \text{ s}^{-1}$ (SD 6.4×10^{-13}).

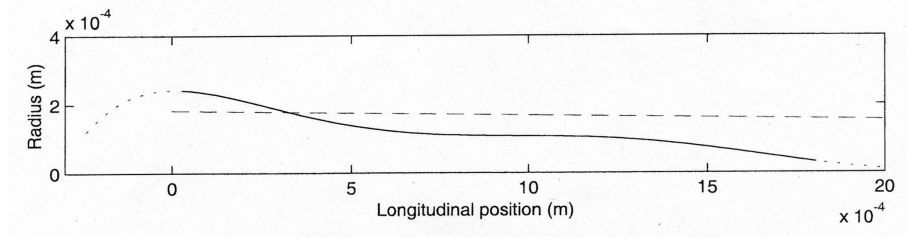


Figure 4.3: The actual height of the embryonic tissue measured perpendicular to the midline (solid line), compared to the embryo profile calculated from nutrient demand (dashed). The heart is located at longitudinal position 0; the dotted extensions of the solid line indicate embryo radius rostral or caudal of the vascular system (see also Fig. 4.1).

4.3.2 Model output

The model calculates embryo profiles with declining radii in caudal direction, both using the nutrient and the oxygen requirements. The predicted size according to oxygen demand, with an initial radius of around 0.6 mm and an infinite length is much larger than the one based on nutrients, which starts at a radius of around 0.2 mm and ends after less than 2 cm. Although the ‘oxygen embryo’ has an infinite length, the blood oxygen supply runs out at around 14 cm from the heart, after which a radius of a bit more than 0.4 mm can be maintained by diffusion through the skin alone. A section of the profile based on nutrient demand is depicted in Fig. 4.3, along with the actual embryo dimensions.

It can be concluded that although the predicted length, based on nutrient demand, exceeds the actual one by around tenfold, the predicted maximum radius lies close to the actual one.

4.4 Discussion

We investigated to what extent the required supply of oxygen and nutrients to tissue restricts embryo morphology in the zebrafish, and what role the vascular system plays. For that purpose we developed a model predicting morphology on the basis of these requirements and compared the results to the actual morphology. On the basis of oxygen requirements, we calculated the model embryo to grow both thicker and longer than the actual one. Even after the blood has been depleted of oxygen,

diffusion through the skin suffices to support a radius considerably larger than the actual one. The model suggests that, in case of oxygen saturated water, zebrafish embryo development is not directly limited by oxygen demand. In this situation the oxygen supplying capacity of the circulatory system is small compared to that of skin diffusion. These conclusions are in agreement with previous findings by Pelster and Burggren (1996) who found disruption of hemoglobin function not to affect aerobic processes in the zebrafish embryo. The nutrient model on the other hand, led to an embryo that was longer than the actual one, but of equal radius. Also, the calculated maximum radius, which can be interpreted as the maximum diffusion distance of nutrients, is several times smaller than the distance between the yolk sac and the tip of the embryo tail (see Fig. 4.1). This suggests the circulatory system to play a crucial role in transporting nutrients to the caudal part of the body.

These model results were achieved using parameter values taken from literature and experiments. The values defining blood characteristics (b , α and β) were determined in other fish species. Although there are reasons to believe they also apply to zebrafish blood (see section 4.3.1), their relevance for the zebrafish has not been experimentally tested. The initial blood nutrient concentration $C_{n,1}$ was calculated using blood flux Φ . Φ has a considerable inaccuracy which on its own would lead to a SD of around 20% in $C_{n,1}$. The calculation was furthermore based on the assumption that all mass loss from the yolk sac corresponds to nutrients metabolized by the embryo. This method leads to an overestimation of the amount of nutrients available if any nutrients are stored within the body (Blaxter, 1988). Also, when estimating the yolk cell volume we ignored the longitudinal section extending from the yolk ball in caudal direction (see Fig. 4.1). The error made in this way is estimated as less than 5%. The nutrient diffusion coefficient D_n was intentionally overestimated. Since yolk supplies several different nutrient molecules it is not possible to give a single D_n for nutrients as a whole. We used the highest possible value for D_n (based on the amino acid glycine) since our goal was to estimate the maximum possible embryo size. The diffusion coefficient of other amino acids is bound to lie in the same order of magnitude as that of glycine, due to their comparable size. The diffusion coefficient of VLDL on the other hand, might be around a hundred times smaller than the one used (see section 4.3.1).

What is the significance of these inaccuracies for the interpretation of our results? Concerning the parameters describing the oxygen carrying characteristics of blood (b ,

α and β) we can safely state that possible variations in these are of no importance to our conclusions. The radius and length of the model embryo are largely determined by oxygen diffusion through the skin rather than from the blood, and widely exceed the actual dimensions. The effect of variation in $C_{n,1}$ should be examined more closely. A higher value of $C_{n,1}$ would lead to larger model embryos, which could affect our conclusions regarding the importance of nutrient requirements. Closer investigation reveals that an altered value of $C_{n,1}$ has only a modest influence on the maximum radius and length of the model embryo. A twofold increase in $C_{n,1}$ leads to an increase in maximum radius and length of around 30% and 20%, respectively. These values indicate that fluctuations within reasonable limits of $C_{n,1}$ would not affect our conclusions. As mentioned, we overestimated the nutrient diffusion coefficient D_n . This has no consequences for our conclusions. Since a smaller value of D_n would lead to a narrower and more elongated model embryo, this overestimation even emphasizes our conclusion that nutrient requirements might constrain the embryo radius. A tenfold decrease of D_n leads to about a twofold decrease of maximum radius and a fourfold increase in length. Finally, variation in Φ would lead to changes in $C_{n,1}$ and also the predicted embryo length. The former was discussed above, and no conclusions were based on the latter, so that variations in this parameter would have no effect on our conclusions. Summarizing, it can be stated that in spite of several uncertainties determining parameter values, our conclusions remain justified.

The embryo size prediction is essentially based on the actual, observed supply of nutrients. This means that if model and parameter values are correct the volume of the model embryo will by definition be identical to the actual volume (in other words: the model embryo volume is a function of $C_{n,1}$ and m_n), yet we calculated an embryo that is larger than the actual one. In addition to the parameter inaccuracies discussed above, we ignored the nutrients being supplied to the embryo section rostral of the heart. This might explain why the calculated embryo volume is larger than the actual one, though it does not affect our predictions on maximum radius.

Our model has several imperfections. Especially the hard to assess problem of nutrient dynamics obliged us to settle for choices that require critical comments ($C_{n,1}$, D_n). In spite of these imperfections we have come to several conclusions that can withstand careful review, so that the notion remains that zebrafish embryos of this developmental stage are restricted in their growth by nutrient but not oxygen demand, and need their circulatory systems for nutrient but not oxygen transport.

Acknowledgements

We would like to thank prof. dr. Johan L. van Leeuwen and dr. Henri W.J. Stroband for their suggestions during research and careful review of the manuscript.

Intermezzo II - Oxygen Transfer to a Sphere in Stokes Flow¹

Introduction

The Reynolds number of a flow around an object is a measure of the relative importance of the inertial forces compared to the viscosity forces. In low Reynolds number flow, or Stokes flow ($Re < 1$), viscosity forces dominate (Purcell, 1977). Biology offers an interesting possibility to apply the theory of mass transfer to spheres in low Reynolds number flow.

Many small organisms (order of magnitude 1 mm) do not have an active internal oxygen transport system and solely depend on diffusion and external convection for their oxygen supply. The lack of an active transport system sets limits on the maximum size of these organisms as anoxic regions are expected to be avoided. Krogh (1941) put it very concisely: ‘...diffusion alone can provide sufficient oxygen only to organisms of 1 mm diameter or less...’. This conclusion, however, is based on the assumption that the oxygen concentration at the body surface equals the free water concentration (well-stirred condition). As many small organisms live in stagnant ponds, this assumption is likely to be invalid, because an oxygen poor boundary layer is expected to develop around the organism. This difficulty is accounted for in models of oxygen transfer in stagnant water (Lee and Strathmann, 1998; Kranenbarg *et al.*, 2000), although these models raise yet another problem. In natural conditions, completely stagnant water is highly unlikely to occur. Even stagnant ponds are continuously being stirred by aerial and thermal advection. The contribution of this advection to the total mass transfer can be accounted for by the introduction of static fluid film around the organism, through which oxygen is transported (Carslaw and Jaeger, 1959; Gielen and Kranenbarg, 2002). The thickness of this layer is translated

¹The mathematical analysis in this chapter is mainly performed by Jan H.G. Verhagen, MSc.

in a so-called mass transfer coefficient.

Flow associated with the stirring effects of aerial and thermal advection is typically in the low Reynolds number regime for small organisms with a diameter of about a millimeter. In this intermezzo, we account for the stirring effects of advection by describing the actual boundary layer morphology and oxygen concentration profile around the spherical organism (contrary to the mass transfer coefficient method, where a spherical boundary layer is forced upon the organism). The theory can be applied to teleost eggs, which are typically spherical and about a millimeter in diameter.

The model

An oxygen consuming sphere of radius a is held fixed in a uniform stream flowing from left to right parallel to the x -axis with constant velocity U , see Fig. II.1. The Reynolds number $2aU/\nu$ is supposed to be small compared to unity, where ν is the kinematic viscosity of the fluid. Oxygen is transported to the sphere across the mass boundary layer. The oxygen transfer consists of two parts: an advective and a diffusive contribution. In a steady state, the equation of oxygen mass conservation can be written as (Bird *et al.*, 1960):

$$\mathbf{q} \cdot \nabla c = D \nabla^2 c \quad (\text{II.1})$$

where \mathbf{q} is the fluid velocity vector, c is the oxygen concentration and D is the oxygen diffusion coefficient in water. The left hand side of equation II.1 represents the advective contribution, while the right hand side represents the diffusive contribution to the oxygen transfer.

Diffusive contribution

The diffusive contribution can be written in a dimensionless form in spherical polar co-ordinates (r, θ) as (Bird *et al.*, 1960):

$$\frac{2}{Pe} \left(\sin \theta \frac{\partial}{\partial \bar{r}} \left(\bar{r}^2 \frac{\partial \bar{c}}{\partial \bar{r}} \right) + \frac{\partial}{\partial \theta} \left(\sin \theta \frac{\partial \bar{c}}{\partial \theta} \right) \right) \quad (\text{II.2})$$

Here

$$\bar{c} = \frac{C_\infty - c_w}{C_\infty - c_s}, \quad \bar{r} = \frac{r}{a}, \quad \bar{\theta} = \frac{\theta}{a}, \quad Pe = \frac{2aU}{D}$$

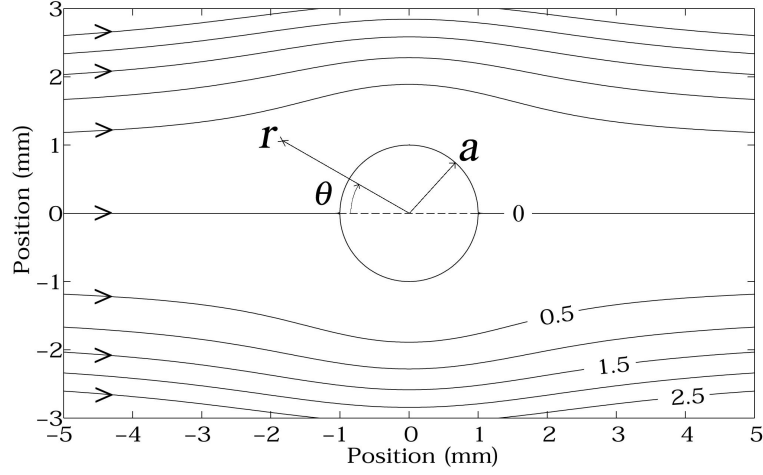


Figure II.1: Streamlines around a sphere in Stokes flow. Values of ψ (mm^3/s) are indicated in the streamlines.

where C_∞ is the bulk oxygen concentration, c_w is the oxygen concentration in the water, c_s is the oxygen concentration at the sphere surface, δ is the mass boundary layer thickness

At the surface of the sphere ($\bar{r} = 1$), the no-slip condition requires all fluid velocity components to be zero. If we assume the oxygen concentration at the sphere surface to be constant (due to mixing inside the sphere, see chapter 8), the tangential diffusion at the surface must be zero, so the boundary conditions that have to be satisfied by \bar{c} at $\bar{r} = 1$ are:

$$\bar{c} = 1, \quad \frac{\partial}{\partial \bar{r}} \left(\bar{r}^2 \frac{\partial \bar{c}}{\partial \bar{r}} \right) = 0 \quad (\text{II.3})$$

At the outer edge of the concentration boundary layer ($\bar{r} = 1 + \bar{\delta}$), the following boundary condition has to be satisfied:

$$\bar{c} = 0 \quad (\text{II.4})$$

Furthermore, we will assume the radial diffusive transport at the outer edge of the concentration boundary layer equal to that in stagnant medium, *i.e.*:

$$\bar{r}^2 \frac{\partial \bar{c}}{\partial \bar{r}} = -1 \quad (\text{II.5})$$

Equation II.1 will be solved using the Von Kármán integral method, which has been successfully applied to many boundary layer problems in the past. In this method

a distribution of the concentration over the thickness of the mass-boundary layer is assumed which satisfies as many boundary conditions as possible (Friedlander, 1957).

The following assumption is made:

$$\bar{r}^2 \frac{\partial \bar{c}}{\partial \bar{r}} = -k(\theta) \left(1 - \left(\frac{\bar{r} - 1}{\bar{\delta}} \right)^2 \right) - 1 \quad (\text{II.6})$$

The concentration distribution follows from equation II.6 together with boundary conditions for \bar{c} at $\bar{r} = 1$ and $\bar{r} = 1 + \bar{\delta}$:

$$\bar{c} = \frac{1}{\bar{r}} \left(k + 1 - \frac{k}{\bar{\delta}^2} \right) - \frac{2k}{\bar{\delta}^2} \ln \bar{r} + k \left(\frac{\bar{r}}{\bar{\delta}^2} - 1 \right) \quad (\text{II.7})$$

where

$$k = \frac{\bar{\delta}^2}{(1 + \bar{\delta})(\bar{\delta}^2 - 2\bar{\delta} + 2 \ln(1 + \bar{\delta}))}$$

This oxygen distribution satisfies all four boundary conditions.

Advective contribution

The flow around the sphere is well known as Stokes flow (see Fig. II.1) and the dimensionless stream function $\bar{\psi}(\bar{r}, \theta)$ (with $\bar{\psi} = \psi/a^2U$) in spherical polar co-ordinates \bar{r} and θ is

$$\bar{\psi} = \bar{r}^2 \left(\frac{1}{2} - \frac{3}{4\bar{r}} + \frac{1}{4\bar{r}^3} \right) \sin^2 \theta \quad (\text{II.8})$$

When F represents the total amount of oxygen transported within the concentration boundary layer across a radius at any θ along the sphere due to advection, $F(\theta)$ can be written as:

$$F(\theta) = - \int_1^0 \bar{\psi} d\bar{c} = - \int_1^{1+\bar{\delta}} \frac{\partial \bar{c}}{\partial \bar{r}} \bar{\psi} d\bar{r} \quad (\text{II.9})$$

Total mass transfer

The equation of oxygen mass conservation (II.1) can be rewritten as the mass balance for a θ -section of the concentration boundary layer by integrating equation II.2 over the boundary layer thickness and differentiating equation II.9 with respect to θ :

$$-\frac{d}{d\theta} \left(\int_1^{1+\bar{\delta}} \frac{\partial \bar{c}}{\partial \bar{r}} \bar{\psi} d\bar{r} \right) = \int_1^{1+\bar{\delta}} \frac{2}{Pe} \left(\sin \theta \frac{\partial}{\partial \bar{r}} \left(\bar{r}^2 \frac{\partial \bar{c}}{\partial \bar{r}} \right) + \frac{\partial}{\partial \theta} \left(\sin \theta \frac{\partial \bar{c}}{\partial \theta} \right) \right) d\bar{r} \quad (\text{II.10})$$

Both $\bar{\psi}$ and \bar{c} are now known functions of \bar{r} , $\bar{\delta}$ and θ . Equation II.10 needs two boundary conditions for $\bar{c}(\theta)$. One condition is $d\bar{c}/d\theta = 0$ for $\theta = 0$. If the other boundary condition would be known, the boundary layer thickness $\bar{\delta}$ could be solved as a function of θ .

If the Péclet number $Pe \gg 1$ the concentration boundary layer $\bar{\delta}$ becomes very small. In that case, equation II.10 can be linearized for $\bar{\delta} \ll 1$ and the tangential diffusion term appears negligible. The resulting first order differential equation needs only one boundary condition and can be solved analytically to:

$$\bar{\delta} = \sqrt[3]{\frac{30}{Pe}} \times \frac{\sqrt[3]{\theta - \frac{1}{2} \sin 2\theta}}{\sin \theta} \quad (\text{II.11})$$

The Sherwood number (Sh) is defined as (Friedlander, 1957):

$$Sh = - \int_0^\pi \left(\frac{\partial \bar{c}}{\partial \bar{r}} \right)_{\bar{r}=1} \sin \theta d\theta = \int_0^\pi (k+1) \sin \theta d\theta \quad (\text{II.12})$$

For $Pe \gg 1$ or $\bar{\delta} \ll 1$, $k(\bar{\delta})$ can be linearized and equation II.12 can be solved analytically to (*cf.* Friedlander (1957, 1961)):

$$Sh = 0.9785 Pe^{1/3} \quad (\text{II.13})$$

For smaller values of Pe , the mass boundary layer thickness is no longer small compared to one. In that case, equation II.10 has to be solved numerically. However, this is not possible because equation II.10 lacks sufficient boundary conditions in θ -direction. The tail length of the mass boundary layer appears to be undetermined and could as well be infinitely long. This is the direct result of the assumption that $\bar{c} = 0$ at $\bar{r} = 1 + \bar{\delta}$ and because the boundary condition for $\partial \bar{c} / \partial \theta$ at $\bar{r} = 1 + \bar{\delta}$ and $\theta = \pi$ is missing.

Applying the linearization procedure for $\bar{\delta} \ll 1$ to equation II.10 and II.12 shows that Sh can be written as:

$$Sh = \alpha Pe^{1/3} + \beta Pe^0 + O(Pe^{-1/3}) \quad (\text{II.14})$$

It can be shown that the contribution of the tangential diffusion to the Sh -number must be $O(Pe^{-1/3})$. So we may solve equation II.12 up to $O(Pe^0)$ numerically without needing a second boundary condition for $\bar{\delta}(\theta)$. (Neglecting the tangential diffusion term in equation II.10 reduces the equation from a second order to a first order differential equation in θ , for which only one boundary condition at $\theta = 0$ is sufficient.)

The numerical solution of equation II.12 without the tangential diffusion term is shown in Fig. II.2. With the effect of the tangential diffusion included, the solution to the right order of accuracy is:

$$Sh = 0.978Pe^{1/3} + 1.38 + O(Pe^{-1/3}) \quad (\text{II.15})$$

This expression together with its confidence interval is valid for all Pe larger than one (Fig. II.2). Fig. II.2 also shows the agreement between our analytical model (solid line) and data points from Friedlander (1957). See Kranenbarg *et al.* (2001) for several other relations between the Sherwood number and the Péclet number from the literature

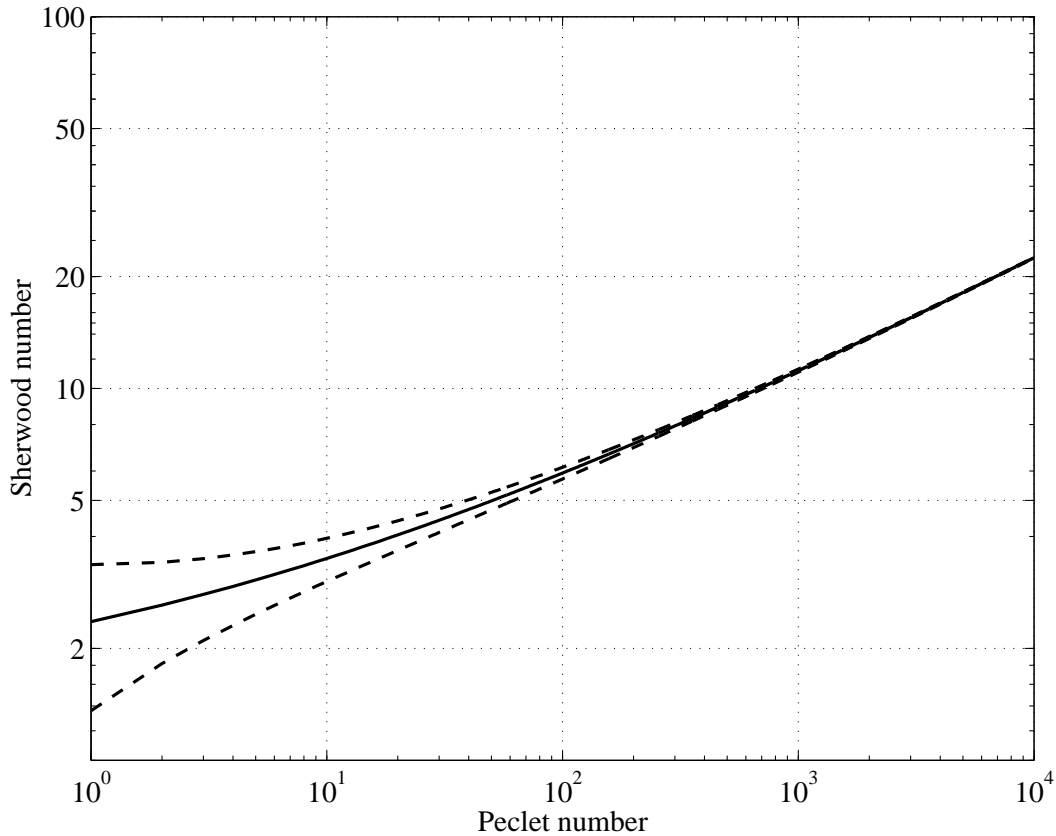


Figure II.2: Sherwood number as a function of the Péclet number. The solid line with dashed confidence intervals represents the general solution of equation II.12 to the right order of magnitude (equation II.15). Black dots represent data cited in Friedlander (1957).

Chapter 5

Consequences of Forced Convection for the Constraints on Size and Shape in Embryos¹

Previously, predictions on maximum size of biological objects based on oxygen availability have been made for both zero and infinite water velocity around the object. In reality however, water velocity is always intermediate between zero and infinity. We predicted maximum size and optimal shape of biological objects, pending the velocity of water around them. We assumed oxygen inside the object to be transported by diffusion and outside the object by diffusion and convection. Fick's first law of diffusion describes the inner transport. For the outer transport, we relied on semi-empirical relations between mass transport and flow conditions (Friedlander's equations). To keep mathematical complexity acceptable, we restricted ourselves to the analysis of a sphere and a cylinder in cross flow. If water velocity is low, a spherical shape is most favorable for gas exchange. If water velocity is high, an elongated and flattened shape is more favorable. A size-dependent intermediate velocity exists where shape does not matter (10^{-4} m/s for teleost embryos). Teleost embryos are typically exposed to flow velocities equal to or larger than 10^{-4} m/s, making an elongated shape more favorable than a spherical one. Although teleost eggs are typically spherical, the oxygen consuming embryos inside are indeed elongated.

5.1 Introduction

Several authors have predicted maximum sizes of biological objects based on oxygen diffusion capacities (McNeill Alexander, 1971; Fenn, 1927; Gerard, 1931; Harvey, 1928; Kranenbarg *et al.*, 2000; Krogh, 1941; Lee and Strathmann, 1998; Strathmann and Chaffee, 1984; Warburg, 1923; Woods, 1999). All of these authors assumed the oxygen

¹Kranenbarg, S., Verhagen, J.H.G., Muller, M. and van Leeuwen, J.L. (2001). *J. Theor. Biol.* 212(4), 521-533. Reproduced with permission of Academic Press.

concentration at the surface of their object to equal the concentration of the free water (infinitely thin concentration boundary layer). In addition, Kranenbarg *et al.* (2000) and Lee and Strathmann (1998) give a model of oxygen diffusion into animals living in completely stagnant water. This situation allows a complete diffusion boundary layer to build up without any perturbations.

A comparison of oxygen diffusion into a spherical, cylindrical and sheet-like animal in the ‘infinitely thin boundary layer’ situation by Kranenbarg *et al.* (2000) showed that a sheet-like animal can become largest in the absence of an additional internal oxygen transport system. This makes the sheet the most optimal shape for gas exchange when water velocity is infinitely large (and presumably much lower). A situation where consumption (independent of local oxygen concentration) by the animal is at equilibrium with the supply by diffusion (steady state) is never reached for an infinitely long cylindrical or sheet-like shape in stagnant water. The optimal shape for gas exchange in stagnant water could therefore not be determined by Kranenbarg *et al.* (2000).

In real life situations, however, it is highly unlikely that an animal lives in either completely stagnant water or in a situation where the boundary layer is infinitely thin. Naturally occurring mechanisms such as parental fin fanning (*e.g.* Cichlidae, Gasterosteidae), positive buoyancy of eggs (Cambalik *et al.*, 1998; Nakatani and Maeda, 1993), cilia-induced convection (Burggren, 1985), flow of the surrounding medium (Johnson, 1980) or natural convection (O’Brien *et al.*, 1978) tend to stir or refresh the oxygen poor boundary layer around the animal.

In this paper, we try to assess the effects of movement of the medium due to external forces (forced convection) on the supply of oxygen to embryos without a functional circulatory system. Our analysis aims to predict a theoretical maximum body size that can be supplied with oxygen solely by diffusion, pending the flow velocity of the external medium. In addition, the optimal body shape for gas exchange is determined for different flow velocities of the surrounding medium.

5.2 Theoretical Analysis

5.2.1 Optimal shape in forced convection with infinite or zero velocity

The volume of respiring tissue of an animal without a circulatory system has to be supplied with oxygen by diffusion through the skin surface. Too large a surface area will be energetically inefficient, as will be too large a tissue volume. Thus, an optimal tuning of the (oxygen supplying) surface area and (oxygen consuming) tissue volume is to be expected. Therefore, volume-to-surface-ratio (V/A) is a relevant definition of size. A maximum volume-to-surface-ratio represents the volume that can be maintained by a specified surface area (and a surface-to-volume-ratio represents the surface area needed to supply a specified volume with sufficient oxygen). Kranenbarg *et al.* (2000) give theoretical maximum volume-to-surface-ratios for sheet-, cylinder- and sphere-shaped embryos living in running water (infinitely thin diffusion boundary layer) in a steady state situation.

$$\text{sheet:} \quad \frac{V}{A} = 1.41 \sqrt{\frac{D_e C_\infty}{m}} \quad (5.1)$$

$$\text{cylinder:} \quad \frac{V}{A} = \sqrt{\frac{D_e C_\infty}{m}} \quad (5.2)$$

$$\text{sphere:} \quad \frac{V}{A} = 0.82 \sqrt{\frac{D_e C_\infty}{m}} \quad (5.3)$$

where V is the volume of the organism, A is the surface area, D_e is the diffusion coefficient of oxygen in embryonic tissue, C_∞ is the free water oxygen concentration and m is the volume-specific oxygen consumption (independent of the oxygen concentration, based on Longmuir (1957); see appendix A). In running water, a sheet-like shape is the most favorable for gas exchange (sheet-like embryos can obtain the largest volume-to-surface-ratio). Equation 5.1 holds for a sheet of infinite planar dimensions and equation 5.2 holds for an infinitely long cylinder. For a finite cylinder in running water, the effect of diffusion through the (plate-like) ends on the oxygen concentration in the center of the cylinder is negligible at a length-radius-ratio of about five (Gielen and Kranenbarg, 2002). In low Reynolds number flow around a finite cylinder, water velocity will be largest around the ends of the cylinder, thereby locally increasing the oxygen concentration. The effect of this faster flow around the ends of the cylinder will at most be a two-fold larger oxygen concentration at the ends as compared to the

middle part of the cylinder (Kranenbarg *et al.*, 2000). It can therefore be argued that the effect of diffusion through the ends of a finite cylinder at low Reynolds number flow on oxygen concentration at the center of the cylinder will cease to exist at a length-radius-ratio of about ten. At a length-radius-ratio between ten and twenty, there is no effect of oxygen diffusion through the ends of a finite cylinder on oxygen concentration at the center of the cylinder, though the maximum volume-to-surface-ratio is still smaller than that of an infinite cylinder. At a length-radius-ratio of about twenty, the maximum volume-to-surface-ratio of a finite cylinder equals 95% of that of an infinite cylinder. In the remainder of this paper we will discuss sheets and cylinders of infinite dimensions with the implicit assumption that the results will reasonably hold for length-radius-ratios larger than about twenty.

If the diffusion coefficient of oxygen in water is assumed to be three times that of oxygen in embryonic tissue (Kranenbarg *et al.*, 2000), the maximum volume-to-surface ratio for a spherical embryo without a circulatory system in stagnant water (complete diffusion boundary layer build-up, zero velocity) in a steady state situation is:

$$\frac{V}{A} = 0.63 \sqrt{\frac{D_e C_\infty}{m}} \quad (5.4)$$

which is (of course) smaller than in running water. Steady state situations do not exist for a cylinder and plane sheet of infinite dimensions in stagnant water as the concentration gradient is described by a logarithmic and linear function of the radial distance, respectively and the oxygen concentration thus never reaches a plateau (Kranenbarg *et al.*, 2000). However, contrary to running water, the sphere appears to be the most favorable shape in stagnant water! This can be shown as follows.

Assume for simplicity the diffusion coefficients of oxygen in tissue and water to be the same ($D_e = D_w$). The oxygen concentration at the center of a spherical embryo in stagnant water, as a function of time t (where t is large) is given by:

$$c(0, t) = C_\infty - \frac{mR^2}{2D} + \frac{mR^3}{3\pi D} \sqrt{\frac{\pi}{Dt}} \quad (5.5)$$

where R is the radius of the organism (Kranenbarg *et al.*, 2000).

For a sheet-like organism, the equivalent expression is:

$$c(0, t) = C_\infty - mt \left(1 - 4 i^2 \operatorname{erfc} \frac{R}{2\sqrt{Dt}} \right) \quad (5.6)$$

for any t (Carslaw and Jaeger, 1959), where R is half the thickness of the sheet and $i^2 \operatorname{erfc}(z)$ is a repeated integral of the error function (Abramowitz and Stegun, 1965).

Table 5.1: Volume-to-surface-ratios (V/A) of spherical or sheet like embryos with their accompanying survival times t_s in stagnant water. Values of the input parameters are those at 25°C (Appendix C).

t_s (s)	sphere V/A (m)	plane sheet V/A (m)
10^3	1.12×10^{-4}	2.69×10^{-5}
10^4	1.08×10^{-4}	9.67×10^{-6}
10^5	1.07×10^{-4}	3.06×10^{-6}
10^6	1.07×10^{-4}	9.67×10^{-7}

Using the first two terms of a power series expansion of $i^2 \operatorname{erfc}(z)$ (Abramowitz and Stegun, 1965), equation 5.6 reduces to:

$$c(0, t) = C_\infty - 1.1284mR\sqrt{\frac{t}{D}} \quad (5.7)$$

for large t .

Now suppose that we want to calculate the volume-to-surface-ratio at which the model embryo can survive t_s seconds, *i.e.* the center of the organism is not allowed to become anoxic for $t < t_s$. If $t = t_s$, the concentration in the center of the model embryo reaches zero:

$$\text{sphere:} \quad 0 = C_\infty - \frac{mR^2}{2D} + \frac{mR^3}{3\pi D} \sqrt{\frac{\pi}{Dt_s}} \quad (5.8)$$

$$\text{sheet:} \quad 0 = C_\infty - 1.1284mR\sqrt{\frac{t_s}{D}} \quad (5.9)$$

From these equations, the volume-to-surface-ratio at $t = t_s$ can be calculated by using appendix C to estimate parameters m and D (Table 5.1).

These results show that although a steady state solution does not exist for a plane sheet (and cylinder) of infinite dimensions in stagnant water, a maximum volume-to-surface-ratio can be predicted for a defined survival time. This predicted maximum volume-to-surface-ratio is larger for a spherical organism than for a sheet- and cylinder-shaped organism (assuming the cylinder to be intermediate between the plane sheet and the sphere), which makes the sphere the most optimal shape in stagnant water (see discussion). Preliminary numerical evaluations of diffusion in plane sheets and cylinders of finite dimensions in FEMLAB 2.1 show similar results, thus indicating that a sphere in stagnant water can indeed obtain the maximum volume-to-surface-ratio.

5.2.2 Effects of forced convection on size and shape; an analytical approach

The plane sheet appears to be a less favorable shape for gas exchange in stagnant water than in running water, while the reverse is true for the sphere. This suggests the existence of a flow condition where shape does not matter! In order to find this condition, we analyzed a moving line sink (as a representation of a cylindrical, oxygen consuming organism in a moving fluid) and a moving point sink (for a spherical, oxygen consuming organism in a moving fluid). In our analysis we only considered the line sink moving perpendicular to its axis.

According to Kranenbarg *et al.* (2000), a steady state situation for the oxygen concentration distribution is reached within several minutes (when theoretically possible). This is very quick compared with the developmental time scale and we therefore adopt a steady state situation in the subsequent analyses.

Moving point sink

If oxygen is consumed at a rate $\frac{4}{3}\pi R^3 m$ per unit time at the origin of a co-ordinate system and the medium moves uniformly past the origin with velocity U parallel to the x-axis, the steady state oxygen concentration in point (x,y,z) is given by (modified after Carslaw and Jaeger (1959)):

$$c(x, y, z) = C_\infty - \frac{mR^3}{3D_w \sqrt{x^2 + y^2 + z^2}} e^{\frac{-U(\sqrt{x^2 + y^2 + z^2} - x)}{2D_w}} \quad (5.10)$$

Note that although we analyzed a point sink, we introduced a radius R . An actual spherical sink would influence the streamlines of the originally parallel flow, while a point sink does not. The effect of introducing a radius in the analysis will be discussed in section 5.3. For now, we will assume the equations of a point sink to hold for a spherical sink as well. For $x = 0$, $y = 0$ and $\sqrt{x^2 + y^2 + z^2} = R$, it follows from equation 5.10 that

$$c(0, 0, R) = C_\infty - \frac{mR^2}{3D_w} e^{\frac{-UR}{2D_w}} \quad (5.11)$$

which gives the oxygen concentration at the outer surface of the spherical embryo (see Fig. 5.1 A for the orientation of the sphere).

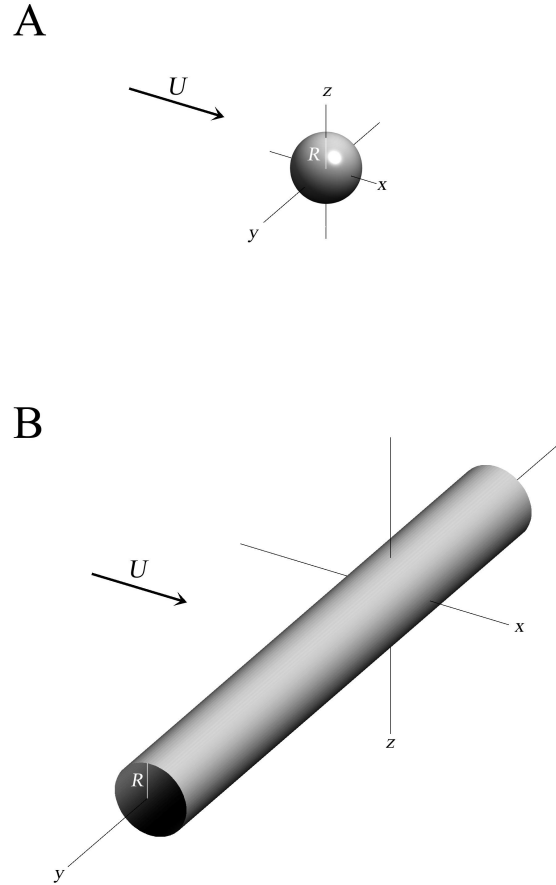


Figure 5.1: Illustration of the orientation of the point (A) and line (B) sink. The artificially introduced radius (see text) is indicated by R . The flow velocity of the surrounding medium is represented by U .

Moving line sink (of infinite length)

If oxygen is consumed at a rate $m\pi R^2$ per unit length and unit time along the y-axis and the medium moves uniformly past the y-axis with velocity U parallel to the x-axis (cross flow), the oxygen concentration in steady state at a point (x,y,z) is given by

(modified after Carslaw and Jaeger (1959)):

$$c(x, z) = C_\infty - \frac{mR^2}{2D_w} e^{\frac{Ux}{2D_w}} K_0 \left(\frac{U\sqrt{x^2 + z^2}}{2D_w} \right) \quad (5.12)$$

where K_0 is the modified Bessel function of the second kind of order 0. Here we again introduced a radius R and again we will assume the equation for a line sink to hold for a cylindrical sink (see also section 5.3).

For $x = 0$ and $\sqrt{x^2 + z^2} = R$, it follows from equation 5.12 that

$$c(0, R) = C_\infty - \frac{mR^2}{2D_w} K_0 \left(\frac{UR}{2D_w} \right) \quad (5.13)$$

gives the oxygen concentration at the outer surface of the cylindrical embryo (see Fig. 5.1 B for the orientation of the cylinder).

It would be interesting to know under what conditions the oxygen concentration for a cylindrical and a spherical shape are equal, or when

$$c_{\text{line}}(0, R) = c_{\text{point}}(0, 0, R) \quad (5.14)$$

This is the case when equations 5.11 and 5.13 are equal:

$$\frac{1}{2} K_0 \left(\frac{UR}{2D_w} \right) = \frac{1}{3} e^{-\frac{UR}{2D_w}} \quad (5.15)$$

which yields after numerical evaluation

$$UR = 6.6D_w \quad (5.16)$$

Since the diffusion coefficient is in the order of magnitude of 10^{-9} m²/s and the embryo radius (volume-to-surface-ratio) in the order of magnitude of 10^{-4} m (Kranenbarg *et al.*, 2000), the flow velocity at which the oxygen concentration at the surface of the model embryo is the same for a cylindrical and spherical shape is in the order of magnitude 10^{-4} m/s, or several hundreds of micrometers per second. When the velocity is higher a cylindrical shape is more favorable, if flow is perpendicular to the axis, when it is lower a spherical shape is more favorable for gas-exchange.

5.2.3 Effects of forced convection on size and shape; a semi-empirical approach

The effects of forced convection on gas exchange in different shapes can also be investigated by employing dimensionless number theory (appendix B). Numerous semi-empirical relations exist between different dimensionless numbers to describe mass

transfer to different shapes, which we used in the following analysis. Again, we compared oxygen diffusion and forced convection to a spherical and cylindrical embryo in cross flow.

We assume diffusion to be the only way of oxygen transport inside the organism, as the animal does not have a functional circulatory system yet. Outside the embryo forced convection occurs in combination with diffusion. It is therefore convenient to divide the problem of oxygen transport to an embryo into an inner and an outer problem. In this paper we assume oxygen transport inside and outside the embryo to be linked by a ‘constant and equal concentration on the skin surface’ principle (Daykin, 1965).

Oxygen transport inside the embryo

Fick’s first law of diffusion applied to the inside of a spherical embryo gives:

$$\frac{4}{3}\pi r^3 m = 4\pi r^2 D_e \frac{dc}{dr} \quad (5.17)$$

where r is the distance to the center of the embryo, c is the oxygen concentration, and the volume-specific oxygen consumption m is independent of the oxygen concentration.

This reduces to:

$$\frac{dc}{dr} = \frac{mr}{3D_e} \quad (5.18)$$

By integrating from the center of the sphere ($r = 0$) to the surface ($r = R$) and assuming $c(0) = 0$, we obtain:

$$c_s = \frac{mR^2}{6D_e} \quad (5.19)$$

where c_s = oxygen concentration at the skin surface.

For a cylindrical embryo an analogous expression can simply be derived by applying Fick’s first law to a cylinder:

$$c_s = \frac{mR^2}{4D_e} \quad (5.20)$$

Thus, equations 5.19 and 5.20 give the oxygen concentration at the body surface of a spherical and cylindrical organism respectively, needed to sustain the maximum possible volume-to-surface-ratio.

Oxygen transport outside the embryo

The effect of forced convection in combination with diffusion on the oxygen transport to the embryo can be assessed by a dimensionless number analysis. A respiring embryo builds up an oxygen concentration boundary layer around it. Oxygen is transferred by diffusion across that boundary layer at a rate proportional to the difference in oxygen concentration on opposite sides of that layer (Daykin, 1965):

$$J = 4\pi R^2(C_\infty - c_s)k \quad (5.21)$$

where J is the mass flux of oxygen to the sphere and k the mass transfer coefficient.

For a sphere with volume-specific oxygen consumption m , equation 5.21 becomes:

$$\frac{Rm}{3} = (C_\infty - c_s)k \quad (5.22)$$

The mass transfer coefficient, the sphere radius and the diffusion coefficient of oxygen in water (D_w) can be combined into a dimensionless number, the Sherwood number (Sh , equivalent to the Nusselt number in heat transfer) (Daykin, 1965):

$$Sh = \frac{2kR}{D_w} \quad (5.23)$$

The Sherwood number is a measure for the ratio of total mass transfer to diffusive mass transfer. By assuming $D_w = 3D_e$ (Kranenbarg *et al.*, 2000), equations 5.20, 5.22 and 5.23 can be combined to obtain:

$$Sh_{\text{sphere}} = \frac{4}{\frac{6D_w C_\infty}{mR^2} - 3} \quad (5.24)$$

For a cylindrical embryo the analogous formula becomes:

$$Sh_{\text{cylinder}} = \frac{4}{\frac{4D_w C_\infty}{mR^2} - 3} \quad (5.25)$$

The effect of forced convection is to reduce the boundary layer thickness and thus enhancing diffusion of oxygen into the embryo. Forced convection can be described in terms of the dimensionless Reynolds number (Re) and Schmidt number (Sc , equivalent to the Prandtl number in heat transfer) (Bird *et al.*, 1960):

$$Re = \frac{2RU}{\nu} \quad (5.26)$$

Table 5.2: Several semi-empirical relations of the Sherwood number (Sh) with the Reynolds (Re) and Schmidt (Sc) or Péclet (Pe) number, together with their origin (mass or heat transfer), their validity domain and author.

	mass / heat	validity region	reference
sphere			
$Sh = (1.21Pe^{2/3} + 4)^{1/2}$	mass	$Re < 1$	Brian and Hales (1969)
$Sh = 1 + (1 + Pe)^{1/3}$	mass	$Re < 1$	Clift <i>et al.</i> (1978)
$Sh = 2 + 0.89Pe^{1/3}$	mass	$Re < 1$ $Pe > 10^3$	Friedlander (1957)
$Sh = 2 + 0.6Re^{1/2}Sc^{1/3}$	heat	$1 < Re < 10^5$	Bird <i>et al.</i> (1960)
$Sh = 2 + 0.8Re^{1/2}Sc^{1/3}$	mass	$Re > 1$ $Sc \approx 10^3$	Daykin (1965)
cylinder			
$Sh = 0.557Pe^{1/3}$	mass	$Re = 0.1$ $Pe \geq 10$	Friedlander (1957)
$Sh = 0.91Re^{0.385}Sc^{0.31}$	heat	$0.1 < Re < 50$	Jakob (1949)
$Sh = 0.86Re^{0.43}Sc^{0.3}$	heat	$0.1 < Re < 200$	McAdams (1951)
$Sh = 0.49Re^{0.53}Sc^{1/3}$	heat	$10^2 < Re < 10^5$	Bird <i>et al.</i> (1960)

where ν is the kinematic viscosity of the surrounding water, U is the flow velocity of the surrounding water. The Reynolds number is a measure for the ratio of inertial forces to viscous forces. The Schmidt number is a measure for the ratio of kinematic viscosity to molecular diffusivity:

$$Sc = \frac{\nu}{D_w} \quad (5.27)$$

The Péclet number (Pe) is often used as the product of the Reynolds and Schmidt numbers and is a measure for the ratio of convective mass transfer to diffusive mass transfer:

$$Pe = ReSc = \frac{2RU}{D_w} \quad (5.28)$$

Several other theoretical and semi-empirical equations exist to relate the Sherwood number to the Reynolds and Schmidt or Péclet number for different flow conditions and different shapes of the object (Table 5.2).

We want to calculate the maximum volume-to-surface-ratio at any flow velocity of the surrounding medium for both a spherical and cylindrical embryo. This can be

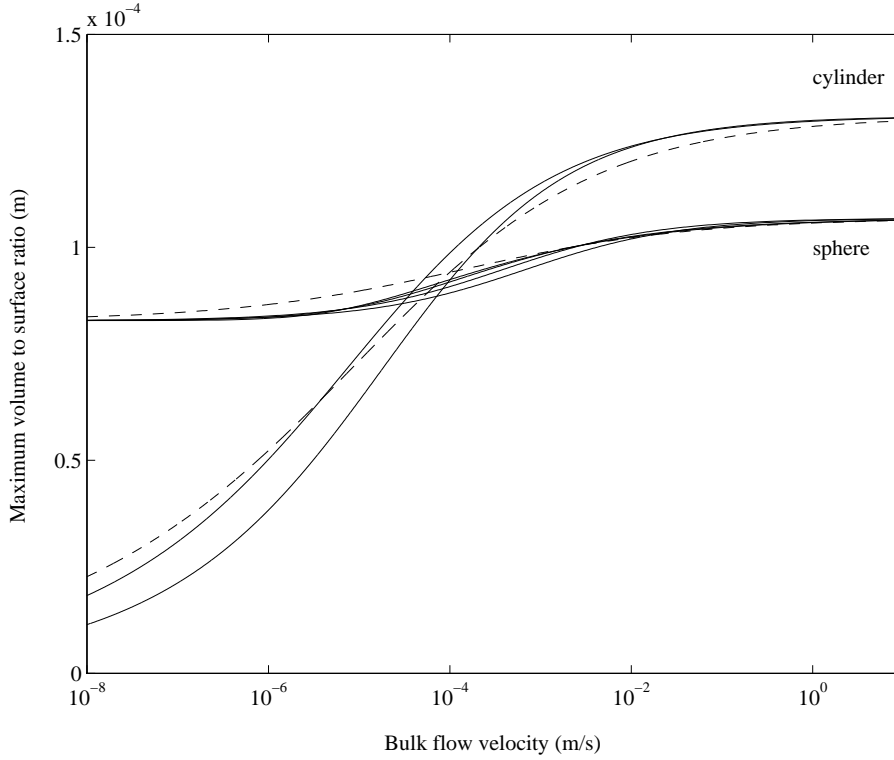


Figure 5.2: Graph of maximum volume-to-surface-ratio of a cylindrical and a spherical animal as a function of flow velocity of the surrounding medium at 25°C. The two sets of lines were calculated using the different relations shown in Table 5.2. The dotted lines were used for further analytical analysis (see text). Note the intersection point of the two sets of lines. Flow velocities above that of the intersection point make a cylindrical shape more efficient. At lower velocities, a spherical shape is more efficient.

done by combining equations 5.24 and 5.25 with the equations in Table 5.2, giving two equations with two variables (R and U) for both the sphere and the cylinder. Fig. 5.2 gives the result of these calculations. Using Friedlander's equations (Table 5.2), the point of intersection of the curves for maximum volume-to-surface-ratio of a sphere and cylinder as a function of flow velocity of the surrounding medium can be calculated (dotted lines in Fig. 5.2). It appears that if

$$U = 9.83 \sqrt{\frac{D_w m}{C_\infty}} \quad (5.29)$$

the maximum volume-to-surface-ratio for a spherical organism is the same as that

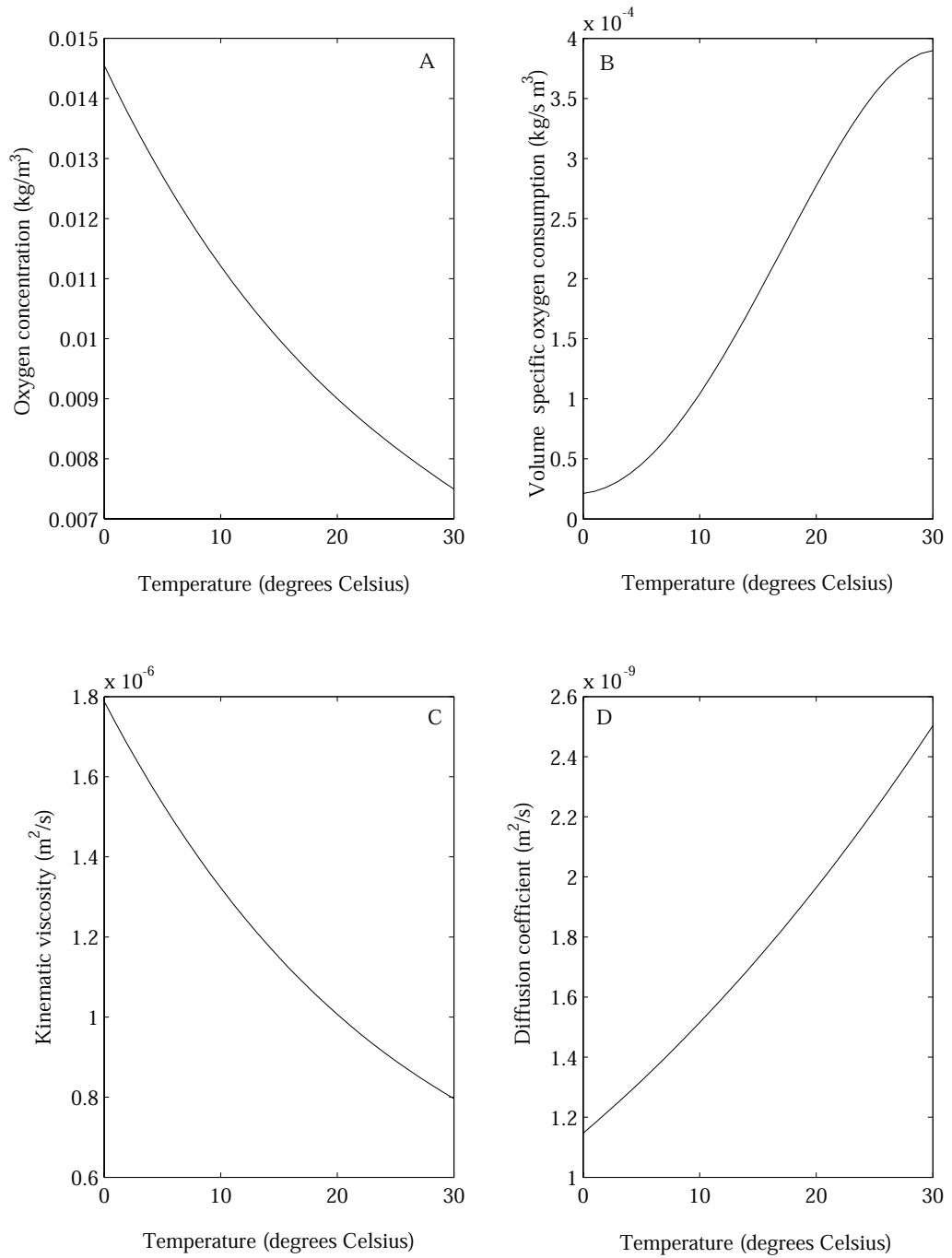


Figure 5.3: Graphs of the four input parameters as a function of temperature: (A) oxygen concentration of the free water (data from Kranenbarg *et al.* (2000)), (B) volume-specific oxygen consumption (data from Rombough (1988)), (C) kinematic viscosity of water (data from Weast (1976)). and (D) diffusion coefficient of oxygen in water (data from Kranenbarg *et al.* (2000)).

of a cylindrical organism and can be expressed as:

$$\frac{V}{A} = 0.41 \sqrt{\frac{D_w C_\infty}{m}} \quad (5.30)$$

cf. equations 5.3 and 5.4, where the coefficients in front of the rooted term are 0.47 and 0.36 respectively if D_e is converted to D_w ($D_w = 3D_e$; Kranenbarg *et al.* (2000)). If the flow velocity of the surrounding medium is lower, the maximum volume-to-surface-ratio for a spherical organism is larger, if this flow velocity is higher, then a cylindrical organism can obtain a larger volume-to-surface-ratio.

If we replace the velocity and radius in the Reynolds number by equations 5.29 and 5.30 respectively, where $R = 2V/A$ in a cylinder and $R = 3V/A$ in a sphere, we obtain the following for the intersection point:

$$\text{for a cylinder:} \quad ReSc = 8.14 \quad (5.31)$$

$$\text{for a sphere:} \quad ReSc = 12.2 \quad (5.32)$$

In terms of the physical parameters, these expressions read $\frac{2RU}{\nu} \frac{\nu}{D_w} \approx 10$, which can be simplified as:

$$RU = 5D_w \quad (5.33)$$

Note that this equation closely resembles equation 5.16 in section 5.2.3.

Obviously, all four input parameters (C_∞ , m , ν and D_w) necessary to create Fig. 5.2, depend on temperature. Appendix C gives this dependency for these four parameters based on literature data. Kranenbarg *et al.* (2000) give the temperature dependencies of the free water oxygen concentration and the diffusion coefficient of oxygen in water. Appendix C gives this relation based on temperature in degrees Celsius instead of Kelvin. Kinematic viscosity of water decreases with temperature, which can be described by a polynomial fitted to data in Weast (1976). Volume-specific oxygen consumption of teleost embryos depends on temperature as given by Rombough (1988). In appendix C, Rombough's regression line is represented as a fourth order polynomial. Fig. 5.3 gives a graphical representation of the above mentioned relations. Using the equations in Appendix C, maximum volume-to-surface-ratio as a function of flow velocity of the surrounding medium can be calculated with temperature as a covariable (Fig. 5.4). As was already shown by Kranenbarg *et al.* (2000), theoretical maximum volume-to-surface-ratio is higher as temperature decreases. However, the flow velocity at which the lines representing maximum volume-to-surface-ratio of a sphere and cylinder intersect show a relatively small effect of temperature (Fig. 5.4).

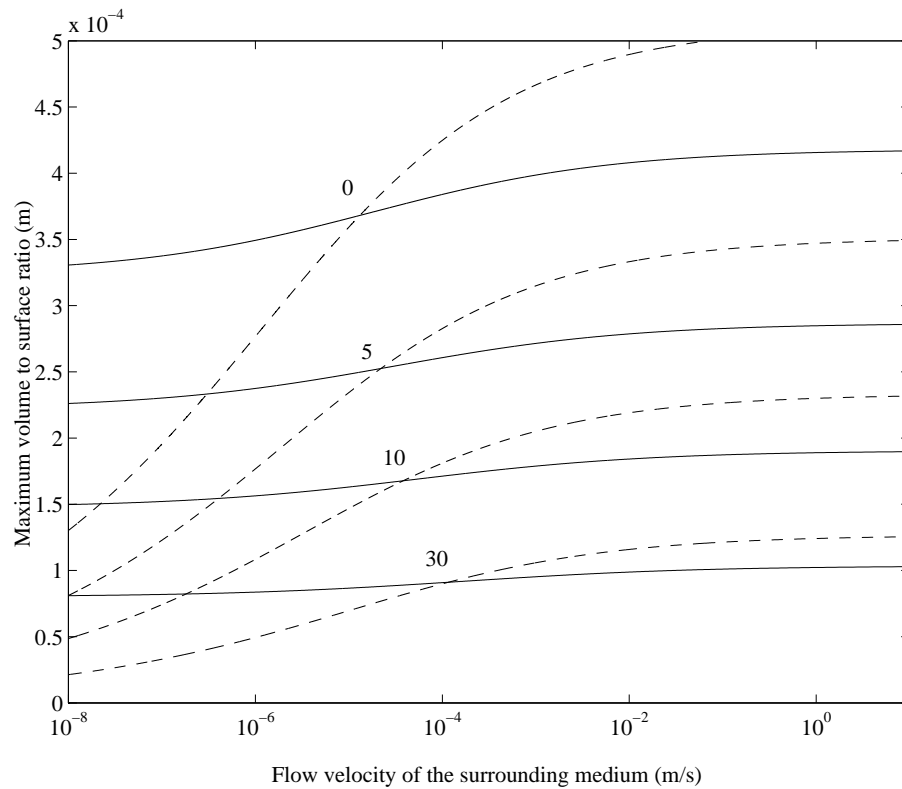


Figure 5.4: Graph of the maximum volume-to-surface-ratio of a cylindrical (dotted lines) and a spherical organism (solid lines) as a function of flow velocity of the surrounding medium (*cf.* Fig. 5.2) and temperature (indicated in °C near the intersection point). The two lines for each temperature are based on Friedlander's equations in Table 5.2. Note the minor effect of temperature on the flow velocity at the intersection point of the lines for a cylinder and sphere.

5.3 Discussion

In our theoretical analysis, we compared oxygen supply to three geometrically simple shapes (sheet, cylinder and sphere). In fact, the analysis of a sheet boils down to the elimination of two out of three dimensions. Oxygen diffuses to a sphere from three dimensions, while a sheet of infinite length and width can be supplied with oxygen from only one dimension (*i.e.* perpendicular to the sheet). In case of the infinite cylinder, one dimension (*i.e.* parallel to the long axis of the cylinder) is excluded. Finite sheets and cylinders will at least partly be supplied with oxygen from less than three dimensions. This is the reason why in stagnant water, a sphere is the most

favorable shape for gas exchange.

In running water ($U > 1$ m/s; Fig. 5.2), the oxygen concentration at the skin surface equals the free water concentration (infinitely thin concentration boundary layer). A given surface area can supply a larger volume of embryonic tissue when arranged in a sheet-like shape. When flow velocity is high, a flattened shape is therefore more favorable for gas exchange. It should be noticed that a large surface area is favorable for gas exchange only if it is available to the underlying tissue. Thin flaps protruding from a body (*e.g.* early finfold of teleosts) cannot serve as a ‘respiratory organ’ unless an integrated oxygen transport system is present to carry away the oxygen and thereby maintaining the oxygen concentration gradient. The maximum volume-to-surface-ratio of a cylindrical organism is intermediate between a sheet-like and a spherical one.

When the flow velocity of the surrounding medium increases from zero to infinity, the advantage of having a larger surface area (sheet) gradually takes over from the advantage of being supplied with oxygen from three dimensions (sphere). In general it can be said that for gas exchange in stagnant water, the sphere is the most favorable shape, while flattening of the body becomes more and more favorable as flow velocity increases.

Since the efficiency (volume of respiring tissue that can be supplied with oxygen per unit surface area) of different shapes with respect to gas exchange appears to reverse with increasing flow velocity, an intermediate flow velocity can be expected where shape does not matter. In order to find this intermediate velocity, we compared the supply of oxygen to a sphere and cylinder in cross flow. Our preference to analyze cross flow instead of parallel flow is based on three arguments. First of all, the analysis of parallel flow would introduce an additional parameter (length of the cylinder) which makes comparison with the sphere rather difficult. Secondly, a symmetrical moving body (at least at Reynolds numbers > 0.1) will take up an orientation with the maximum cross-sectional area normal to the direction of motion (McNown and Malaika, 1950; Vogel, 1994), *i.e.* cross flow. Thirdly, there is a vast amount of empirical data on mass and heat transfer to cylinders and spheres in cross flow. Mass and heat transfer to cylinders in flow parallel to its axis is much less well investigated. Analysis of diffusion and convection in and around other shapes such as ellipsoids and eventually actual embryo shapes would be very interesting. However, such analyses become mathematically extremely difficult and even impossible when

performed analytically. To overcome these limits of analytical mathematics, numerical evaluation of the equations of diffusion and motion in arbitrary three-dimensional shapes are required.

The flow regime, at which shape does not matter, can be defined by analyzing an oxygen consuming point and line (section 5.2.3). This leads to the condition that if flow velocity of the surrounding medium times radius of the model organism is about seven times the diffusion coefficient of oxygen in water, a spherical and cylindrical shape can obtain an equal volume-to-surface-ratio. From the semi-empirical dimensionless number analysis, the analogous proportionality factor is five (instead of seven). In fact, the conditions assumed in the point and line sink analysis are more favorable for the model organism than in the dimensionless number analysis. In the point and line sink analysis, water is allowed to flow inside the artificially introduced boundaries of the model organism (because a point and line are infinitely thin). This enhances oxygen transport and thus it is not surprising that for a specified flow velocity and oxygen diffusion coefficient, the maximum radius calculated from the point and line sink analysis is a little bit larger than that calculated from the semi-empirical analysis.

Despite this small difference, the apparent similarity in the order of magnitude of the results of the analytical and semi-empirical approach suggest that the analysis of point and line sinks can be used to predict the effects of forced convection on maximum volume-to-surface-ratio and optimal shape. At a flow velocity of about 10^{-5} to 10^{-4} m/s and larger, a cylindrical shape can obtain a larger volume-to-surface-ratio than a spherical one (Fig.5.4). Bearing the analysis in section 5.2.1 in mind, this statement holds true for cylindrical shapes with length-radius-ratios larger than about twenty.

Kranenbarg *et al.* (2000) presented a graph of theoretical maximum volume-to-surface-ratios of spherical, cylindrical and sheet-like organisms with continuous refreshment of the oxygen poor boundary layer (Fig. 5.5). The same graph includes the maximum volume-to-surface-ratio of a spherical organism in stagnant water. Actual volume-to-surface-ratios of several teleost embryos are smaller than or equal to the maximum volume-to-surface-ratio of a spherical embryo in stagnant water. This suggests that in stagnant water diffusive oxygen supply is sufficient if the embryos were spherical. However, the theory presented in this paper indicates that deviation from the spherical shape (which is of course the case) would create problems with the oxygen supply if the water were stagnant (at least for the embryos scattered around

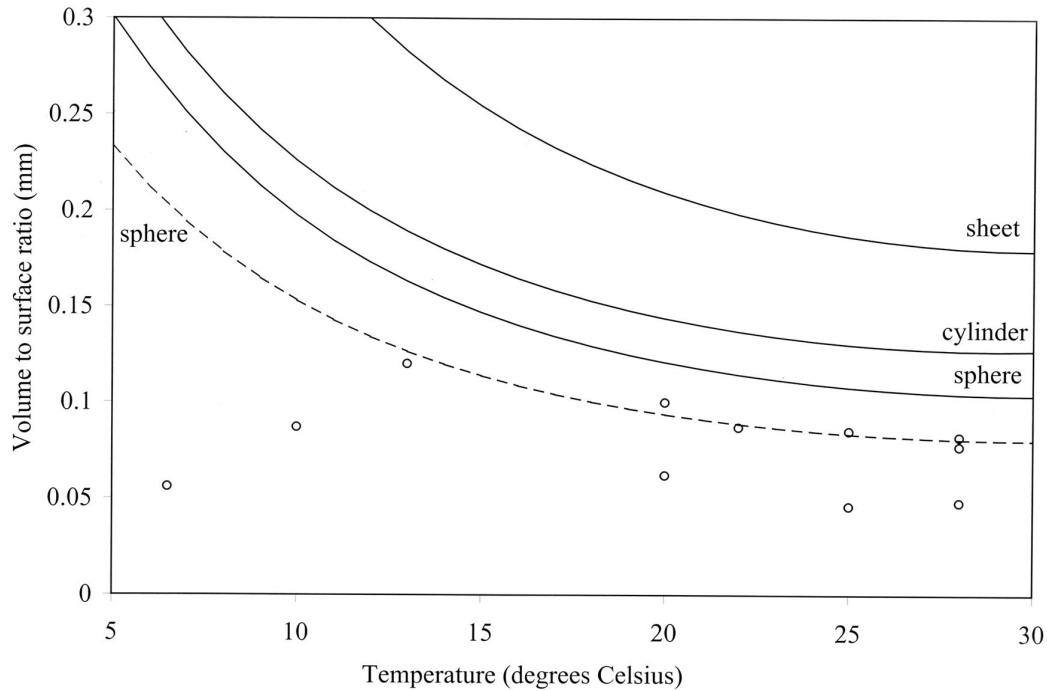


Figure 5.5: Graph of the calculated maximum volume-to-surface-ratios of a spherical, cylindrical and sheetlike organism in a situation of continuous diffusion boundary layer refreshment ('running water') as a function of temperature (solid lines). The dotted line represents the maximum volume-to-surface-ratio for a spherical organism in a completely stagnant medium. The open circles indicate literature data for several teleost embryos (for further explanation, see Kranenbarg *et al.* (2000).

the dotted line in Fig. 5.5).

According to Johnson (1980), measured Reynolds numbers for forced convection over gravel-like substrates vary from 0.1 - 75. For salmonid eggs this suggest a water velocity of 10^{-4} to 10^{-1} m/s (assuming an egg diameter in the order of magnitude of a millimeter). Several marine buoyant teleost eggs rise to the surface with a velocity of typically 1×10^{-3} to 2×10^{-3} m/s (Nakatani and Maeda, 1993; Cambalik *et al.*, 1998). Burggren (1985) found a convective flow inside the egg capsule of the pickerel frog (*Rana palustris*) due to the activity of a ciliated epithelium. The velocities of this convection varied between 1×10^{-4} and 3×10^{-4} m/s. Even in the absence of forced convection, natural convection can generate water velocities around a teleost egg of about 2×10^{-4} m/s on average (O'Brien *et al.*, 1978). Furthermore, the perivitelline

fluid of Atlantic salmon (*Salmo salar*) eggs exchanges within a few minutes with the external medium (Potts and Rudy, 1969). These data suggest that teleost eggs typically develop in a moving external medium, with flow velocities of at least 10^{-4} m/s.

Eggs of teleosts are generally spherical, though elongated eggs also occur; *e.g.* some Gobiidae (Moser, 1996). The embryos at the stage where a circulatory system becomes functional, however, can reasonably accurately be modelled as a finite cylinder of length-radius-ratio of about twenty, although this does not take the actual curvature of the long axis of the embryo into account (Moser, 1996). Fig. 5.2 shows that under the prevalent flow conditions, such a shape is indeed more favorable with respect to diffusive oxygen supply than a more spherical one. And however small, flow velocities of 10^{-4} m/s appear necessary to supply the actual cylindrical embryo with sufficient oxygen. Lower flow velocities would predict maximum volume-to-surface-ratios for the cylindrical embryo below the dotted line in Fig 5.5.

It is conceivable that a sheet-like shape would be even more favorable than a cylindrical one at the prevalent flow velocities, though our model is not suitable to analyze this shape properly. In addition, it is likely that other constraints such as strength and stability would prevent the actual embryo from adopting a sheet-like shape.

Another way of utilizing the high oxygen transfer properties of running water is increasing respiration rate, while the same amount of tissue is to be maintained as in stagnant water. Increase of respiration rate may lead to faster growth and reproduction. According to equations 5.3 and 5.4, running water can supply enough oxygen to an equally sized, but 1.7 times higher respiring animal as compared to an animal in stagnant water. Indeed, it is known that individuals of the freshwater wood louse (*Asellus aquaticus*) that live in fast running water have a respiration rate one and a half times that of individuals living in slowly running water (Hynes, 1970). Although the theory presented in this paper cannot simply be extrapolated to animals with a circulatory system like the freshwater wood louse, the opportunities are clear.

Acknowledgements

J.L.W. Gielen from the subdepartment of mathematics of the Wageningen University is gratefully acknowledged for his contribution to the manuscript. An anonymous referee is thanked for his valuable comments.

Appendix A Abbreviations and units

A	Surface area of the embryo	$[\text{m}^2]$
c	Oxygen concentration	$[\text{kg}/\text{m}^3]$
c_s	Oxygen concentration at the skin surface	$[\text{kg}/\text{m}^3]$
C_∞	Oxygen concentration of the free water	$[\text{kg}/\text{m}^3]$
D_e	Diffusion coefficient of oxygen in embryonic tissues	$[\text{m}^2/\text{s}]$
D_w	Diffusion coefficient of oxygen in water	$[\text{m}^2/\text{s}]$
J	Mass flux of oxygen	$[\text{kg}/\text{s}]$
k	Oxygen transfer coefficient	$[\text{m}/\text{s}]$
m	Volume-specific oxygen consumption	$[\text{kg}/\text{m}^3 \text{ s}]$
r	Distance to the center of the embryo	$[\text{m}]$
R	Radius of the embryo	$[\text{m}]$
t	Time	$[\text{s}]$
t_s	Survival time	$[\text{s}]$
T_c	Temperature	$[\text{°C}]$
U	Flow velocity of the surrounding medium	$[\text{m}/\text{s}]$
V	Volume of embryonic tissue	$[\text{m}^3]$
ν	Kinematic viscosity	$[\text{m}^2/\text{s}]$

Appendix B Dimensionless numbers in convective mass transfer theory

For symbols see appendix A.

name	abbr.	equivalent number in heat transfer	equation	description
Péclet number	Pe		$\frac{2RU}{D_w}$	$\frac{\text{convective mass transfer}}{\text{diffusive mass transfer}}$
Reynolds number	Re		$\frac{2RU}{\nu}$	$\frac{\text{inertia}}{\text{viscosity}}$
Schmidt number	Sc	Prandtl number	$\frac{\nu}{D_w}$	$\frac{\text{kinematic viscosity}}{\text{molecular diffusivity}}$
Sherwood number	Sh	Nusselt number	$\frac{2kR}{D_w}$	$\frac{\text{total mass transfer}}{\text{diffusive mass transfer}}$

Appendix C Temperature dependency of input parameters

Values of constants in the polynomial describing the temperature dependency of three input parameters. Parameter value = $a + bT_c + cT_c^2 + dT_c^3 + eT_c^4$. Furthermore, $D_w = 3.051 \times 10^{-6} e^{-17900/8.314(T_c+273)}$.

	C_∞	m	ν
a	1.455×10^{-2}	2.122×10^{-5}	1.789×10^{-6}
b	-4.052×10^{-4}	9.687×10^{-7}	-5.567×10^{-8}
c	7.831×10^{-6}	7.967×10^{-7}	1.003×10^{-9}
d	-7.207×10^{-8}	-2.772×10^{-9}	-9.310×10^{-12}
e	0	-3.736×10^{-10}	3.355×10^{-14}

Chapter 6

Oxygen Balance for Small Organisms: an Analytical Model¹

An analytical model is developed that describes oxygen transport and oxygen consumption for small biological structures without a circulatory system. Oxygen inside the organism is transported by diffusion alone. Oxygen transfer towards the organism is retarded by a thin static fluid film at the surface of the organism. The thickness of this film models the outward water conditions, which may range from completely stagnant water conditions to so-called well-stirred water conditions. Oxygen consumption is concentration-independent above a specified threshold concentration (regulator behavior) and is proportional to the oxygen concentration below this threshold (conformer behavior). The model takes into account shape and size of the organism and predicts the transition from (pure) regulator behavior to (pure) conformer behavior, as well as the mean oxygen consumption rate. Thereby the model facilitates a proper analysis of the physical constraints set on shape and size of organisms without an active internal oxygen transport mechanism. This analysis is carried out in some detail for six characteristic shapes (infinite sheet, cylinder and beam; finite cylinder, sphere and block). In a well-stirred external medium, a flattened shape appears to be the most favorable for oxygen supply, while a compact shape (cube) is more favorable if the external medium is nearly stagnant. The theoretical framework is applied to oxygen consumption data of eight teleost embryos. This reveals relative insensitivity to external flow conditions in some species (*e.g.* winter flounder, herring) while others appear to rely on external stirring for a proper oxygen supply (*e.g.* largemouth bass). Interestingly, largemouth bass is the only species in our analysis that exhibits ‘fin-fanning’.

¹Gielen, J.L.W. and Kranenbarg, S. (2002). *Bull. Math. Biol.* 64(1), 175-207. Reproduced with permission of the Society for Mathematical Biology.

6.1 Introduction

Molecular diffusion is an important mechanism by which oxygen is transported to respiring biological structures. However, molecular diffusion is only efficient over relatively short distances, or as formulated by Krogh (1941): ‘diffusion alone can provide sufficient oxygen only to organisms of 1mm diameter or less’. Molecular diffusion thus poses a physical constraint on the size and shape of an organism that does not (yet) have an additional way of oxygen transport (Graham, 1988). Mathematical models of oxygen transport may serve to gain quantitative insight in these constraints and the parameters involved.

Models of oxygen flow to biological structures date back to Warburg (1923), Fenn (1927) and Harvey (1928), who modelled steady-state diffusion of oxygen from a well-stirred solution to liver slices, frog nerves and bacteria, respectively. Warburg (1923) and Fenn (1927) calculated maximum diffusion distances, while Harvey (1928) calculated a minimum surface oxygen tension for the bacterium to maintain an adequate respiration. Gerard (1931) extended this model for a varying diffusion constant and oxygen consumption pattern in the sphere. These authors modelled steady-state diffusion of oxygen from a well-stirred solution into a one-dimensional structure (only the radius is a variable shape-factor) under the assumption that volume-specific oxygen consumption is independent of oxygen concentration (regulator behavior).

Strathmann and Chaffee (1984) elaborated on these models to formulate size constraints for invertebrate egg masses, while Lee and Strathmann (1998) included the depletion of oxygen in a boundary layer around a spherical egg or egg-mass. Seymour and Bradford (1987) modelled the effect of an impeding gelatinous capsule on the oxygen delivery to a spherical egg and predicted maximum sizes of amphibian eggs and egg capsules.

Daykin (1965) and Wickett (1975) applied mass transfer theory to oxygen transport to respiring fish eggs. They predicted the bulk flow velocity required for proper egg development. Kranenbarg *et al.* (2000) employed mass transfer theory to predict maximum size and optimal shape of small organisms for any bulk flow velocity.

The assumption of concentration-independent consumption was alleviated by Byatt-Smith *et al.* (1991) in their non steady-state models of oxygen diffusion to mouse and human preimplantation embryos in the absence of stirring. They modelled the volume-specific oxygen consumption of the embryos both as being independent of the oxygen concentration (regulator) and as being directly proportional to the oxygen

concentration (conformer), though both models were mutually exclusive.

This short historical sketch shows three important aspects in models of oxygen transport to small organisms: shape and size of the organism, oxygen consumption pattern of the organism and flow condition of the medium around the organism. In the present paper we incorporate all these aspects of the oxygen transport problem in one analytical model. We represent the actual organism by a region G in space, which determines the size and shape of the organism. Analytical solutions of the resulting formalism for some special one-dimensional cases (infinite sheet, infinite cylinder, sphere) and some higher dimensional cases (infinite beam, rectangular parallelepiped and finite cylinder) are included. The oxygen consumption behavior of our model organism is, in essence, a mixed form of conformer behavior (at low oxygen concentrations) and regulator behavior (at higher oxygen concentrations), as is generally found by experiment (*e.g.* Longmuir (1957)). Pure regulator and pure conformer behavior are included as limiting cases in our model. Convective oxygen transport to the organism is incorporated in our model by the introduction of a thin static fluid film around the organism, through which oxygen is transported (Carslaw and Jaeger, 1959; Rosen, 1952). The thickness of this layer will be translated in a transport coefficient k_{eff} . A well-stirred external medium is represented by a layer of (almost) zero thickness, while more or less stagnant water conditions are represented by a positive thickness of the encapsulating layer, and hence by a finite value for k_{eff} .

With the inclusion of these aspects in our model we are able to make a proper analysis of the constraint oxygen transport sets on the size and shape of organisms that do not have an active internal oxygen transport mechanism.

6.2 The Model

6.2.1 Preliminaries

We wish to describe the stationary oxygen concentration inside a small organism surrounded by water as a function of (1) the shape and size of the organism, (2) the oxygen consumption pattern the organism exhibits, (3) the outside conditions the organism experiences. The organism is modelled as a region G in 3-dimensional space; the surface of the organism is denoted as ∂G . The oxygen concentration inside the organism at place \vec{x} and time t is described by the function $u(\vec{x}, t)$, with $\vec{x} \in G$ and $t > 0$. Then the stationary (equilibrium) oxygen concentration inside the organism

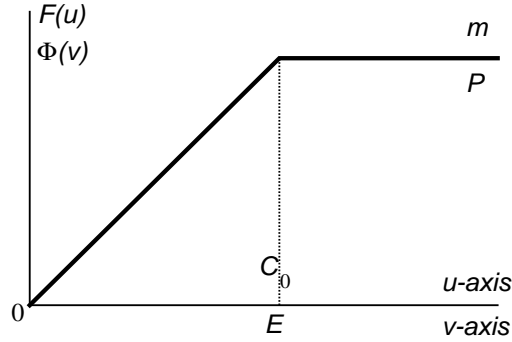


Figure 6.1: The oxygen consumption rate $F(u)$ of the organism (dimensionless: $\Phi(v)$). For $u < C_0$ (dimensionless: $v < E$) there is conformer behavior; for $u > C_0$ (dimensionless: $v > E$) there is regulator behavior. The maximum consumption rate equals m (dimensionless: P).

is given by $u(\vec{x}) = u(\vec{x}, \infty)$, with $\vec{x} \in G$.

Oxygen inside the organism is transported by diffusion; the (constant) diffusion coefficient is denoted as D . It is assumed that barriers to oxygen diffusion and possible movements of the protoplasm or interstitial fluid can be adequately accounted for in the value of this diffusion coefficient (*e.g.* Desaulniers *et al.* (1996); Dowse *et al.* (2000); Krogh (1919)). These authors show that the diffusion coefficient of oxygen in animal tissue is about three times smaller than its value in water.

Furthermore oxygen will be consumed inside the organism. We suppose that the oxygen consumption rate F at place \vec{x} and time t is in the following way a function of the oxygen concentration $u = u(\vec{x}, t)$:

$$F(u) = \begin{cases} m & \text{if } u \geq C_0 \\ mu/C_0 & \text{if } u \leq C_0 \end{cases} \quad (6.1)$$

This assumption implies a uniform oxygen consumption throughout the embryo, while in reality oxygen is consumed by a large number of point sinks, *i.e.* the mitochondria. To reduce mathematical complexity, however, we assume the effect of all these point sinks on the final oxygen distribution to be the same as a uniform oxygen consumption. Preliminary measurements of the oxygen concentration inside a zebrafish (*Danio rerio*) embryo *in vivo* indeed supports this assumption.

The threshold concentration C_0 marks the transition between so-called regulator behavior and conformer behavior. We say the organism exhibits at place \vec{x} and time

t regulator behavior if $u(\vec{x}, t) \geq C_0$. This means that the oxygen concentration is locally sufficiently high for the organism to consume all the oxygen it can use. The consumption rate at such a point will therefore be at its maximum value m . If $u(\vec{x}, t) < C_0$ we say the organism exhibits at place \vec{x} and time t conformer behavior. This means that the oxygen concentration is locally too low to satisfy all the needs of the organism. Accordingly it scales down its consumption to a (constant) fraction of the available oxygen; see Fig. 6.1. Of course the organism as a whole can be in a mixed state: then there is only lack of oxygen and thus conformer behavior in (typically) some small interior part of G , while the outer parts of G still exhibit regulator behavior. We designate an organism as a pure regulator (conformer) if it exhibits regulator (conformer) behavior in all points of G .

It can be expected that the transition from pure regulator behavior to mixed case behavior triggers certain biological modifications in the organism, for instance, the onset of the formation of blood vessels in the oxygen deprived region. Also the transition from mixed case behavior to pure conformer behavior is interesting from a biological point of view: then the organism as a whole experiences oxygen shortage, which may eventually lead to the complete shut-down of certain biological functions inside the organism (Padilla and Roth, 2001). For these reasons we will pay special attention to the parameter values for which these transitions occur.

In general the free water oxygen concentration C_∞ does not equal the oxygen concentration at the surface of the organism. The first reason for this phenomenon stems from the solubility of oxygen in the organism's tissue. With K the (dimensionless) Henry coefficient for oxygen with respect to water and tissue, the oxygen concentration in water directly at the surface ∂G equals $u(\vec{x}, t)/K$. For biological tissue K will generally equal or be close to one. The second reason is found in the formation of a thin static fluid film of water at the surface of the organism (Carslaw and Jaeger, 1959; Rosen, 1952). The average thickness of this layer depends on the water movement around the organism. In more or less stagnant water conditions this film will be relatively thick, while in running water conditions this layer will be practically non-existent. We suppose that oxygen transport through this layer obeys Fick's first law. This leads to the equation:

$$D \frac{\partial}{\partial \vec{n}} u(\vec{x}, t) = k_{\text{eff}} \left[C_\infty - \frac{u(\vec{x}, t)}{K} \right], \quad \text{for } \vec{x} \in \partial G \text{ and } t > 0 \quad (6.2)$$

The so-called mass transfer coefficient $k_{\text{eff}} = D_w/\delta$, where δ represents the (averaged) thickness of the static film and D_w the diffusion coefficient of oxygen in water. In

this way k_{eff} delivers a measure for the thickness of the static layer, and thereby for the outward water conditions. Running water conditions can be characterized by the equation:

$$u(\vec{x}, t) = KC_{\infty}, \quad \text{for } \vec{x} \in \partial G \text{ and } t > 0 \quad (6.3)$$

Because for $k_{\text{eff}} \rightarrow \infty$ equation 6.2 transforms into 6.3, we may say that the case $k_{\text{eff}} = \infty$ represents running water conditions. The value of k_{eff} under (completely) stagnant water conditions will be discussed in Section 6.3.3.

6.2.2 The model equations

The foregoing considerations lead to the following partial differential equation on G and matching boundary condition on ∂G for the oxygen concentration $u(\vec{x}, t)$:

$$\text{PDE: } \frac{\partial}{\partial t} u(\vec{x}, t) = D \Delta_{\vec{x}} u(\vec{x}, t) - F(u(\vec{x}, t)), \quad \text{for } \vec{x} \in G \text{ and } t > 0 \quad (6.4)$$

$$\text{BC: } D \frac{\partial}{\partial \vec{n}} u(\vec{x}, t) + \frac{k_{\text{eff}}}{K} u(\vec{x}, t) = k_{\text{eff}} C_{\infty}, \quad \text{for } \vec{x} \in \partial G \text{ and } t > 0 \quad (6.5)$$

Since the time scale for diffusion equilibrium is very much smaller than the time scale for growth of the organism, we can safely assume diffusion equilibrium at any stage during a growth process. That is why we are, in this paper, mainly interested in the stationary (equilibrium) solution of equations 6.4 and 6.5, which means that an initial condition is not needed.

At this point we introduce in the following way a characteristic length L for the region G :

$$L = V/A \quad \text{with } V = \int_G 1 \, d\omega \quad \text{and } A = \int_{\partial G} 1 \, d\sigma \quad (6.6)$$

So L equals the volume to surface area ratio of the organism, which is in the present context a meaningful notion indeed, as it represents the volume of respiring tissue to be supplied with oxygen per unit surface area (Kranenbarg *et al.*, 2000).

Next we introduce, with the help of this characteristic length L , the following dimensionless parameters:

$$\begin{aligned} \vec{\xi} &= \vec{x}/L && \text{dimensionless place co-ordinates} \\ \tau &= Dt/L^2 && \text{dimensionless time} \\ v(\vec{\xi}, \tau) &= u(\vec{x}, t)/C_{\infty} && \text{dimensionless concentration} \end{aligned} \quad (6.7)$$

The co-ordinate transformation $\vec{x} \rightarrow \vec{\xi}$ is a simple contraction with its center in the origin, and transforms the region G into a unique ‘standard’ region G' with the same shape as G , but with a (dimensionless) volume to surface area ratio equal to one. Note that the (dimensionless) time scale τ obtained on G' depends on the size of G .

With the help of equation 6.7 we deduce in a straightforward way the following dimensionless forms for 6.4 and 6.5:

$$\text{PDE: } \frac{\partial}{\partial \tau} v(\vec{\xi}, \tau) = \Delta_{\vec{\xi}} v(\vec{\xi}, \tau) - \Phi(v(\vec{\xi}, \tau)) \quad \text{for } \vec{\xi} \in G' \text{ and } \tau > 0 \quad (6.8)$$

$$\text{BC: } \frac{\partial}{\partial \vec{n}'} v(\vec{\xi}, \tau) + \frac{Q}{K} v(\vec{\xi}, \tau) = Q \quad \text{for } \vec{\xi} \in \partial G' \text{ and } \tau > 0 \quad (6.9)$$

Here the dimensionless consumption rate Φ is defined as (see Fig. 6.1):

$$\Phi(v) = \begin{cases} P & \text{if } v \geq E \\ Pv/E & \text{if } v \leq E \end{cases} \quad (6.10)$$

and the dimensionless parameters P , Q and E are given by:

$$\begin{aligned} P &= m L^2 / (D C_{\infty}) && \text{dimensionless maximum consumption rate} \\ Q &= k_{\text{eff}} L / D && \text{dimensionless mass transfer coefficient} \\ E &= C_0 / C_{\infty} && \text{dimensionless threshold concentration} \end{aligned} \quad (6.11)$$

In this way we have reduced the parameter set D [$\text{m}^2 \text{s}^{-1}$], m [$\text{kg m}^{-3} \text{s}^{-1}$], C_0 [kg m^{-3}], C_{∞} [kg m^{-3}], k_{eff} [m s^{-1}], L [m] and K to the dimensionless parameter set P , Q , E and K ; also the region G is transformed into a matching standard region G' .

As already said before in this paper we are mainly interested in the stationary (equilibrium) state of the organism. From equations 6.8 and 6.9 we infer for the dimensionless equilibrium concentration $v(\vec{\xi}) = v(\vec{\xi}, \infty)$ the following boundary value problem:

$$\text{PDE: } \Delta_{\vec{\xi}} v(\vec{\xi}) - \Phi(v(\vec{\xi})) = 0 \quad \text{for } \vec{\xi} \in G' \quad (6.12)$$

$$\text{BC: } \frac{\partial}{\partial \vec{n}'} v(\vec{\xi}) + \frac{Q}{K} v(\vec{\xi}) = Q \quad \text{for } \vec{\xi} \in \partial G' \quad (6.13)$$

From this equilibrium concentration $v(\vec{\xi})$ on G' we retrieve with the help of equation 6.7 the original equilibrium concentration $u(\vec{x})$ on G . Now we can divide G into two parts: $G = G_{\text{reg}} \cup G_{\text{conf}}$, with $G_{\text{reg}} = \{\vec{x} \in G \mid u(\vec{x}) \geq C_0\}$ and $G_{\text{conf}} = \{\vec{x} \in G \mid u(\vec{x}) \leq C_0\}$. On G_{reg} the organism exhibits regulator behavior; and on G_{conf} there is conformer behavior. Roughly speaking, we expect ‘unimpeded growth’ on G_{reg} and we expect ‘adaptive behavior’ on G_{conf} .

Table 6.1: Parameter values for eight teleost embryos. To the left: L , volume to surface area ratio [m]; m , maximum consumption rate [$\text{kg m}^{-3} \text{s}^{-1}$]; D , diffusion coefficient [$\text{m}^2 \text{s}^{-1}$]; C_∞ , free water oxygen concentration [kg m^{-3}]. The mass transfer coefficient $k_{\text{eff}} = 3.00 \times 10^{-5} \text{ m s}^{-1}$ for all eight embryos. To the right: P , dimensionless consumption rate; Q , dimensionless mass transfer coefficient. The dimensionless parameters S and T are defined in Section 6.5.

	L	m	D	C_∞	P	Q	S	T
	$\times 10^{-5}$	$\times 10^{-4}$	$\times 10^{-10}$	$\times 10^{-3}$				
African catfish <i>Clarias gariepinus</i>	8.50	3.80	7.41	8.19	0.45	3.44	5.12	0.67
Common carp <i>Cyprinus carpio</i>	6.20	11.0	6.55	9.00	0.72	2.84	3.35	0.85
Herring <i>Clupea harengus</i>	12.0	.430	5.47	10.5	0.11	6.58	20.0	0.33
Largemouth bass <i>Micropterus salmoides</i>	10.0	3.70	6.55	9.00	0.63	4.58	5.78	0.79
Plaice <i>Pleuronectes platessa</i>	8.70	1.70	5.05	11.2	0.23	5.17	10.8	0.48
Rabbitfish <i>Siganus randalli</i>	4.80	2.80	7.96	7.76	0.10	1.81	5.60	0.32
Winter flounder <i>Pseudopleuronectes americanus</i>	5.60	4.80	4.59	12.2	0.03	3.66	22.3	0.38
Zebrafish <i>Danio rerio</i>	4.60	4.10	7.41	8.19	0.14	1.86	4.93	0.38

To exemplify the presented theory, we used the oxygen dynamics data from Kraenbarg *et al.* (2000) for eight teleost embryos to calculate the corresponding values of the dimensionless parameters used in this paper. These embryos do not have a circulatory system yet and are therefore dependent on diffusion for their internal oxygen supply. The value of the mass transfer coefficient was chosen to represent a bulk flow velocity ranging from $10^{-4} - 10^{-3} \text{ m s}^{-1}$, which is the minimum convection velocity found in natural situations. For this purpose we used the relation between mass transfer coefficient and bulk flow velocity for a spherical particle given by Clift *et al.* (1978). The value for the threshold concentration was obtained from Longmuir (1957). Both the mass transfer coefficient and the threshold concentration were chosen to be equal for all eight embryos: $k_{\text{eff}} = 3.00 \times 10^{-5} \text{ m s}^{-1}$ and $C_0 = 6.40 \times 10^{-5} \text{ kg}$

m^{-3} . This means $E \approx 0.01$; to be complete: for the (dimensionless) Henry coefficient K the value 1 is chosen. Table 6.1 shows the result.

6.2.3 Critical points and mean consumption rate

The equilibrium concentration profile $v(\vec{\xi})$ predicted by 6.12 and 6.13 for an organism of shape G' depends of course on the actual parameter values P , Q , E , and K . Also the minimum and maximum values v_{\min} and v_{\max} which $v(\vec{\xi})$ takes on G' are functions of these parameters. For a given type G' we define in the associated (four-dimensional) parameter space two so-called critical (hyper-)surfaces S_{reg} and S_{conf} by their respective equations:

$$\begin{aligned} S_{\text{reg}} : \quad v_{\min}(P, Q, E, K) &= E \\ S_{\text{conf}} : \quad v_{\max}(P, Q, E, K) &= E \end{aligned} \tag{6.14}$$

Surfaces S_{reg} and S_{conf} divide parameter space in three parts. For $v_{\min}(P, Q, E, K) \geq E$ the organism is a (pure) regulator: $G = G_{\text{reg}}$. For $v_{\max}(P, Q, E, K) \leq E$ the organism is a (pure) conformer: $G = G_{\text{conf}}$. For all other cases the organism is in a mixed state.

If we vary (in some continuous way) the parameters of the model, the result will be a trajectory in parameter space. A point of intersection of such a trajectory with S_{reg} or S_{conf} we call a critical point: in passing one of these surfaces we expect an essential change in the behavior of the organism.

For instance, it is to be expected that most of the parameters of our model are a function of the ambient temperature T . Thus, for a (slowly) varying temperature T the organism follows a trajectory $\langle P(T), Q(T), E(T), K(T) \rangle$ in parameter space. A critical temperature arises whenever this trajectory crosses a critical surface.

One more example: because we are particularly interested in how the size of an organism affects its equilibrium state, it is worthwhile noting that if we multiply the size of G by κ , P changes into $P\kappa^2$, Q into $Q\kappa$ (and, to be complete, τ into τ/κ). Therefore, points in parameter space representing different sizes of the organism, all other circumstances unchanged, are to be found on a simple parabola parallel with the PQ -plane. A critical size for an organism corresponds with a point of intersection of this parabola and S_{reg} or S_{conf} .

Another measurable quantity predicted by our model is the mean (oxygen) consumption rate γ , that is the consumption rate per unit of volume:

$$\gamma = \frac{1}{V} \int_G F(u(\vec{x})) \, d\omega = \frac{D}{V} \int_{\partial G} \frac{\partial}{\partial \vec{n}} u(\vec{x}) \, d\sigma \tag{6.15}$$

With dimensionless volume $V' = \int_{G'} 1 \, d\omega'$ and dimensionless surface area $A' = \int_{\partial G'} 1 \, d\sigma'$ (remember: $V'/A' = 1$) the corresponding dimensionless mean consumption rate Γ is given by:

$$\Gamma = \frac{1}{V'} \int_{G'} \Phi(v(\vec{\xi})) \, d\omega' = \frac{1}{A'} \int_{\partial G'} \frac{\partial}{\partial \vec{n}'} v(\vec{\xi}) \, d\sigma' \quad (6.16)$$

which means that Γ also equals the mean dimensionless surface flux. The relation between γ and Γ is given by the equality: $\gamma t = \Gamma \tau C_\infty$.

Of course Γ is a function of the model parameters P, Q, E, K , but Γ also depends on the type G' of the organism under consideration. For a pure regulator we have of course $\Gamma = P$; for other cases we can use Γ to determine what shape of an organism is a more favorable one (that is, admits a higher value for Γ , or, allows a better overall respiration), given all other circumstances are the same (see Fig. 6.3 b).

6.3 One-dimensional Cases

In this section we demonstrate the principles set out in the previous section for three simple cases: the infinite sheet, the infinite cylinder and the sphere. At first glance an organism in the form of an infinite sheet or an infinite cylinder seems strange. But firstly, we need only a perpendicular cross-section of such a sheet or cylinder; the resulting extra surface we render ineffective by taking there a homogeneous boundary condition of the second kind (a no-flow boundary condition). And secondly, later on we will see that the case of a (thin) finite sheet or a (long) finite cylinder may be readily approximated by the corresponding infinite case.

The common feature of these three cases is their inherent symmetry, which allows for the use of only one place variable: all three cases are effectively one-dimensional. Consequently, for all these cases 6.12 and 6.13 reduce to simple ordinary differential equations with matching boundary conditions. The case of the infinite sheet we will discuss in some detail. For the infinite cylinder and the sphere we will only give the final results.

6.3.1 The infinite sheet

The volume to surface area ratio for (any perpendicular cross-section of) a plane infinite sheet with diameter $2R$ equals R . Therefore the (dimensionless) diameter of the ‘standard’ infinite sheet equals 2. Hence we may reduce 6.12 and 6.13 to the

following boundary value problem on $[0, 1]$:

$$\text{ODE: } \frac{\partial^2}{\partial \xi^2} v(\xi) - \Phi(v(\xi)) = 0 \quad \text{for } 0 < \xi < 1 \quad (6.17)$$

$$\text{BC}_1: \frac{\partial}{\partial \xi} v(0) = 0, \quad \text{BC}_2: \frac{\partial}{\partial \xi} v(1) + \frac{Q}{K} v(1) = Q \quad (6.18)$$

This boundary value problem is easily solved for the (pure) regulator or (pure) conformer case. The regulator case occurs if (and only if) $v(0) \geq E$. Now $\Phi(v) = P$ and it follows that

$$v(\xi) = \frac{P}{2} \xi^2 + K - \frac{KP}{Q} - \frac{P}{2} \quad (6.19)$$

The conformer case occurs if (and only if) $v(1) \leq E$. Now $\Phi(v) = Pv/E$ and it follows that

$$v(\xi) = \frac{KQ \cosh(\xi \sqrt{P/E})}{K \sqrt{P/E} \sinh(\sqrt{P/E}) + Q \cosh(\sqrt{P/E})} \quad (6.20)$$

Expressions for the critical surfaces follow already from equations 6.19 and 6.20:

$$S_{\text{reg}} : (K - E)Q = KP + PQ/2 \quad (6.21)$$

$$S_{\text{conf}} : (K - E)Q = KE \sqrt{P/E} \tanh(\sqrt{P/E}) \quad (6.22)$$

For a mixed case there will be, for some ρ between 0 and 1, conformer behavior on $[0, \rho]$ and regulator behavior on $[\rho, 1]$. By means of the (continuity) conditions

$$\lim_{\xi \uparrow \rho} v(\xi) = E, \quad \lim_{\xi \downarrow \rho} v(\xi) = E, \quad \text{and} \quad \lim_{\xi \uparrow \rho} \frac{\partial}{\partial \xi} v(\xi) = \lim_{\xi \downarrow \rho} \frac{\partial}{\partial \xi} v(\xi) \quad (6.23)$$

we find for $0 \leq \xi \leq \rho$:

$$v(\xi) = E \frac{\cosh(\xi \sqrt{P/E})}{\cosh(\rho \sqrt{P/E})} \quad (6.24)$$

and for $\rho \leq \xi \leq 1$:

$$v(\xi) = \frac{P}{2} \xi^2 + \frac{2(K - E)Q - 2KP - PQ(1 - \rho^2)}{2K + 2Q(1 - \rho)} (\xi - 1 - \frac{K}{Q}) + K - \frac{KP}{Q} - \frac{P}{2} \quad (6.25)$$

with ρ the (unique) root between 0 and 1 of the following transcendental equation:

$$E \sqrt{P/E} \tanh(\rho \sqrt{P/E}) = \frac{2(K - E)Q - 2KP(1 - \rho) - PQ(1 - \rho)^2}{2K + 2Q(1 - \rho)} \quad (6.26)$$

Obviously we should give ρ the value 0 for a (pure) regulator, while for a (pure) conformer ρ should get the value 1. Then, as expected, equation 6.26 reduces for $\rho = 0$ to 6.21 and for $\rho = 1$ to 6.22.

The dimensionless mean consumption rate Γ follows from 6.16. For this simple one-dimensional case it holds that

$$\Gamma = \frac{\partial}{\partial \xi} v(1) \quad (6.27)$$

Hence from equations 6.19, 6.20 and 6.25 we infer, respectively:

$$\Gamma = P \quad \text{for a regulator} \quad (6.28)$$

$$\Gamma = \frac{KQ}{K + Q\sqrt{E/P} \coth(\sqrt{P/E})} \quad \text{for a conformer} \quad (6.29)$$

$$\Gamma = \frac{2(K - E)Q + PQ(1 - \rho)^2}{2K + 2Q(1 - \rho)} \quad \text{for a mixed case} \quad (6.30)$$

The result for a regulator is, of course, not a surprise: it follows also from first principles or, for that matter, from 6.16. Note that equation 6.30 on S_{reg} reduces to 6.28 and on S_{conf} to 6.29.

6.3.2 The infinite cylinder and the sphere

The case of the infinite cylinder and the sphere can be treated in exactly the same way. For that reason we mention in this subsection only the relevant model equations and their most important consequences.

First we discuss the case of the infinite cylinder. The (dimensionless) radius of the ‘standard’ infinite cylinder equals 2; therefore we have to solve the following boundary value problem on $[0, 2]$:

$$\text{ODE: } \frac{1}{\xi} \frac{\partial}{\partial \xi} \left[\xi \frac{\partial}{\partial \xi} v(\xi) \right] - \Phi(v(\xi)) = 0 \quad \text{for } 0 < \xi < 2 \quad (6.31)$$

$$\text{BC}_1: \lim_{\xi \rightarrow 0} \xi \frac{\partial}{\partial \xi} v(\xi) = 0, \quad \text{BC}_2: \frac{\partial}{\partial \xi} v(2) + \frac{Q}{K} v(2) = Q \quad (6.32)$$

The expressions for the critical surfaces are:

$$S_{\text{reg}}: (K - E)Q = KP + PQ \quad (6.33)$$

$$S_{\text{conf}}: (K - E)Q = KE\sqrt{P/E} \, \text{I}_1(2\sqrt{P/E})/\text{I}_0(2\sqrt{P/E}) \quad (6.34)$$

where I_0 and I_1 are modified Bessel functions (Abramowitz and Stegun, 1965). The transcendental equation for the radius ρ of the region with conformer behavior reads:

$$E\sqrt{P/E} \frac{I_1(\rho\sqrt{P/E})}{I_0(\rho\sqrt{P/E})} = \frac{2(K-E)Q - 2(PQ + KP)(1 - \rho^2/4) - PQ\rho^2 \ln(\rho/2)}{K\rho - 2Q\rho \ln(\rho/2)} \quad (6.35)$$

This time ρ should get the value 2 for a (pure) conformer. As expected, equation 6.35 reduces for $\rho = 0$ to 6.33 and for $\rho = 2$ to 6.34.

The (dimensionless) mean consumption rate Γ for this case is given by:

$$\Gamma = P \quad \text{for a regulator} \quad (6.36)$$

$$\Gamma = \frac{KQ\sqrt{P/E} I_1(2\sqrt{P/E})}{K\sqrt{P/E} I_1(2\sqrt{P/E}) + Q I_0(2\sqrt{P/E})} \quad \text{for a conformer} \quad (6.37)$$

$$\Gamma = \frac{(K-E)Q - PQ(1 - \rho^2/4) - 2PQ \ln(\rho/2)}{K - 2Q \ln(\rho/2)} \quad \text{for a mixed case} \quad (6.38)$$

Note again that equation 6.38 reduces on S_{reg} to 6.36 and on S_{conf} to 6.37.

Next we discuss the case of a spherical organism. The (dimensionless) radius of the ‘standard’ sphere equals 3; therefore we have to solve the following boundary value problem on $[0, 3]$:

$$\text{ODE: } \frac{1}{\xi^2} \frac{\partial}{\partial \xi} [\xi^2 \frac{\partial}{\partial \xi} v(\xi)] - \Phi(v(\xi)) = 0 \quad \text{for } 0 < \xi < 3 \quad (6.39)$$

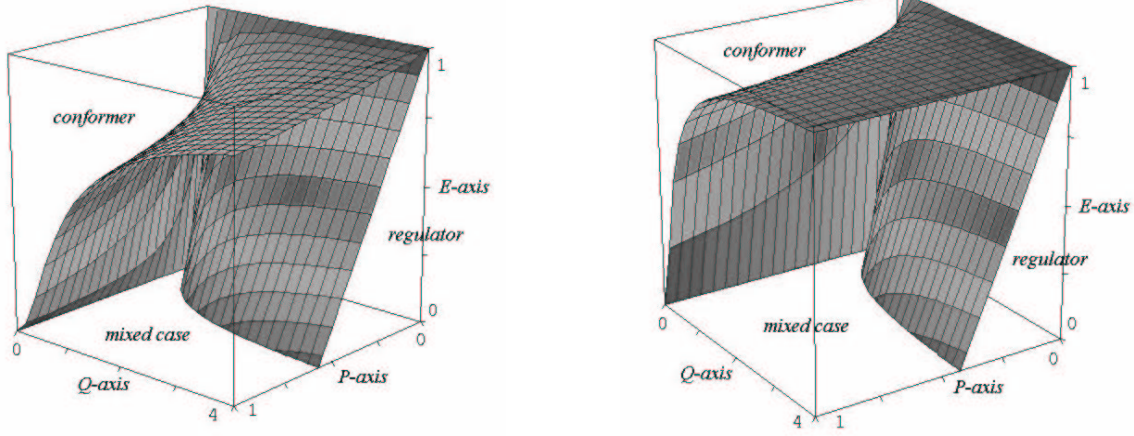
$$\text{BC}_1: \lim_{\xi \rightarrow 0} \xi^2 \frac{\partial}{\partial \xi} v(\xi) = 0, \quad \text{BC}_2: \frac{\partial}{\partial \xi} v(3) + \frac{Q}{K} v(3) = Q \quad (6.40)$$

The expressions for the critical surfaces (see Fig. 6.2 a) are:

$$S_{\text{reg}}: (K-E)Q = KP + 3PQ/2 \quad (6.41)$$

$$S_{\text{conf}}: (K-E)Q = KE(\sqrt{P/E} \coth(3\sqrt{P/E}) - 1/3) \quad (6.42)$$

Comparison of the values for P and Q in Table 6.1 with Fig. 6.2 shows, as follows from 6.41, that for the chosen values of E (≈ 0.01) and K ($= 1$), zebrafish, rabbitfish, winter flounder, plaice and herring are clearly in the regulator area (in both the sphere and the cube model). Common carp and largemouth bass are in the mixed case area. African catfish enters the mixed case area when going from the sphere to the cube model.



(a) Critical surfaces for the sphere.

(b) Critical surfaces for the cube.

Figure 6.2: For $K = 1$: the critical surfaces S_{reg} and S_{conf} divide the reduced parameter space $\langle P, Q, E, 1 \rangle$ into three parts: the regulator domain (oxygen deficiency nowhere in the organism), the mixed domain (oxygen deficiency somewhere in the organism), the conformer domain (oxygen deficiency everywhere in the organism). For differently shaped organisms the picture is essentially the same.

The transcendental equation for the radius ρ of the region with conformer behavior is given by:

$$E(\rho\sqrt{P/E} \coth(\rho\sqrt{P/E}) - 1) = \frac{9(K-E)Q - 9KP(1 - \rho^3/27) - 9PQ(1 - \rho/3)^2(\rho + 3/2)}{K\rho + 3Q(3 - \rho)} \quad (6.43)$$

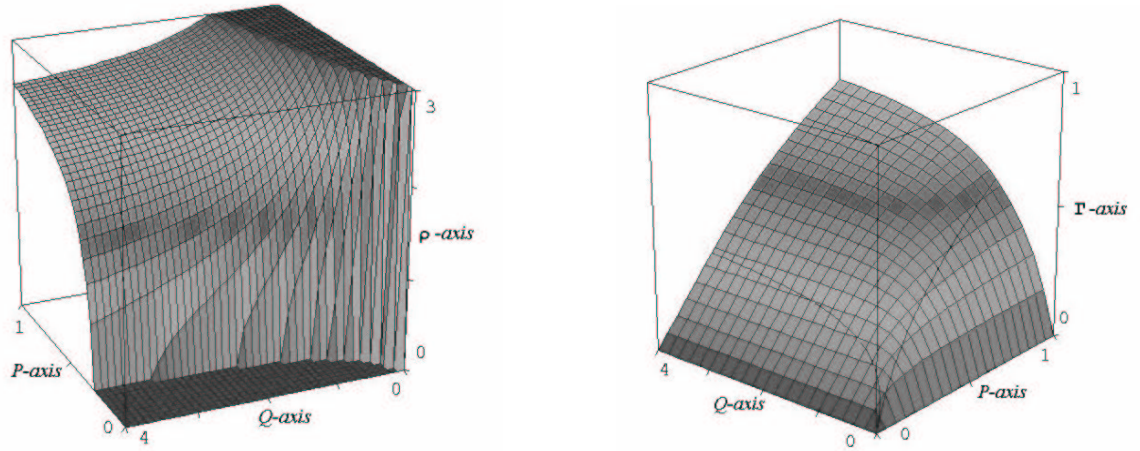
For this case ρ should get the value 3 for a (pure) conformer; see Fig. 6.3 a. Again, equation 6.43 reduces for $\rho = 0$ to 6.41 and for $\rho = 3$ to 6.42. Finally, the (dimensionless) mean consumption rate Γ is given by:

$$\Gamma = P \quad \text{for a regulator} \quad (6.44)$$

$$\Gamma = \frac{KQ(\sqrt{P/E} \coth(3\sqrt{P/E}) - 1/3)}{K(\sqrt{P/E} \coth(3\sqrt{P/E}) - 1/3) + Q} \quad \text{for a conformer} \quad (6.45)$$

$$\Gamma = \frac{(K-E)Q\rho + 9PQ(1 - \rho/3)^2(1 + \rho/6)}{K\rho + 9Q(1 - \rho/3)} \quad \text{for a mixed case} \quad (6.46)$$

see Fig. 6.3 b. Again, equation 6.46 reduces to 6.44 on S_{reg} and reduces to 6.45 on S_{conf} .



(a) The dimensionless radius ρ of the region with oxygen deficiency.

(b) The dimensionless mean consumption rate Γ .

Figure 6.3: For the sphere and for $K = 1$, $E = \frac{1}{2}$. (a) The radius ρ of the region with conformer behavior as a function of the dimensionless maximum consumption rate P and the dimensionless mass transfer coefficient Q . For a pure regulator $\rho = 0$; for a pure conformer $\rho = 3$. (b) The dimensionless mean consumption rate Γ as a function of the dimensionless maximum consumption rate P and the dimensionless mass transfer coefficient Q . The two extra curves on the surface separate pure regulator behavior from mixed case behavior and mixed case behavior from pure conformer behavior.

6.3.3 Limit cases and critical sizes

Several interesting special cases are neatly incorporated in our formalism. We discuss these cases mainly for an infinite sheet. It is easily verified that analogous results can be achieved for the infinite cylinder and for the sphere, or even for arbitrarily shaped organisms.

(1) In the literature (Byatt-Smith *et al.*, 1991) the term conformer is used if the oxygen consumption rate F the organism exhibits, is modelled by a linear function: $F(u) = au$ (in dimensionless form: $\Phi(v) = pv$), while the term regulator is used if F is modelled by a constant function: $F(u) = m$ (in dimensionless form: $\Phi(v) = P$).

The first of these two special cases is represented within our model by the condition $E \geq K$. Because K obviously is an upper limit for the dimensionless oxygen

concentration v inside the organism, the condition $E \geq K$ compels conformer behavior everywhere in the organism's interior, independent of all other parameter values. We could introduce for this case the new (dimensionless) variable $p = P/E$, thereby removing one parameter from our model (note the occurrence of the term P/E in 6.20 and 6.29). The model equations for this case are linear: now even the time-dependent equations are easily solvable.

The second special case is represented within our model by the condition $E = 0$. It should be noted that this case still leaves open the possibility of conformer behavior somewhere in the organism. Conformer behavior in this case just means that the oxygen concentration v in part of the organism is equal to zero, see equation 6.24. The transition from pure regulator behavior to partial conformer behavior is still given by 6.21. Even pure conformer behavior is possible for this case: this also happens if $Q = 0$, as follows from 6.22. Because $Q = 0$ stands for a homogeneous boundary condition of the second kind (a no-flow boundary condition), this is as expected. For $E = 0$ the transcendental equation 6.26 for the 'radius' ρ of the region with conformer behavior reduces to a simple quadratic equation. So for this special case it follows from 6.26 and 6.30 that the dimensionless consumption rate $\Gamma = P(1 - \rho)$, which for this simple case also follows from first principles.

(2) That leaves the case $0 < E < K$. Now all three behavioral patterns are possible: the organism may be a pure regulator, or may be in a mixed state, or may be a pure conformer. The critical surfaces S_{reg} and S_{conf} separate these three possibilities in parameter space; see Fig. 6.2.

As already said before the limiting case $Q = \infty$, that is $k_{\text{eff}} = \infty$, is tied in with so-called running water conditions, or well-stirred water conditions (Carslaw and Jaeger, 1959; Kranenbarg *et al.*, 2000). For this special case the second boundary condition (6.18 b) changes into a simple boundary condition of the first kind, BC_2 : $v(1) = K$. The expressions for the critical surfaces, given by 6.21 and 6.22, simplify to S_{reg} : $K - E = P/2$ and S_{conf} : $K - E = 0$; therefore pure conformer behavior is impossible for this limit case (unless $E \geq K$).

(3) Special attention is often devoted to that size of a (slowly growing) organism, for which it first encounters, somewhere in its interior, oxygen deficiency. Such a size is called a critical size. Because oxygen is needed to perform essential biological processes, natural selection will favor organisms that prevent oxygen deficiency in

their interior. These organisms can either stay of subcritical size or develop an additional oxygen transport system (*e.g.* a circulatory system) by the time they reach their critical size. Within our model oxygen deficiency starts when the representation $\langle P, Q, E, K \rangle$ of this organism in parameter space passes the critical surface S_{reg} . Therefore, as follows from equations 6.21, 6.33 and 6.41, for such a critical point it holds that

$$(K - E)Q = KP + nPQ/2 \quad (6.47)$$

where it is understood that n takes the value 1 for an infinite sheet, 2 for an infinite cylinder and 3 for a sphere. We divide equation 6.47 by Q , rewrite the result with the help of 6.11 in terms of the original model parameters, to find, after some rearrangements:

$$\frac{n}{2}L^2 + \frac{KD}{k_{\text{eff}}}L - \frac{D}{m}(KC_{\infty} - C_0) = 0 \quad (6.48)$$

Hence for the critical value of the volume to surface area ratio we obtain:

$$L_{\text{crit}} = -\frac{KD}{nk_{\text{eff}}} + \sqrt{\frac{K^2D^2}{n^2k_{\text{eff}}^2} + \frac{2D}{nm}(KC_{\infty} - C_0)} \quad (6.49)$$

Note that L_{crit} represents the maximum volume of respiring tissue that can be fully supplied with oxygen per unit surface area. With R_{crit} the critical radius (half the diameter) of the object under consideration, it follows from the relation $L = V/A = R/n$ that

$$R_{\text{crit}} = -\frac{KD}{k_{\text{eff}}} + \frac{KD}{k_{\text{eff}}} \sqrt{1 + 2n \frac{k_{\text{eff}}^2}{mKD} (C_{\infty} - \frac{C_0}{K})} \quad (6.50)$$

The special case $C_0 = 0$, $K = 1$ and $k_{\text{eff}} = \infty$ yields

$$R_{\text{crit}} = \sqrt{2n \frac{DC_{\infty}}{m}} \quad (6.51)$$

a well-known result (*e.g.* Graham (1988)). Note that it is possible to determine in exactly the same way critical values for other model parameters.

(4) One more interesting limit case arises when we take the thickness δ of the static fluid film that surrounds the organism to infinity. This situation can be simulated in the laboratory by placing one small organism at the center of a large water-filled tank. For an infinite sheet and an infinite cylinder taking δ to infinity means that

k_{eff} goes to zero. The reason for this is the non-existence of a stationary solution for the diffusion problem outside the organism for these two shapes. For a sphere-like organism, say with radius R , such an external stationary solution does exist: $u_{\text{ex}}(x) = C_{\infty} + (u(R)/K - C_{\infty})R/x$, with $x > R$ the distance from the center of the sphere. It follows that k_{eff} takes the value $D_w/R = D_w/(3L)$, with D_w again the diffusion coefficient of oxygen in water. Substituting this value for k_{eff} in 6.48, we obtain:

$$\left(\frac{3}{2} + \frac{3KD}{D_w}\right) L^2 - \frac{D}{m} (KC_{\infty} - C_0) = 0 \quad (6.52)$$

So the critical value of the volume to surface area ratio for this case is:

$$L_{\text{crit}} = \sqrt{\frac{2D_w D (KC_{\infty} - C_0)}{3m(D_w + 2KD)}} \quad (6.53)$$

The special case $C_0 = 0$ and $K = 1$ yields:

$$L_{\text{crit}} = \sqrt{\frac{2D_w DC_{\infty}}{3m(D_w + 2D)}} \quad (6.54)$$

also a well-known result (*e.g.* Lee and Strathmann (1998)).

(5) Finally we discuss the question: what happens at the critical surface S_{conf} ? Will a growing organism, beyond its critical size, eventually change into a pure conformer, or will it always remain in a mixed state? For the infinite sheet this question is answered by means of equation 6.22. Rewriting this equation in terms of the original model parameters, see 6.11, we obtain after some rearrangements:

$$k_{\text{eff}}(C_{\infty} - \frac{C_0}{K}) = \sqrt{mDC_0} \tanh\left(L\sqrt{\frac{m}{DC_0}}\right) \quad (6.55)$$

Therefore, if it holds that

$$k_{\text{eff}}(C_{\infty} - \frac{C_0}{K}) \geq \sqrt{mDC_0} \quad (6.56)$$

a growing organism of this shape will always retain a region with regulator behavior, which is the case for all eight teleost embryos in Table 6.1. A simple inspection of the right-hand side of equations 6.34 and 6.42 shows that the same condition applies for an infinite cylinder and for a sphere.

We will show that this condition also holds for an organism of arbitrary shape. With that goal in mind we put a given point on a smooth part of the surface ∂G of

the organism under a magnifying-glass: in this way we interpret the organism in the neighborhood of this point as a (left) half-space. Then, assuming that the organism is a pure conformer, the following initial value problem describes the tendency of the system in the neighborhood of this point, see equations 6.8 and 6.9:

$$\text{PDE: } \frac{\partial}{\partial \tau} v(\xi, \tau) = \frac{\partial^2}{\partial \xi^2} v(\xi, \tau) - \frac{P}{E} v(\xi, \tau) \quad \text{for } \xi < 0 \text{ and } \tau > 0 \quad (6.57)$$

$$\text{BC: } \frac{\partial}{\partial \xi} v(0, \tau) + \frac{Q}{K} v(0, \tau) = Q, \quad \text{IC: } v(\xi, 0) = v_0 \quad (6.58)$$

Next we apply the Laplace transformation: $v(\xi, \tau) \rightarrow V(\xi, s)$. A straightforward calculation yields:

$$V(\xi, s) = \frac{v_0}{s + P/E} + \left(\frac{Q}{s} - \frac{v_0 Q/K}{s + P/E} \right) \frac{\exp(\xi \sqrt{s + P/E})}{Q/K + \sqrt{s + P/E}} \quad (6.59)$$

It follows:

$$\lim_{\tau \rightarrow \infty} v(0, \tau) = \lim_{s \downarrow 0} sV(0, s) = \frac{Q}{Q/K + \sqrt{P/E}} \quad (6.60)$$

Thus a condition for regulator behavior in the neighborhood of this point is:

$$\frac{Q}{Q/K + \sqrt{P/E}} \geq E \quad (6.61)$$

If we rewrite this result with the help of 6.11 in terms of the original model parameters, we retrieve equation 6.56.

6.4 Higher Dimensional Cases

In Section 6.3 we provided a complete analytical solution of the non-linear boundary value problem stated in equations 6.12 and 6.13 for three one-dimensional cases. Such a general solution is not feasible for higher dimensional cases. The difficulty here is the description of the surface inside the organism that separates the region with regulator behavior from the region with conformer behavior. But if we restrict ourselves to the pure regulator case or to the pure conformer case the problem simplifies to a linear boundary value problem and a solution by the method of eigenfunction expansion becomes possible. This method enables us to obtain useful expressions for the critical surfaces S_{reg} and S_{conf} for higher dimensional cases.

6.4.1 A formal solution

We consider the following eigenvalue problem, which will prove to be central to our purpose:

$$\text{PDE: } \Delta_{\vec{\xi}} X(\vec{\xi}) + \lambda X(\vec{\xi}) = 0 \quad \text{for } \vec{\xi} \in G' \quad (6.62)$$

$$\text{BC: } \frac{\partial}{\partial \vec{n}'} X(\vec{\xi}) + \frac{Q}{K} X(\vec{\xi}) = 0 \quad \text{for } \vec{\xi} \in \partial G' \quad (6.63)$$

Such an eigenvalue problem admits an infinite number of (positive) eigenvalues λ_n with corresponding eigenfunctions $X_n(\vec{\xi})$ ($n = 1, 2, 3, \dots$) (cf. Churchill (1955)). If we expand the constant function $g(\vec{\xi}) = 1$ on G' with respect to this (orthogonal) set of eigenfunctions, the result is:

$$1 = \sum_{n=1}^{\infty} \gamma_n X_n(\vec{\xi}) \quad (6.64)$$

$$\text{with } \gamma_n = (g, X_n) / (X_n, X_n) = \int_{G'} X_n(\vec{\xi}) d\omega' / \int_{G'} X_n(\vec{\xi})^2 d\omega'$$

As we will shortly see, both special cases mentioned above, are solvable in terms of the eigenfunctions $X_n(\vec{\xi})$, the eigenvalues λ_n , and the Fourier coefficients γ_n .

For a *pure regulator* it holds that $v(\vec{\xi}) \geq E$ for all $\vec{\xi} \in G'$. This means that $\Phi(v) = P$, as follows from 6.10. Then equations 6.12 and 6.13 reduce to:

$$\text{PDE: } \Delta_{\vec{\xi}} v(\vec{\xi}) = P \quad \text{for } \vec{\xi} \in G' \quad (6.65)$$

$$\text{BC: } \frac{\partial}{\partial \vec{n}'} v(\vec{\xi}) + \frac{Q}{K} v(\vec{\xi}) = Q \quad \text{for } \vec{\xi} \in \partial G' \quad (6.66)$$

The formal solution of this problem is:

$$v_{\text{reg}}(\vec{\xi}) = K - P \sum_{n=1}^{\infty} \frac{\gamma_n}{\lambda_n} X_n(\vec{\xi}) \quad (6.67)$$

as follows easily by inspection. The critical surface S_{reg} is given by $\min_{\vec{\xi} \in G'} [v_{\text{reg}}(\vec{\xi})] = E$, see 6.14. This yields the following equation for the critical surface

$$S_{\text{reg}} : \quad K - E = P \max_{\vec{\xi} \in G'} \left(\sum_{n=1}^{\infty} \frac{\gamma_n}{\lambda_n} X_n(\vec{\xi}) \right) \quad (6.68)$$

For a *pure conformer* it holds that $v(\vec{\xi}) \leq E$ for all $\vec{\xi} \in G'$. Hence $\Phi(v) = Pv/E$, see, again, 6.10. So this time equations 6.12 and 6.13 reduce to:

$$\text{PDE: } \Delta_{\vec{\xi}} v(\vec{\xi}) - \frac{P}{E} v(\vec{\xi}) = 0 \quad \text{for } \vec{\xi} \in G' \quad (6.69)$$

$$\text{BC: } \frac{\partial}{\partial \vec{n}'} v(\vec{\xi}) + \frac{Q}{K} v(\vec{\xi}) = Q \quad \text{for } \vec{\xi} \in \partial G' \quad (6.70)$$

The formal solution of this problem is:

$$v_{\text{conf}}(\vec{\xi}) = K - K(P/E) \sum_{n=1}^{\infty} \frac{\gamma_n}{P/E + \lambda_n} X_n(\vec{\xi}) \quad (6.71)$$

as follows again by inspection. Critical surface S_{conf} is given by $\max_{\vec{\xi} \in G'} [v_{\text{conf}}(\vec{\xi})] = E$, see, again, 6.14. This yields the following equation for the critical surface

$$S_{\text{conf}} : \quad K - E = K(P/E) \min_{\vec{\xi} \in G'} \left(\sum_{n=1}^{\infty} \frac{\gamma_n}{P/E + \lambda_n} X_n(\vec{\xi}) \right) \quad (6.72)$$

For a pure regulator the *dimensionless oxygen consumption rate* $\Gamma = P$, as follows from first principles or, for that matter, from the first equality in equation 6.16. For a pure conformer it follows from 6.71 and the second equality in equation 6.16 that

$$\Gamma = -K(P/E)/A' \sum_{n=1}^{\infty} \frac{\gamma_n}{P/E + \lambda_n} \int_{\partial G'} \frac{\partial}{\partial \vec{n}'} X_n(\vec{\xi}) \, d\sigma' \quad (6.73)$$

An application of Green's identity on the surface integral in the right-hand side of equation 6.73 yields, together with 6.62:

$$\Gamma = K(P/E)/A' \sum_{n=1}^{\infty} \frac{\gamma_n \lambda_n}{P/E + \lambda_n} \int_{G'} X_n(\vec{\xi}) \, d\omega' \quad (6.74)$$

Parseval's relation for the constant function $g(\vec{\xi}) = 1$ on G' yields, together with 6.64:

$$V' = (g, g) = \sum_{n=1}^{\infty} (g, X_n)^2 / (X_n, X_n) = \sum_{n=1}^{\infty} \gamma_n \int_{G'} X_n(\vec{\xi}) \, d\omega' \quad (6.75)$$

$$\text{Next we define: } g_n = \frac{\gamma_n}{V'} \int_{G'} X_n(\vec{\xi}) \, d\omega', \quad \text{which means: } \sum_{n=1}^{\infty} g_n = 1 \quad (6.76)$$

In this way we obtain from 6.74 and 6.76, and with the equality $V' = A'$ in mind, the following concise expression for the dimensionless consumption rate Γ for a pure conformer:

$$\Gamma = K(P/E) \sum_{n=1}^{\infty} \frac{g_n \lambda_n}{P/E + \lambda_n} \quad (6.77)$$

Note that the parameter combination Q/K plays a role in the determination of the eigenvalues λ_n and the weight factors g_n .

6.4.2 Three characteristic shapes

It should be noted that it is not always possible to find an analytical solution for the eigenvalue problem stated in 6.62 and 6.63. For exotic regions G' we have to use numerical methods, for instance, a Galerkin procedure (Fairweather, 1978). But for (from a mathematical point of view) reasonably shaped organisms an explicit solution is attainable (*cf.* Gielen (2000)). The regions G' discussed in the following three examples, are determined by one or two shape-parameters. We use these parameters in Section 6.5 to distinguish and compare between elongated, compact and sheet-like organisms.

Infinite beam

First we discuss in some detail the case of a (rectangular) infinite beam with length $2R_1$ and breadth $2R_2$. We may take $R_1 \leq R_2$, which means that $\alpha = R_2/R_1 \geq 1$. Note that α defines the shape of the beam and that the ‘dimensions’ of the standard beam of this shape are $2(1+1/\alpha)$ and $2(1+\alpha)$, respectively. With $G' = [-1-1/\alpha, 1+1/\alpha] \times [-1-\alpha, 1+\alpha]$ equations 6.12 and 6.13 constitute a two-dimensional boundary value problem.

Because of the inherent symmetry of the case under consideration, it is obvious that in the equilibrium situation there will be no oxygen transport through the planes $\xi_1 = 0$ and $\xi_2 = 0$. Therefore it is possible to restrict the problem to the region $[0, 1+1/\alpha] \times [0, 1+\alpha]$ by taking no-flow boundary conditions on these planes. Then the eigenvalue problem stated in 6.62 and 6.63 may be written as:

$$\text{PDE: } \frac{\partial^2}{\partial \xi_1^2} X(\xi_1, \xi_2) + \frac{\partial^2}{\partial \xi_2^2} X(\xi_1, \xi_2) + \lambda X(\xi_1, \xi_2) = 0 \quad (6.78)$$

$$\text{BC}_1: \frac{\partial}{\partial \xi_1} X(0, \xi_2) = 0, \quad \text{BC}_2: \frac{\partial}{\partial \xi_1} X(1+1/\alpha, \xi_2) + \frac{Q}{K} X(1+1/\alpha, \xi_2) = 0 \quad (6.79)$$

$$\text{BC}_3: \frac{\partial}{\partial \xi_2} X(\xi_1, 0) = 0, \quad \text{BC}_4: \frac{\partial}{\partial \xi_2} X(\xi_1, 1+\alpha) + \frac{Q}{K} X(\xi_1, 1+\alpha) = 0 \quad (6.80)$$

Applying the well-known separation of variables technique: $X(\xi_1, \xi_2) = \tilde{X}_1(\xi_1)\tilde{X}_2(\xi_2)$, we get two (almost identical) so-called regular Sturm-Liouville problems:

$$\begin{cases} \tilde{X}_1''(\xi_1) + \lambda_1 \tilde{X}_1(\xi_1) = 0 & \text{for } 0 < \xi_1 < 1+1/\alpha \\ \tilde{X}_1'(0) = 0 \\ \tilde{X}_1'(1+1/\alpha) + (Q/K)\tilde{X}_1(1+1/\alpha) = 0 \end{cases} \quad (6.81)$$

$$\left\{ \begin{array}{l} \tilde{X}_2''(\xi_2) + \lambda_2 \tilde{X}_2(\xi_2) = 0 \quad \text{for } 0 < \xi_2 < 1 + \alpha \\ \tilde{X}_2'(0) = 0 \\ \tilde{X}_2'(1 + \alpha) + (Q/K) \tilde{X}_2(1 + \alpha) = 0 \end{array} \right. \quad (6.82)$$

Because $Q/K > 0$ the eigenvalues $\lambda_{1,n}$ and $\lambda_{2,n}$ are positive: we write $\lambda_{1,n} = \mu_{1,n}^2$ with $\mu_{1,n} > 0$, and $\lambda_{2,n} = \mu_{2,n}^2$ with $\mu_{2,n} > 0$ ($n = 1, 2, 3, \dots$). A straightforward calculation yields the eigenfunctions:

$$\tilde{X}_{1,n}(\xi_1) = \cos(\mu_{1,n}\xi_1) \quad \text{and} \quad \tilde{X}_{2,n}(\xi_2) = \cos(\mu_{2,n}\xi_2) \quad (6.83)$$

where $\mu_{1,n}$ is the n th positive root of the first and where $\mu_{2,n}$ is the n th positive root of the second of the following two characteristic equations for μ :

$$\begin{aligned} -\mu K \sin(\mu(1 + 1/\alpha)) + Q \cos(\mu(1 + 1/\alpha)) &= 0 \\ -\mu K \sin(\mu(1 + \alpha)) + Q \cos(\mu(1 + \alpha)) &= 0 \end{aligned} \quad (6.84)$$

Hence the eigenfunctions $X_{i,j}(\xi_1, \xi_2)$ and corresponding eigenvalues $\lambda_{i,j}$ of the original problem are:

$$X_{i,j}(\xi_1, \xi_2) = \cos(\mu_{1,i}\xi_1) \cos(\mu_{2,j}\xi_2) \quad \text{with } \lambda_{i,j} = \mu_{1,i}^2 + \mu_{2,j}^2 \quad (6.85)$$

Following the guideline set out in Section 6.4.1, we determine the Fourier coefficients $\gamma_{i,j}$ of the constant function $f(\xi_1, \xi_2) = 1$ with respect to this orthogonal set of eigenfunctions $X_{i,j}(\xi_1, \xi_2)$. It follows from equation 6.64 that

$$\gamma_{i,j} = \frac{\int_0^{1+1/\alpha} \tilde{X}_{1,i}(\xi_1) d\xi_1}{\int_0^{1+1/\alpha} \tilde{X}_{1,i}(\xi_1)^2 d\xi_1} \times \frac{\int_0^{1+\alpha} \tilde{X}_{2,j}(\xi_2) d\xi_2}{\int_0^{1+\alpha} \tilde{X}_{2,j}(\xi_2)^2 d\xi_2} \quad (6.86)$$

which leads, with the shorthand $Q/K = q$, to

$$\gamma_{i,j} = \frac{2(-1)^{i+1} q \sqrt{q^2 + \mu_{1,i}^2}}{(1 + 1/\alpha)(\mu_{1,i}^3 + q^2 \mu_{1,i}) + q \mu_{1,i}} \times \frac{2(-1)^{j+1} q \sqrt{q^2 + \mu_{2,j}^2}}{(1 + \alpha)(\mu_{2,j}^3 + q^2 \mu_{2,j}) + q \mu_{2,j}} \quad (6.87)$$

Once $\gamma_{i,j}$ is known, the dimensionless concentration $v_{\text{reg}}(\xi_1, \xi_2)$ follows from 6.67 and 6.85, and the dimensionless concentration $v_{\text{conf}}(\xi_1, \xi_2)$ follows from 6.71 and 6.85.

The next step, still following the path set out in Section 6.4.1, is the determination of the minimum value of $v_{\text{reg}}(\xi_1, \xi_2)$ and the maximum value of $v_{\text{conf}}(\xi_1, \xi_2)$ on G' . In general this is not an easy task; numerical methods may be needed, though for the highly symmetrical case we are dealing with here the problem is not that difficult. The minimum value of (any stationary) $v(\xi_1, \xi_2)$ on an infinite beam will always be found on the central axis of the beam and the maximum value will always be attained

on the edges of the beam. In this way we infer from 6.68 and 6.72 for the critical surfaces the following equations:

$$S_{\text{reg}} : \quad K - E = P \sum_{i,j=1}^{\infty} \frac{\gamma_{i,j}}{\mu_{1,i}^2 + \mu_{2,j}^2} \quad (6.88)$$

$$S_{\text{conf}} : \quad K - E = K(P/E) \sum_{i,j=1}^{\infty} \frac{\gamma_{i,j} \cos(\mu_{1,i}(1 + 1/\alpha)) \cos(\mu_{2,j}(1 + \alpha))}{P/E + \mu_{1,i}^2 + \mu_{2,j}^2} \quad (6.89)$$

Note that the infinite sum in the right-hand side of 6.88 is a function of Q/K alone, while the infinite sum in the right-hand side of 6.89 is a function of Q/K and P/E .

Rectangular parallelepiped

Next we discuss the case of a (rectangular) parallelepiped with length $2R_1$, breadth $2R_2$ and height $2R_3$. We may take $R_1 \leq R_2 \leq R_3$, which means that $\alpha = R_2/R_1 \geq 1$ and $\beta = R_3/R_1 \geq \alpha$. The shape of the parallelepiped is fixed by α and β , and the ‘dimensions’ of the standard parallelepiped of this shape are $2(1 + 1/\alpha + 1/\beta)$, $2(1 + \alpha + \alpha/\beta)$ and $2(1 + \beta + \beta/\alpha)$, respectively. The symmetry argument already used for the case of an infinite beam yields, this time, a three-dimensional eigenvalue problem for an unknown function $X(\xi_1, \xi_2, \xi_3)$ on the region $[0, 1 + 1/\alpha + 1/\beta] \times [0, 1 + \alpha + \alpha/\beta] \times [0, 1 + \beta + \beta/\alpha]$.

The same reasoning as applied for the case of the infinite beam leads to the following eigenfunctions $X_{i,j,k}(\xi_1, \xi_2, \xi_3)$ and corresponding eigenvalues $\lambda_{i,j,k}$:

$$X_{i,j,k}(\xi_1, \xi_2, \xi_3) = \cos(\mu_{1,i}\xi_1) \cos(\mu_{2,j}\xi_2) \cos(\mu_{3,k}\xi_3) \quad (6.90)$$

$$\text{with } \lambda_{i,j,k} = \mu_{1,i}^2 + \mu_{2,j}^2 + \mu_{3,k}^2$$

where $\mu_{1,n}$ is the n th positive root of the first, $\mu_{2,n}$ is the n th positive root of the second and $\mu_{3,n}$ is the n th positive root of the third of the following three characteristic equations for μ ($n = 1, 2, 3, \dots$):

$$\begin{aligned} -\mu K \sin(\mu(1 + 1/\alpha + 1/\beta)) + Q \cos(\mu(1 + 1/\alpha + 1/\beta)) &= 0 \\ -\mu K \sin(\mu(1 + \alpha + \alpha/\beta)) + Q \cos(\mu(1 + \alpha + \alpha/\beta)) &= 0 \\ -\mu K \sin(\mu(1 + \beta + \beta/\alpha)) + Q \cos(\mu(1 + \beta + \beta/\alpha)) &= 0 \end{aligned} \quad (6.91)$$

The Fourier coefficients $\gamma_{i,j,k}$ of the constant function $f(\xi_1, \xi_2, \xi_3) = 1$ with respect to this new orthogonal set of eigenfunctions are:

$$\gamma_{i,j,k} = \frac{2(-1)^{i+1} q \sqrt{q^2 + \mu_{1,i}^2}}{(1 + 1/\alpha + 1/\beta)(\mu_{1,i}^3 + q^2 \mu_{1,i}) + q \mu_{1,i}} \times \quad (6.92)$$

$$\frac{2(-1)^{j+1}q\sqrt{q^2 + \mu_{2,j}^2}}{(1 + \alpha + \alpha/\beta)(\mu_{2,j}^3 + q^2\mu_{2,j}) + q\mu_{2,j}} \times \frac{2(-1)^{k+1}q\sqrt{q^2 + \mu_{3,k}^2}}{(1 + \beta + \beta/\alpha)(\mu_{3,k}^3 + q^2\mu_{3,k}) + q\mu_{3,k}}$$

where, again, the shorthand $q = Q/K$ is used.

The minimum value of (any stationary) $v(\xi_1, \xi_2, \xi_3)$ on a rectangular parallelepiped will always be found in the center and the maximum value will always be attained on the vertices. With these facts in mind we infer from 6.68 and 6.72 the following equations for the critical surfaces (see Fig. 6.2 b)

$$S_{\text{reg}} : \quad K - E = P \sum_{i,j,k=1}^{\infty} \frac{\gamma_{i,j,k}}{\mu_{1,i}^2 + \mu_{2,j}^2 + \mu_{3,k}^2} \quad (6.93)$$

$$S_{\text{conf}} : \quad K - E = K(P/E) \times \sum_{i,j,k=1}^{\infty} \frac{\gamma_{i,j,k} \cos(\mu_{1,i}(1 + 1/\alpha + 1/\beta)) \cos(\mu_{2,j}(1 + \alpha + \alpha/\beta)) \cos(\mu_{3,k}(1 + \beta + \beta/\alpha))}{P/E + \mu_{1,i}^2 + \mu_{2,j}^2 + \mu_{3,k}^2} \quad (6.94)$$

If, for instance, we let β tend to infinity, than equations 6.91 a,b transform into 6.84 a,b; hence the roots of 6.91 a,b change into the roots of 6.84 a,b. And for the roots $\mu_{3,n}$ of 6.91 c it holds that $\mu_{3,n} \rightarrow 0$, but $\mu_{3,n}(1 + \beta + \beta/\alpha) \rightarrow (2n - 1)\pi/2$. Thus $\gamma_{i,j,k}$ changes into $\gamma_{i,j}(4/\pi)(-1)^{k+1}/(2k - 1)$, with $\gamma_{i,j}$ given by 6.87. By means of the well-known equality $\sum_{k=1}^{\infty} (-1)^{k+1}/(2k - 1) = \pi/4$ it follows that equation 6.93 transforms into 6.88. So we see that in this respect an elongated parallelepiped resembles an infinite beam. The same result can be obtained for equations 6.94 and 6.89, using a slightly more involved argument.

Finite cylinder

Finally we discuss the case of a finite cylinder with diameter $2R_1$ and length $2R_2$. The shape of the cylinder is again fixed by $\alpha = R_2/R_1$, this time with $0 < \alpha < \infty$, and the ‘dimensions’ of the standard finite cylinder of this shape are $2(2 + 1/\alpha)$ and $2(1 + 2\alpha)$, respectively. Symmetry arguments yield this time, in accordance with 6.62 and 6.63, a two-dimensional eigenvalue problem for an unknown function $X(\xi_1, \xi_2)$ on the region $[0, 2 + 1/\alpha] \times [0, 1 + 2\alpha]$:

$$\text{PDE: } \frac{1}{\xi_1} \frac{\partial}{\partial \xi_1} [\xi_1 \frac{\partial}{\partial \xi_1} X(\xi_1, \xi_2)] + \frac{\partial^2}{\partial \xi_2^2} X(\xi_1, \xi_2) + \lambda X(\xi_1, \xi_2) = 0 \quad (6.95)$$

$$\text{BC}_1: \lim_{\xi_1 \rightarrow 0} \xi_1 \frac{\partial}{\partial \xi_1} X(\xi_1, \xi_2) = 0, \quad \text{BC}_2: \frac{\partial}{\partial \xi_1} X(2 + 1/\alpha, \xi_2) + \frac{Q}{K} X(2 + 1/\alpha, \xi_2) = 0 \quad (6.96)$$

$$\text{BC}_3: \frac{\partial}{\partial \xi_2} X(\xi_1, 0) = 0, \quad \text{BC}_4: \frac{\partial}{\partial \xi_2} X(\xi_1, 1 + 2\alpha) + \frac{Q}{K} X(\xi_1, 1 + 2\alpha) = 0 \quad (6.97)$$

The separation of variables technique: $X(\xi_1, \xi_2) = \tilde{X}_1(\xi_1)\tilde{X}_2(\xi_2)$, yields:

$$\begin{cases} (1/\xi_1)(\xi_1 \tilde{X}_1'(\xi_1))' + \lambda_1 \tilde{X}_1(\xi_1) = 0 & \text{for } 0 < \xi_1 < 2 + 1/\alpha \\ \lim_{\xi_1 \rightarrow 0} \xi_1 \tilde{X}_1'(\xi_1) = 0 \\ \tilde{X}_1(2 + 1/\alpha) + (Q/K)\tilde{X}_1(2 + 1/\alpha) = 0 \end{cases} \quad (6.98)$$

$$\begin{cases} \tilde{X}_2''(\xi_2) + \lambda_2 \tilde{X}_2(\xi_2) = 0 & \text{for } 0 < \xi_2 < 1 + 2\alpha \\ \tilde{X}_2'(0) = 0 \\ \tilde{X}_2'(1 + 2\alpha) + (Q/K)\tilde{X}_2(1 + 2\alpha) = 0 \end{cases} \quad (6.99)$$

Also for this case the eigenvalues $\lambda_{1,n}$ and $\lambda_{2,n}$ are positive: we write again $\lambda_{1,n} = \mu_{1,n}^2$ with $\mu_{1,n} > 0$, and $\lambda_{2,n} = \mu_{2,n}^2$ with $\mu_{2,n} > 0$ ($n = 1, 2, 3, \dots$). With the help of the Bessel functions J_0 and J_1 (Abramowitz and Stegun, 1965) we obtain the eigenfunctions:

$$\tilde{X}_{1,n}(\xi_1) = J_0(\mu_{1,n}\xi_1) \quad \text{and} \quad \tilde{X}_{2,n}(\xi_2) = \cos(\mu_{2,n}\xi_2) \quad (6.100)$$

where $\mu_{1,n}$ is the n th positive root of the first and where $\mu_{2,n}$ is the n th positive root of the second of the following two characteristic equations for μ :

$$\begin{aligned} -\mu K J_1(\mu(2 + 1/\alpha)) + Q J_0(\mu(2 + 1/\alpha)) &= 0 \\ -\mu K \sin(\mu(1 + 2\alpha)) + Q \cos(\mu(1 + 2\alpha)) &= 0 \end{aligned} \quad (6.101)$$

Hence the eigenfunctions $X_{i,j}(\xi_1, \xi_2)$ and corresponding eigenvalues $\lambda_{i,j}$ of the original problem are:

$$X_{i,j}(\xi_1, \xi_2) = J_0(\mu_{1,i}\xi_1) \cos(\mu_{2,j}\xi_2) \quad \text{with } \lambda_{i,j} = \mu_{1,i}^2 + \mu_{2,j}^2 \quad (6.102)$$

The Fourier coefficients $\gamma_{i,j}$ of the constant function $f(\xi_1, \xi_2) = 1$ with respect to this new orthogonal set of eigenfunctions $X_{i,j}(\xi_1, \xi_2)$ follow again from 6.64:

$$\gamma_{i,j} = \frac{\int_0^{2+1/\alpha} \xi_1 \tilde{X}_{1,i}(\xi_1) d\xi_1}{\int_0^{2+1/\alpha} \xi_1 \tilde{X}_{1,i}(\xi_1)^2 d\xi_1} \times \frac{\int_0^{1+2\alpha} \tilde{X}_{2,j}(\xi_2) d\xi_2}{\int_0^{1+2\alpha} \tilde{X}_{2,j}(\xi_2)^2 d\xi_2} \quad (6.103)$$

which leads, with the shorthand $Q/K = q$, to

$$\gamma_{i,j} = \frac{2q^2}{\mu_{1,i}(2 + 1/\alpha)(q^2 + \mu_{1,i}^2)J_1(\mu_{1,i}(2 + 1/\alpha))} \times \frac{2(-1)^{j+1}q\sqrt{q^2 + \mu_{2,j}^2}}{(1 + 2\alpha)(\mu_{2,j}^3 + q^2\mu_{2,j}) + q\mu_{2,j}} \quad (6.104)$$

The minimum value of (any stationary) $v(\xi_1, \xi_2)$ on a finite cylinder will be found in the center and the maximum value will be attained on the border circles of the cylinder. In this way we infer from 6.64 and 6.73 for the critical surfaces the following equations,

$$S_{\text{reg}} : \quad K - E = P \sum_{i,j=1}^{\infty} \frac{\gamma_{i,j}}{\mu_{1,i}^2 + \mu_{2,j}^2} \quad (6.105)$$

$$S_{\text{conf}} : K - E = K(P/E) \sum_{i,j=1}^{\infty} \frac{\gamma_{i,j} J_0(\mu_{1,i}(2 + 1/\alpha)) \cos(\mu_{2,j}(1 + 2\alpha))}{P/E + \mu_{1,i}^2 + \mu_{2,j}^2} \quad (6.106)$$

If we apply to this case the line of reasoning already developed in the last paragraph of Section 6.4.2 we get for $\alpha \rightarrow \infty$ the case of an infinite cylinder and for $\alpha \rightarrow 0$ the case of an infinite sheet: an elongated cylinder resembles an infinite cylinder and a flattened cylinder resembles an infinite sheet.

6.5 Critical Size for Differently Shaped Organisms

Due to growth of the organism or to changes in the environmental conditions the organism experiences, the representation $\langle P, Q, E, K \rangle$ of the organism follows a path in parameter space. Also in parameter space we find, subject to the shape of the organism, the critical surfaces S_{reg} and S_{conf} . If the organism changes shape during its growth process these critical surfaces will shift accordingly in parameter space. A critical point arises whenever the path the organism follows intersects one of its critical surfaces. From a biological point of view the arrival at a critical point is important: we then expect an essential change in the behavior of the organism.

In this section we discuss what happens at the critical surface S_{reg} for some constant value of E and for $K = 1$. As a result of these restrictions the critical surface S_{reg} degenerates into a critical curve in the reduced parameter space $\langle P, Q \rangle$. In this section we also pay special attention to block-like organisms (block: short for rectangular parallelepiped, see Section 6.4.2). The reason for this is the possibility to distinguish within this class between compact, elongated or flat structures. The numerical justification of the results in this section rests upon equations 6.21, 6.33, 6.41, 6.88, 6.93 and 6.105.

Figure 6.4 shows, for $E = 0$ and $K = 1$, the critical curves for six organisms of different shape and a possible trajectory an organism, that goes through an otherwise undisturbed growth process, could follow in the reduced parameter space $\langle P, Q \rangle$. During such a growth process only the volume to surface area ratio L of the organism increases, while all other parameter values are constant. In this way we obtain, with the help of equation 6.11, the trajectory $\langle Q(L), P(L) \rangle_L = \langle k_{\text{eff}} L/D, mL^2/(DC_{\infty}) \rangle_L$, which is a simple parabola. An equation for this parabola is: $P = RQ^2$, with $R = P/Q^2 = mD/(k_{\text{eff}}^2 C_{\infty})$. Such a parabola is completely determined by the parameter R . The intersection of this parabola with one of the critical curves yields a critical

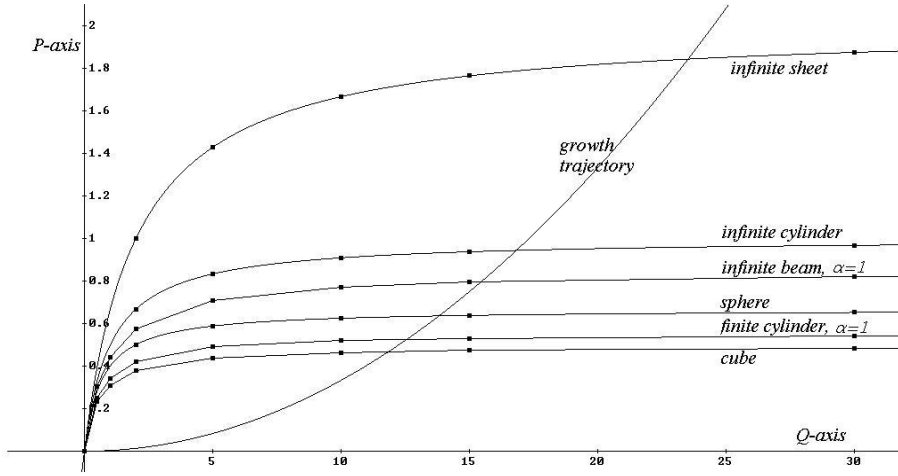


Figure 6.4: For $E = 0$ and $K = 1$: a parabolic growth trajectory representing undisturbed growth and critical curves for six different shapes. Whenever a growth trajectory crosses a critical curve from below an organism of corresponding shape starts to experience oxygen deficiency.

point $(Q_{\text{crit}}, P_{\text{crit}})$. Thus it becomes obvious that the value of Q_{crit} , and therefore the value of L_{crit} , depends solely on the value of the dimensionless parameter combination R (for a given value of E and K and for a given shape of the organism).

From Q_{crit} we can deduce L_{crit} (see 6.11): $L_{\text{crit}} = DQ_{\text{crit}}/k_{\text{eff}}$. In Fig. 6.5 we have plotted, for $E = 0.01$ and $K = 1$, the dimensionless parameter $T_{\text{crit}} = Q_{\text{crit}}\sqrt{R}$ as a function of the dimensionless parameter $S = 1/\sqrt{R}$. Because $T_{\text{crit}} = L_{\text{crit}}\sqrt{m/(DC_{\infty})}$ is directly proportional to L_{crit} (and does not depend on k_{eff}) and $S = k_{\text{eff}}\sqrt{C_{\infty}/(mD)}$ is directly proportional to k_{eff} , Fig. 6.5 shows the dependency of the critical volume to surface area ratio L_{crit} on the mass transfer coefficient k_{eff} . Remember: k_{eff} is a measure for the outward water conditions the organism experiences; the limit $S \rightarrow \infty$ ($k_{\text{eff}} \rightarrow \infty$) represents well-stirred water conditions. Figure 6.5 also shows that, at least for large k_{eff} , a flattened shape allows for a larger L_{crit} and is therefore more favorable for oxygen supply than a compact one.

In Fig. 6.5, again, zebrafish, rabbitfish, winter flounder, plaice and herring are smaller than the critical size T_{crit} even for the most disadvantageous shape (*i.e.* the cube) under the given value of the mass transfer coefficient. This value of the mass transfer coefficient is not large enough to fully meet the oxygen demands of common carp, African catfish and largemouth bass (though note the effect of the shape used

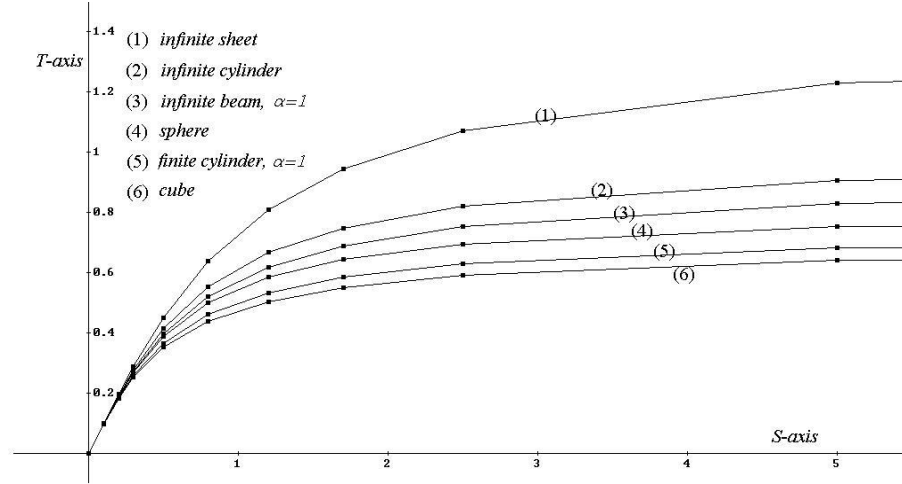
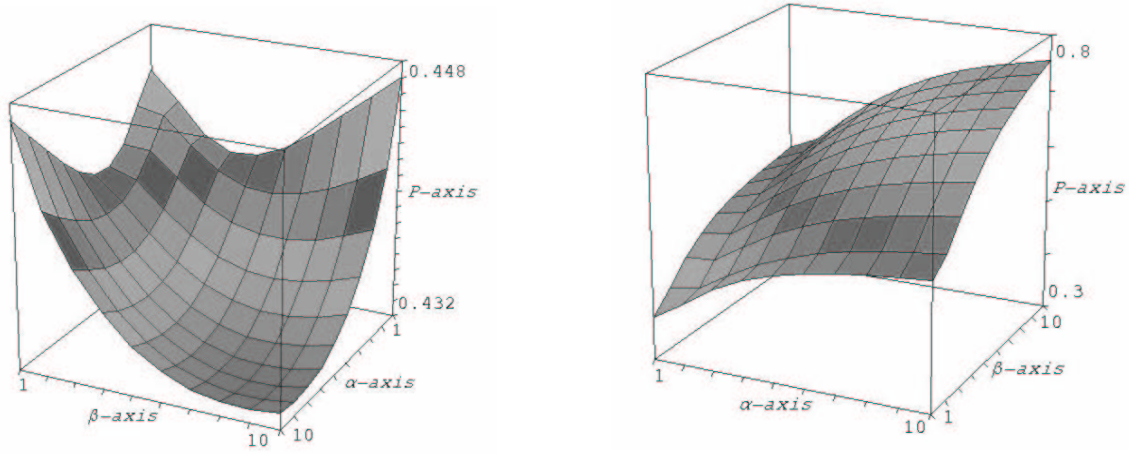


Figure 6.5: For $E = 0.01$ and $K = 1$; T_{crit} as a function of S for six different shapes: infinite sheet (1), infinite cylinder (2), infinite beam with $\alpha = 1$ (3), sphere (4), finite cylinder with $\alpha = 1$ (5), cube (6). Because $T_{\text{crit}} \propto L_{\text{crit}}$ and $S \propto k_{\text{eff}}$, this picture shows how the outward water conditions influence the critical size of the organism. Also the results for S and T from Table 6.1 are plotted in this figure: African catfish (ac), common carp (cc), herring (hg), largemouth bass (lb), plaice (pl), rabbitfish (rf), winter flounder (wf), zebrafish (zf).

to model the embryo).

Next we turn our attention to block-like organisms. A structure from this class is determined by its proportions: $1 : \alpha : \beta$, with $\alpha \geq 1$, $\beta \geq \alpha$ (see Sec. 6.4.2). This yields a multitude of critical curves $S_{\text{reg}}^{\alpha,\beta}$ in the reduced parameter space $\langle P, Q \rangle$. The positioning of these curves in parameter space is not obvious and is, for instance, quite different for small and large values of Q ; see Fig. 6.6. It can be seen, for instance, that $P_{\text{crit}}^{1,1}(0.05) > P_{\text{crit}}^{10,10}(0.05)$ and $P_{\text{crit}}^{1,1}(2) < P_{\text{crit}}^{10,10}(2)$. Therefore, the critical curves of a cube and a sheet with proportions $1 : 10 : 10$ coincide somewhere between $Q = 0.05$ and $Q = 2$. Numerical evaluation yields $(Q, P) = (0.0874, 0.072)$ for this common point. It follows that, for conditions compatible with $R = P/Q^2 = 9.425$, a cube and a sheet with proportions $1 : 10 : 10$ share the same value for L_{crit} and hence are equally well equipped for oxygen supply.

As before, we determine for a given value of S (or, equivalently, a given value of R) for all allowed values of α and β a critical value $Q_{\text{crit}}^{\alpha,\beta}$ (or, equivalently, $T_{\text{crit}}^{\alpha,\beta}$ or $L_{\text{crit}}^{\alpha,\beta}$). Using the cube ($\alpha = 1$, $\beta = 1$) as a gauge, we define the relative critical size



(a) A cross-section of $\{S_{\text{crit}}^{\alpha,\beta}\}$ for $Q = 0.05$.

(b) A cross-section of $\{S_{\text{crit}}^{\alpha,\beta}\}$ for $Q = 2$.

Figure 6.6: For a block with proportions $1 : \alpha : \beta$ and for $E = 0$, $K = 1$: the critical dimensionless consumption rate P_{crit} as a function of α and β for two values of Q . Note the symmetry in α and β : a block with proportions $1 : \alpha : \beta$ behaves the same as a block with proportions $1 : \beta : \alpha$.

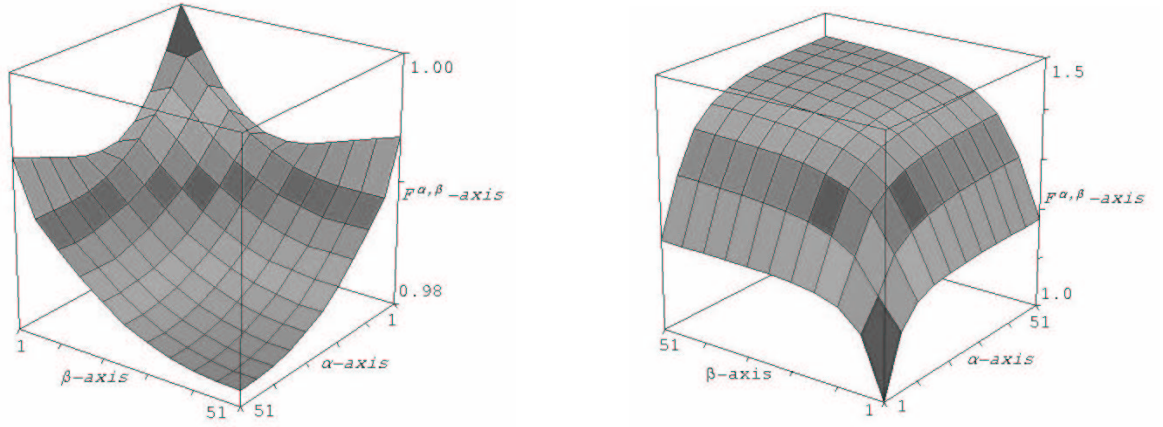
$F^{\alpha,\beta}(S)$ by:

$$F^{\alpha,\beta}(S) = \frac{Q_{\text{crit}}^{\alpha,\beta}(S)}{Q_{\text{crit}}^{1,1}(S)} = \frac{T_{\text{crit}}^{\alpha,\beta}(S)}{T_{\text{crit}}^{1,1}(S)} = \frac{L_{\text{crit}}^{\alpha,\beta}(S)}{L_{\text{crit}}^{1,1}(S)} \quad (6.107)$$

Hence, if it holds for a given value of S that $F^{\alpha,\beta}(S) < 1$, then the critical size of a block-like organism with proportions $1 : \alpha : \beta$ is smaller than the critical size of a cube, which means that a cube for the given value of S is more favorable for oxygen supply.

In Fig. 6.7 a we have plotted $F^{\alpha,\beta}$ for a small value of S (*i.e.* a small value of k_{eff}) and in Fig. 6.7 b we have plotted $F^{\alpha,\beta}$ for a large value of S (*i.e.* a large value of k_{eff}). The results show that for almost stagnant water a compact structure is more favorable for oxygen supply and that for well-stirred water conditions a flat shape is more favorable. This concurs with the predictions already made by Kranenbarg *et al.* (2000).

Apart from pure growth an organism may also (slowly) change its shape. During such a process, supposing all other parameter values are kept constant, again only the



(a) $F^{\alpha,\beta}$ for $S = 0.05$. A cube appears to be the most favorable shape for oxygen supply.

(b) $F^{\alpha,\beta}$ for $S = 1$. A cube appears to be the least favorable shape for oxygen supply.

Figure 6.7: For a block with proportions $1 : \alpha : \beta$ and for $E = 0$, $K = 1$: the relative critical size $F^{\alpha,\beta}(S)$ as a function of α and β for two values of S .

volume to surface area ratio L of the organism changes. Hence the organism follows again a parabola in parameter space. In addition the change of shape of the organism also results in a new corresponding critical curve.

If we take, for instance, a block-like organism with proportions $1 : \alpha_0 : \beta_0$, with volume V_0 and with volume to surface area ratio L_0 , we have:

$$V_0 = \frac{(\alpha_0 + \beta_0 + \alpha_0\beta_0)^3}{\alpha_0^2\beta_0^2} 8L_0^3 \quad (6.108)$$

Hence, if a block with proportions $1 : \alpha_0 : \beta_0$ and with volume to surface area ratio L_0 alters into a block with proportions $1 : \alpha_1 : \beta_1$ and with volume to surface area ratio L_1 , at the same time changing its volume V_0 into $V_1 = g^3V_0$, we have:

$$L_1 = \frac{\alpha_0 + \beta_0 + \alpha_0\beta_0}{\alpha_1 + \beta_1 + \alpha_1\beta_1} \left(\frac{\alpha_1\beta_1}{\alpha_0\beta_0} \right)^{2/3} gL_0 \quad (6.109)$$

By comparing, for a given value of S , L_0 with $L_{\text{crit}}^{\alpha_0,\beta_0}(S)$ and L_1 with $L_{\text{crit}}^{\alpha_1,\beta_1}(S)$ it is possible to see if the proposed growth-spurt of the organism will result in a change of its oxygen consumption pattern and, therefore, of its behavior. Following this procedure it can be shown, for example, that a critical cube would change into a supercritical sphere if the volume were kept constant in the transition.

6.6 Discussion

We presented a model that describes the oxygen balance in small organisms without an active internal oxygen transport mechanism, *e.g.* flatworms (Platyhelminthes) or precirculation embryos of higher organisms. In three important aspects this model expands on earlier models of oxygen transport. Firstly, we included the effect of a moving medium on the oxygen balance. Secondly, we modelled the consumption pattern of the organism as a combination of regulator behavior above a specified threshold oxygen concentration and conformer behavior below the threshold. This is a more realistic oxygen consumption pattern than a pure regulator or a pure conformer pattern as adopted in previous models. And thirdly, by using the method of eigenfunction expansion, we were able to treat within our model organisms with a wide variety of shapes, contrary to existing analytical models that mainly analyze infinite sheets, infinite cylinders or spheres.

We defined four dimensionless parameters that completely describe the state of the organism. This state includes the value of tissue variables (oxygen diffusion coefficient, maximum respiration rate, oxygen consumption concentration threshold), outward conditions variables (mass transfer coefficient, free water oxygen concentration), and size and shape of the organism. For a given shape of the organism and based on the oxygen consumption concentration threshold, we were able to define the critical surfaces S_{reg} and S_{conf} . These surfaces divide parameter space into three domains: the regulator domain (oxygen deficiency nowhere in the organism), the mixed domain (oxygen deficiency at least somewhere in the organism), and the conformer domain (oxygen deficiency everywhere in the organism). Oxygen deficiency is defined here as a local oxygen concentration below the threshold concentration.

A change in the four parameters describing the state of the organism may, for instance, occur due to a variation in environmental conditions (for instance, a change of the ambient temperature) or due to growth of the organism. Such a change triggers a journey along a certain trajectory in parameter space. Whenever this trajectory crosses a critical surface in parameter space, an essential change in the behavior of the organism is expected. If, for example, such a trajectory enters the conformer domain (*i.e.* passes S_{conf}), the organism experiences oxygen deficiency everywhere in its tissues and lowers its respiration rate. Eventually, this may lead to the complete shut down of certain biological processes, *cf.* the suspended animation observed in zebrafish embryos after they had been transferred to an anoxic environment (Padilla

and Roth, 2001).

If a trajectory in parameter space enters the mixed domain from the regulator domain, (*i.e.* passes S_{reg}), this marks the onset of oxygen shortage somewhere in the organism. Because oxygen is needed to perform essential biological processes such as aerobic respiration and growth, we expect natural selection to favor residence of an organism without a circulatory system in the regulator domain. This enabled us to define a critical size for an organism: the largest size for which it can maintain pure regulator behavior. Size is defined here as the volume to surface area ratio, so the critical size represents the maximum volume of respiring tissue that can be fully supplied with oxygen per unit surface area.

The shape of an organism, apart from its size, acts in our model as a ‘fifth’ independent variable. Contrary to the prevailing models of oxygen supply to small organism, this feature of our model enabled us to analyze the class of block-like organisms. In fact, even more exotically shaped organisms can be analyzed, though this would require numerical methods, such as Galerkin procedures. The analysis of the class of block-like structures allowed us to distinguish between cube-like, elongated and sheet-like organisms. In this way we were able to confirm a conjecture of Kranenbarg *et al.* (2000): they stated that for almost stagnant water a flat shape is more favorable for oxygen supply, while for well-stirred water conditions a compact shape is more favorable.

The analysis of oxygen dynamics data of teleost embryos from Kranenbarg *et al.* (2000) illustrates a useful application of the presented theoretical framework. Several teleost embryos (zebrafish, rabbitfish, winter flounder, plaice and herring) appear to be relatively insensitive to external flow conditions. These species will not experience oxygen deficiency even in nearly stagnant water. Other species however (common carp, African catfish and largemouth bass) apparently need a certain amount of external stirring to fully meet their oxygen demands.

Oxygen consumption data of common carp and African catfish are considerably higher than the average oxygen consumption of teleost embryos (Kranenbarg *et al.*, 2000). This could be indicative for rearing conditions with excess oxygen. The predictions for maximum size for these specimens should therefore be interpreted with caution.

Interestingly, largemouth bass is the only species in our analysis in which the male fans the nest in which the eggs are deposited (Scott and Crossman, 1973). This

fanning greatly enhances external stirring and might explain the large size of the largemouth bass embryo.

Intermezzo III - Diffusivity and solubility

Steady state oxygen diffusion into a homogeneous sphere with radius R that consumes oxygen at a rate m per unit volume from a well stirred solution of concentration C_∞ is described by:

$$\frac{D}{r^2} \frac{d}{dr} \left(r^2 \frac{dc}{dr} \right) - m = 0 \quad (\text{III.1})$$

where D is the oxygen diffusion coefficient in water, r is the distance from the center of the sphere and c is the local oxygen concentration.

Integration reveals the general solution of (III.1):

$$c = \frac{mr^2}{6D} - \frac{P}{r} + Q \quad (\text{III.2})$$

where P and Q are integration constants, the values of which still have to be determined.

If the solubility of the diffusing substance in the sphere is α_d times its solubility in the surrounding medium (α_d is called the **distribution coefficient**), then the boundary conditions are: BC1: $dc/dr = 0$ for $r = 0$ (no transport at the center of the sphere) and BC2: $c = \alpha_d C_\infty$ for $r = R$. Applying the boundary conditions to the general solution (III.2) yields:

$$c = \alpha_d C_\infty + \frac{m}{6D} (r^2 - R^2) \quad (\text{III.3})$$

When the concentration reaches a value zero in the center of the sphere, the maximum size without a central anoxic region is attained:

$$R_{\max} = \sqrt{\frac{6\alpha_d D C_\infty}{m}} \quad (\text{III.4})$$

Contrary to the diffusion coefficient of a substance, its solubility does not explicitly appear in the partial differential equation describing the diffusion process. However,

differences in solubility of a substance between two (or more) compartments lead to a discontinuity in concentration at the boundary. Possible differences in solubility therefore show up in the boundary conditions determining the system (see above).

As can be seen from the examples described above, both diffusivity and solubility determine the magnitude of the transport barrier. Furthermore, differences in the diffusion coefficient can either counteract or enforce differences in solubility. Chapter 7 provides an example of a biological system in which compartments with different diffusion coefficients do occur (embryo, yolk and surrounding medium).

Chapter 7

Oxygen Profile in Zebrafish Embryo (*Danio rerio*) Elucidated by Theory and Experiment¹

We present a numerical-experimental diffusion study in which we elucidate the spatial oxygen profile around and inside a zebrafish embryo in the pre-circulation stage (24-28 hpf). Lowest oxygen partial pressures are found in the head with a gradient of posteriorly increasing pressure along the midline of the embryo. Furthermore, instead of being a barrier to oxygen diffusion, this study shows the yolk mass to have a relatively high oxygen permeability. The oxygen permeability in the rest of the body in this stage is close to that of water. Knowledge of the details of the oxygen distribution are important for an understanding of vasculogenesis and angiogenesis since oxygen levels influence the expressions of endothelial growth factors.

7.1 Introduction

Animals without a specialized internal oxygen transporting mechanism have to rely on diffusion through the body surface for their oxygen supply (Graham, 1988). Krogh (1941) formulated the general rule that “diffusion alone can provide sufficient oxygen only to animals of 1 mm diameter or less”. The circulatory system in vertebrate embryos is highly variable in its time of appearance (Richardson, 1995), and before it becomes established, oxygen is distributed by diffusion.

Exactly how oxygen is distributed in and around a vertebrate embryo without a circulatory system is still unknown. Previous theoretical studies have predicted minimum oxygen concentrations, yet the actual shape of the embryo was grossly simplified (Daykin, 1965; Lee and Strathmann, 1998; Seymour, 1994; Seymour and

¹In preparation: Kranenbarg, S., van den Boogaart, J.G.M. and Van Leeuwen, J.L.

Bradford, 1995; Strathmann and Chaffee, 1984; Woods, 1999). The experimental testing of these of oxygen diffusion models is extremely limited (Rombough, 1998). To our knowledge, no complete spatial oxygen distribution in early vertebrate embryos has been measured before.

Vascularization of the embryo is determined at least in part by environmental factors such as local oxygen concentration (Risau, 1997; Semenza, 2001; Weinstein, 1999; Yancopoulos *et al.*, 2000). Several angiogenic factors (*e.g.* vascular endothelial growth factor VEGF) are known to respond to hypoxia by stimulating vascularization (Boussat *et al.*, 2000; Gassmann *et al.*, 1996; Ladoux and Frelin, 1993; Liu *et al.*, 1995; Namiki *et al.*, 1995; Shweiki *et al.*, 1992; Tufro-McReddie *et al.*, 1997). In this respect it is very interesting to know the internal oxygen profile of a vertebrate embryo.

Here we show micro-electrode measurements of the external and internal oxygen profile of a zebrafish embryo (*Danio rerio*) in which a circulatory system is not functional yet (24-28 hours post fertilization hpf, 28°C) (Kimmel *et al.*, 1995). The measured oxygen profiles are compared with a numerical model of the oxygen consumption and diffusion dynamics inside and around a realistic representation of the shape of the embryo.

This numerical-experimental procedure (Oomens *et al.*, 1993) elucidates the internal and external oxygen profile in the zebrafish embryo. Furthermore, interesting physical properties of the embryonic tissues and yolk are revealed. These results provide a quantitative basis for a functional understanding of vertebrate vascularization.

7.2 Materials and Methods

7.2.1 Oxygen measurements

Fertilized zebrafish embryos (*Danio rerio* Hamilton) were kept in a petri-dish in a constant temperature chamber (27°C). Approximately 26 hpf (24-28 hpf), an embryo was decapsulated with two syringe needles. One embryo was embedded in the center of a cylindrical 1% low melting agarose gel (1 cm in diameter, 2 cm high) to allow a proper boundary layer build-up all around the embryo. This gel was transferred to a small water-filled box and placed underneath a clark style micro-electrode with guard cathode (Diamond General). The micro-electrode had a tip-diameter of 20 μm . A motorized x,y,z-micro-manipulator (Märzhäuser) was used to position the micro-electrode with an accuracy of 0.1 μm . The micro-electrode was forced along

the measuring trajectory through the embryo with approximately 100 μm per second. Then the micro-electrode was retracted along the same trajectory with steps of 10 μm per second and during each step the local oxygen partial pressure at the electrode tip was recorded by an Apple Macintosh II computer. The temperature of the water during the oxygen measurements was 27°C.

7.2.2 Numerical simulation

A three-dimensional equidistant ($59 \times 61 \times 67$) grid was constructed in which the medium surrounding the embryo, the embryonic tissue and the yolk were represented (Fig. 7.1).

Fick's second law of diffusion in equilibrium situation:

$$K \nabla^2 p = m \quad (7.1)$$

where K is the Krogh diffusion constant or permeability of oxygen (which in turn is the product of the oxygen diffusion coefficient D and the oxygen solubility α), p is the oxygen partial pressure and m is an oxygen consumption term, was rewritten as a difference equation using the explicit (forward-difference) method in three dimensions (Crank, 1975). The system was considered a composite medium and the continuity of flux condition across boundaries was satisfied (Crank, 1975). The difference equation was solved with a Runge-Kutta method in Matlab 6.1.

7.2.3 Input parameter values

During the simulations, the oxygen partial pressure was kept constant at the grid boundaries with a value equal to the measured bulk oxygen partial pressure. The oxygen permeability in water (Van Stroe and Janssen, 1993) at 27°C is $6.3 \times 10^{-13} \text{ m}^2/(\text{s kPa})$. The agarose gel was assumed not to significantly impede oxygen diffusion compared to water (Westrin and Axelsson, 1991). The nature of the discontinuities found in the measured oxygen profiles implied an oxygen permeability in the embryonic tissues equal to that in the surrounding medium while the oxygen permeability in yolk is higher than in the surrounding medium. The exact value of the permeability of oxygen in the yolk, as well as that of the (constant) oxygen consumption rate was determined by comparing the numerical results with the measurements and adjusting the value of the model input parameters to optimally describe the measured profile. This procedure yielded a value for the oxygen permeability in yolk which is 2.5 times higher than in the surrounding medium and an oxygen consumption rate of 5.1×10^{-4}

ml oxygen / (ml tissue s), which is about twice the routine metabolic rate previously determined for teleost embryos (Rombough, 1988). The oxygen consumption rate was taken zero for both the surrounding medium and yolk.

7.3 Results

Our micro-electrode measurements reveal a previously unknown physical property of the yolk material of a zebrafish embryo. The measurements showed clear discontinuities in the slope of the oxygen partial pressure profile. The oxygen profile in the surrounding medium was characterized by a slope at the ventral surrounding medium - yolk boundary, which was consistently steeper than that of the profile inside the yolk (Fig. 7.1 A). This implies that the permeability of oxygen in yolk is larger than the oxygen permeability in the surrounding medium, since transport over the boundary has to be continuous (Crank, 1975). The slope of the measured oxygen profiles did not show discontinuities at the boundary between the animal tissue and the surrounding medium (Fig. 7.1 A), implying an equal oxygen permeability in the surrounding medium and the embryonic tissue. This is in contrast with the observation that the oxygen permeability of adult animal tissue of various types is much lower than of water (Krogh, 1919).

Fig. 7.1 shows two representative examples of measured oxygen profiles. Profile (A) shows how oxygen partial pressure changes in a ventro-dorsal direction through the surrounding medium, the yolk material, the tissue of the embryo, and the surrounding medium again. The relatively high oxygen permeability of the yolk permits an easy oxygen transport within it and causes an increased boundary layer thickness inside the yolk at the ventral side of the embryo. The oxygen partial pressure in the center of the animal tissue falls to about one quarter of the surrounding oxygen partial pressure. Profile (B) shows oxygen partial pressure change in a lateral direction through the yolk. Here again the discontinuity representing the sudden change in oxygen permeability is prominent, while the minimum oxygen partial pressure is somewhat higher than in profile (A).

Previous oxygen distribution models for early embryos have considerably simplified the morphology (Kranenbarg *et al.*, 2000). In our numerical model, Fick's second law of diffusion is solved for an equidistant three-dimensional grid in which a zebrafish embryo (consisting of tissue and yolk) and the surrounding medium are distinguished.

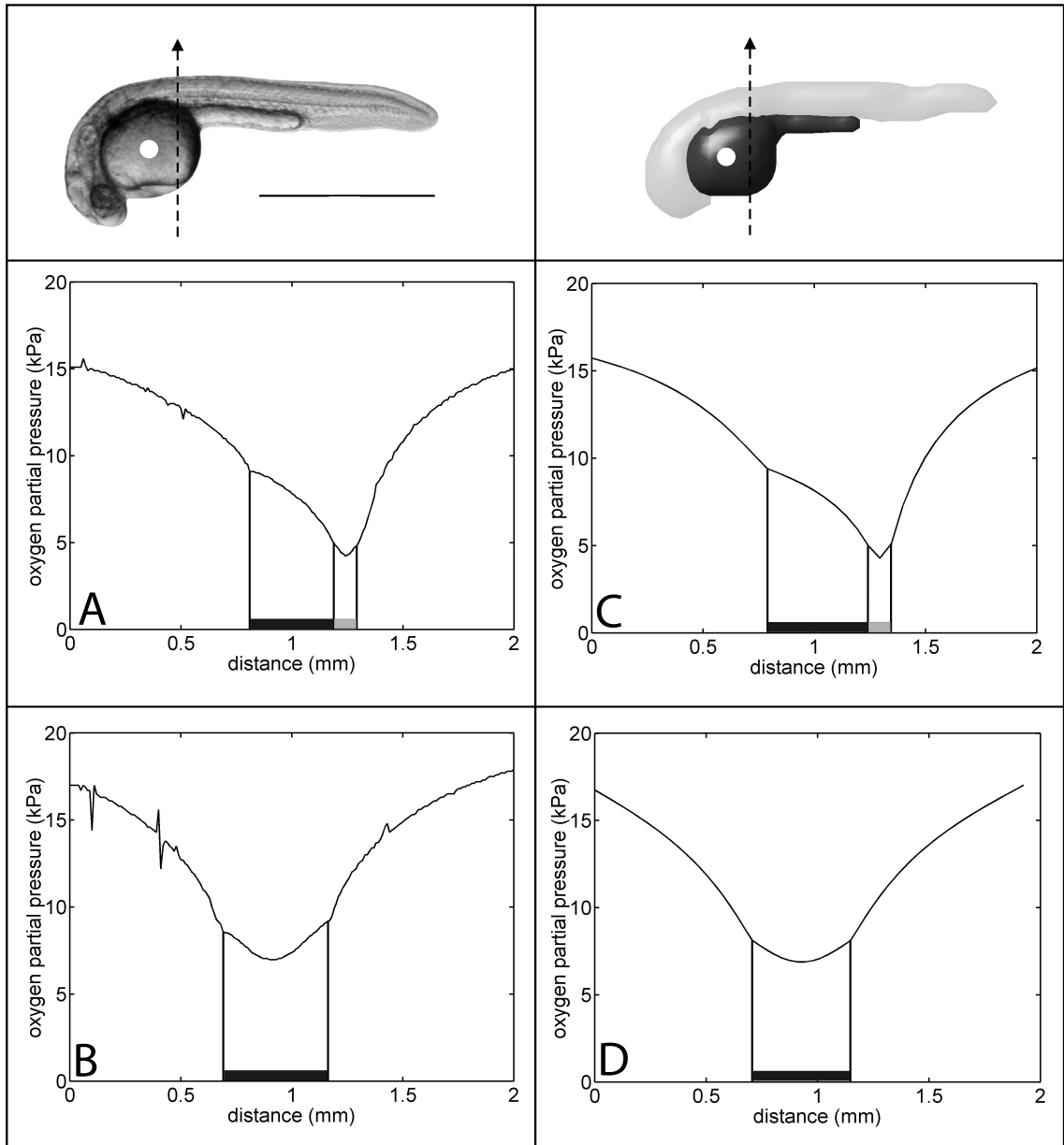


Figure 7.1: Comparison between measured (A and B) and modelled (C and D) oxygen profiles in the zebrafish embryo. (A) and (C), Oxygen partial pressure (in kPa) in ventro-dorsal direction (dashed arrow in the heading figures). B and D, Oxygen partial pressure in lateral direction through the yolk (at the level of the white spot in the heading figures). Note the discontinuity in the slope of the oxygen partial pressure profile at the surrounding medium - yolk boundary. Profile parts inside the yolk are indicated with a light bar, while profile parts inside the tissue of the embryo are indicated with a dark bar. Scale bar is 1 mm.

The shape of the embryo is realistically represented. Trajectories through the resulting three-dimensional oxygen profile, equivalent to the paths of the micro-electrode are shown in Fig. 7.1 C and D. Realistic estimates of input parameter values (see Methods section) yield predicted oxygen partial pressure profiles in close agreement with the micro-electrode measurements. Both the shape of the experimental curves and the measured values for the oxygen partial pressure are surprisingly accurately represented by the model.

Fig. 7.2 shows the complete three-dimensional oxygen profile in and around the zebrafish embryo, based on our numerical model. Fig. 7.2 A represents a sagittal section through the embryo, clearly showing the thicker boundary layer in the yolk when compared to that in the surrounding medium. As in the micro-electrode experiments, the minimum oxygen pressures are observed in the center of the animal tissues. A decrease in oxygen partial pressure along the central axis of the embryo can be observed from posterior to anterior. The thicker boundary layer in the yolk is also present in the horizontal (Fig. 7.2 B) and transverse (Fig. 7.2 C) sections.

7.4 Discussion

The oxygen permeability or Krogh diffusion constant of teleost yolk material has - to our knowledge - not been measured before. A relatively high value for this permeability in zebrafish embryos as found in our study is very advantageous to the animal. As the oxygen permeability in the yolk is higher than in the surrounding medium, the yolk sac effectively mediates oxygen transport to the oxygen consuming embryonic tissues. Replacing the yolk in our model with surrounding medium yields oxygen partial pressures close to zero inside the head of the embryo. Also the value of the oxygen permeability in embryonic tissues as found in our study implies a more rapid diffusion of oxygen into the embryo compared to adult animal tissue, which is highly advantageous when completely relying on oxygen diffusion through the skin.

The agreement between our model and experiments shows that the oxygen distribution inside the zebrafish embryo can be accurately simulated with a physically simple model. The only input parameters to the model are the bulk oxygen partial pressure, the distribution of the oxygen permeability and the oxygen consumption rate of the embryonic tissue.

Apparently, diffusion alone can meet the oxygen demands of an early zebrafish

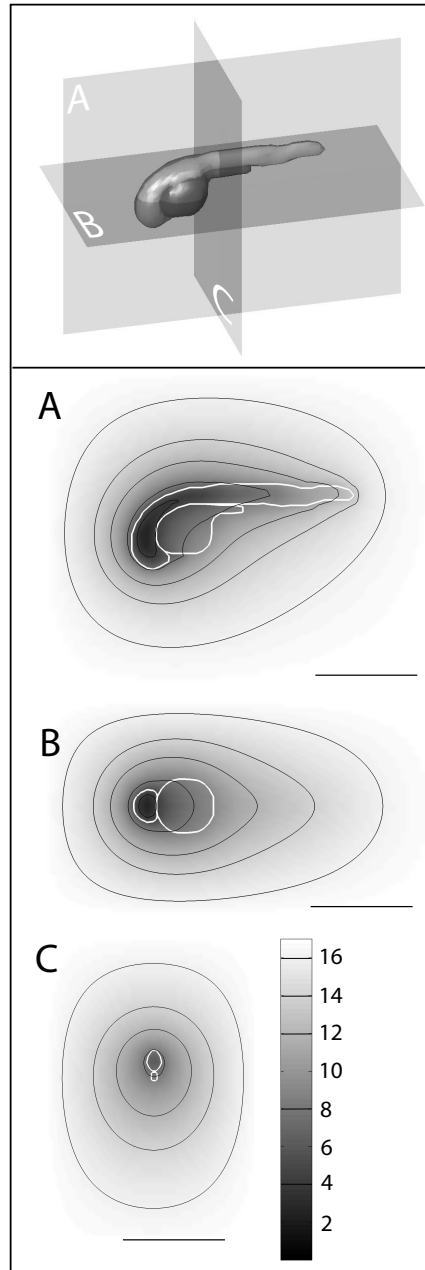


Figure 7.2: Three-dimensional predicted oxygen field surrounding the zebrafish embryo (indicated by the solid white line). A, Sagittal section through the predicted oxygen field. B, Horizontal section through the predicted oxygen field. C, Transverse section through the predicted oxygen field. The figures were obtained from the same simulation as Fig. 7.1. The pressure boundary layer extends both inside the embryo and in the medium surrounding the embryo. Oxygen partial pressure decreases along the long axis of the embryo from posterior to anterior. Minimum oxygen pressures are observed in the center of the tissue of the embryo in the anterior region. Contours of the yolk and animal tissue are indicated in the subfigures. The color bar represents oxygen partial pressure in kPa. The black contour lines represent oxygen partial pressures as indicated in the color bar. Scale bar is 1 mm.

embryo. This is in agreement with previous experiments in which haemoglobin ablation did not noticeably affect the zebrafish embryo (Pelster and Burggren, 1996). Acute anoxic stress is not likely to trigger blood vessel maturation. The predicted three dimensional oxygen profile predicts minimum oxygen partial pressures along the long axis of the embryo. Hypoxia is known to cause vascular growth factor expression (*e.g. vegf*) (Shweiki *et al.*, 1992). Therefore, we suggest that the observed oxygen gradients play a key role in vasculogenesis and angiogenesis in the zebrafish embryo (Gassmann *et al.*, 1996).

Acknowledgements

We thank dr. R.J. Wootton (University of Exeter), dr. M. Muller (Wageningen University) and dr. L. Hoofd (University of Nijmegen) for valuable comments on the manuscript.

Chapter 8

Effect of Oxygen Partial Pressure on *vegf* Expression in the Zebrafish Embryo (*Danio rerio*)¹

Vascularization of the early vertebrate embryo is comprised of vasculogenesis and angiogenesis. Vasculogenesis is thought to be mainly genetically determined, while external cues play an important role in angiogenesis. From a functional point of view, we investigated the role of oxygen on zebrafish vascularization by showing the expression pattern of the oxygen sensitive angiogenic factor *vegf* in normoxic and hypoxic conditions. Furthermore, we show a numerical simulation of the oxygen dynamics in a zebrafish embryo and correlate the predicted oxygen partial pressure profile with the *vegf* expression pattern. No differences in the *vegf* expression pattern between the normoxic and hypoxic group were observed, while the general regions showing *vegf* expressions correlate with regions of low oxygen partial pressure, predicted by the model. This led us to suggest that early vascularization of the zebrafish embryo is mainly genetically determined, where this developmental program represents functional physical constraints trapped in the genome.

8.1 Introduction

8.1.1 Vasculogenesis and angiogenesis

Vasculogenesis is the first step of cardiovascular development in the vertebrate embryo (Risau, 1997; Yancopoulos *et al.*, 2000). Vasculogenesis can be defined as ‘the differentiation of angioblasts from mesoderm and the formation of primitive blood vessels from angioblasts at or near the site of their origin’ (Risau and Flamme, 1995). Vasculogenesis is followed by ‘the vascularization of tissues as a result of sprouting

¹In preparation: Kranenbarg, S., Van der Meulen, T., Samallo, J., Schipper, H., Schutter, M., Stroband, H.W.J. and Van Leeuwen, J.L.

of new vessels from preexisting ones' which is defined as angiogenesis (Maltepe and Simon, 1998; Risau and Flamme, 1995; Weinstein, 1999). The combination of vasculogenesis and angiogenesis leads to a proper development of the early primitive vessels into functional vascular networks (Patan, 2000). An increase in the relative importance of angiogenesis in the functional development of the axial vessels can be observed from lower to higher vertebrates (Weinstein, 1999).

A complex set of vascular-specific growth factors is required for a proper cardiovascular development (*e.g.* Beck *et al.* (2000); Maltepe and Simon (1998); Patan (2000); Risau (1997); Yancopoulos *et al.* (2000)). Vascular endothelial growth factor (VEGF²) and its receptors Flt1, Flk1/KDR and Flt4 (VEGF receptors 1-3) are part of this set and play a critical role in both vasculogenesis and angiogenesis (Beck and D'Amore, 1997; Patan, 2000; Risau, 1997; Weinstein, 1999; Yancopoulos *et al.*, 2000). The respective roles of these genes are exemplified by the result of targeted disruption studies in mice embryos, which cause impaired or blocked vessel formation (Carmeliet *et al.* (1996); Ferrara *et al.* (1996) for *Vegf*^{-/-} embryos; Fong *et al.* (1995) for *Flt-1*^{-/-} embryos; Shalaby *et al.* (1995, 1997) for *Flk-1*^{-/-} embryos).

8.1.2 Effect of hypoxia

The embryonic circulatory plan of vertebrates shows a high amount of evolutionary conservation. Furthermore, the establishment of the major vessels is highly reproducible from embryo to embryo, suggesting that vasculogenesis is a largely hard wired developmental process (Weinstein, 1999), which is not influenced by the local oxygen pressure. This idea is supported by several studies. First, the notochord is shown to play an important role in signalling on the developing axial endothelium in zebrafish embryos (Brown *et al.*, 2000; Sumoy *et al.*, 1997). Second, mice embryos without a proper oxygen sensing mechanism (*Hif-1α*^{-/-}) showed no vascular abnormalities and the heart and dorsal aorta appear nearly normal up to E8.5-E8.75 (Iyer *et al.*, 1997). Finally, VEGF receptor 2/Flt-1/KDR (the only gene product known to be absolutely required for vasculogenesis in mice as no blood vessels can be observed at any stage in *Vegf* receptor 2/*Flk-1*^{-/-} embryos (Shalaby *et al.*, 1995, 1997)) is not directly up-regulated by hypoxia in human cells (Brogi *et al.*, 1996; Gerber *et al.*, 1997).

²We will adopt the following typesetting for genes and proteins, respectively, in this chapter. Referring to the human system: *VEGF* and VEGF, murine system: *Vegf* and Vegf and zebrafish: *veg*f and Vegf.

In contrast to vasculogenesis, angiogenesis appears largely dependent on environmental cues such as local oxygen pressure (Risau, 1997; Semenza, 2001; Weinstein, 1999; Yancopoulos *et al.*, 2000). Hypoxia can promote intensified vascularization through the liberation of angiogenic agents. As one of those agents, VEGF induces angiogenesis (reviewed by Dor *et al.* (2001)) since endothelial cells are stimulated to grow up a VEGF gradient (Maltepe and Simon, 1998). Hypoxia increases *VEGF* mRNA levels in mammals and birds (Boussat *et al.*, 2000; Gassmann *et al.*, 1996; Ladoux and Frelin, 1993; Namiki *et al.*, 1995; Shweiki *et al.*, 1992; Tufro-McReddie *et al.*, 1997; Yue and Tomanek, 1999) due to both an increased transcription rate (transcriptional regulation) (Ikeda *et al.*, 1995; Levy *et al.*, 1995; Liu *et al.*, 1995) and an increase in *VEGF* mRNA stability (posttranscriptional regulation) (Ikeda *et al.*, 1995; Levy *et al.*, 1996; Shima *et al.*, 1995). VEGF protein levels are also increased in mammals by hypoxia (Boussat *et al.*, 2000; Lee *et al.*, 2001).

8.1.3 Oxygen gradients and vessel development

Before the development of a cardiovascular system, embryos depend solely on diffusion for their oxygen supply. This results in the formation of oxygen gradients inside the embryo (Kranenbarg *et al.*, 2000, 2002), which constitute the environmental cues thought to be important in vascularization of the vertebrate embryo (Lee *et al.*, 2001; Maltepe and Simon, 1998).

The formation of oxygen gradients has been simulated using three-dimensional numerical methods (Kranenbarg *et al.*, 2002) and measured using oxygen micro-electrodes (Gassmann *et al.*, 1996; Kranenbarg *et al.*, 2002; Rombough, 1998). The three-dimensional oxygen profile in a zebrafish embryo as found in both the numerical predictions and the micro-electrode measurements, shows a region of lowest oxygen partial pressure in the head with a gradient of posteriorly increasing partial pressure along the midline of the embryo (Kranenbarg *et al.*, 2002).

From a functional perspective, it is interesting to explore whether oxygen (as an environmental cue) both spatially and temporally regulates vascularization of the embryo. Therefore, we analyzed the spatial and temporal expression of *vegf* in the zebrafish embryo under normoxic and hypoxic conditions. The results were compared with numerical simulations of the oxygen transport and consumption dynamics in a realistically shaped model embryo to obtain physical insight in the process of early vertebrate vascularization.

8.2 Materials and Methods

8.2.1 Embryos and oxygen treatment

Newly fertilized zebrafish embryos (*Danio rerio*) were collected. Subsequently, the batch was randomly divided into a normoxic and a hypoxic group, each consisting of approximately 75 eggs. One hour post fertilization (hpf), the eggs from the normoxic group were placed in a tea strainer inside a water-filled 1 liter beaker. A continuous air-flow was led through the water to ensure a constant, air-saturated oxygen partial pressure. The beaker was covered with a plexiglass lid to reduce evaporation. Eggs from the hypoxic group were placed in a similar set-up at the same time, yet with a continuous flow of nitrogen gas, to ensure a constant, low oxygen partial pressure. The oxygen partial pressure in the hypoxic group was continuously monitored during the experiment with a clark style micro-electrode (Diamond General). The temperature in both beakers was 28°C during the entire experiment. The air-saturated oxygen partial pressure was 21.6 kPa, while the oxygen partial pressure in the hypoxic group was 4.5 ± 1.6 kPa, which amounts to about 21 % of the air air-saturated partial pressure.

The developing embryos were sampled (6-10 eggs per sample) from both the normoxic and the hypoxic groups at 1 hpf, 8.75 hpf, 10.5 hpf, 12.5 hpf, 18.5 hpf, 24 hpf and 30 hpf. The eggs were fixed in 4% paraformaldehyde (PFA) in PBS and stored at 4°C.

8.2.2 Whole mount *in situ* hybridisation and cryosectioning

An α -sense digoxigenin labelled *vegf* probe was generated starting from a pBluescript SK vector containing a 1.1 kb 5'RACE zebrafish *vegf* insert, which was kindly provided by dr. Ruowen Ge from the Department of Biological Sciences of the National University of Singapore. The insert encodes the 5' end of *vegf* coding region and 5' untranslated region (5'UTR) (Liang *et al.*, 1998).

The *vegf*-probe was used to carry out whole mount *in situ* hybridisation. The *in situ* hybridisation method used here is essentially as described in Stroband *et al.* (1995), with the following modifications. After fixation in 4% PFA at 4°C for at least 24 hours, the embryos were mechanically decapsulated and washed in PBST (PBS buffer/0.1% Tween-20). Before the 2 hours incubation in prehybridization

mix at 70°C, the embryos were incubated for 7 min in prehybridization mix without tRNA and heparin. Hybridization took place overnight at 70°C using the *vegf*-probe. The optimal probe dilution was determined experimentally. The embryos were rinsed at 70°C in prehybridisation mix and subsequently washed at 70°C in 50% formamid/2×SSCT (SSC solution/0.1% Tween-20) for 15 min, 25% formamid/2×SSCT for 15 min, 2×SSCT for two times 15 min, 0.2×SSCT for two times 30 min, 0.2×SSCT for 15 min and allowed to cool to room temperature (RT) during this last washing step. The embryos were washed two times 10 min in PBST at RT and incubated 4 hours at RT with 1% blocking solution (PBST-BL, Roche Biochemicals), before overnight probe detection at 4°C with alkaline phosphatase labelled α -DIG-Fab fragments. Embryos were rinsed and subsequently washed six times 15 min in PBST-BL and two times 5 min in PBST. After a three times 5 min wash in AP buffer (0.1 M Tris/0.1 M NaCl/0.05 M MgCl₂/0.1% Tween-20), the probe was visualized by incubation with nitro blue tetrazolium (NBT, Roche Biochemicals) and 5'-bromo-4'-chloro-3'-indolyl phosphatase (BCIP, Roche Biochemicals) according to the manufacturers protocol. When the resulting deep purple color was first seen intense enough in some embryos, all embryos were washed simultaneously three times 5 min in PBST, fixed in 4% PFA in PBS, and stored at 4°C.

The embryos were photographed in PBST with a Zeiss Stemi SV11 dissecting microscope in combination with an Olympus DP50 digital camera with accompanying analySIS[®] software. After photographing, sections of whole-mount stained embryos were prepared by cryosectioning as essentially described by Stevens *et al.* (1998). The postfixation in 4% PFA/0.2% glutaraldehyde/PBS was omitted. The sections were photographed with the Olympus DP50 digital camera, mounted on a Nikon microphot-FXA microscope.

8.2.3 Simulation of oxygen dynamics

In order to realistically simulate the oxygen dynamics inside a zebrafish embryo, an analysis of the oxygen transport mechanisms in the surrounding medium is inevitable. Dimensionless number theory provides a suitable framework to carry out this analysis.

The dimensionless Sherwood number (Sh) is a measure for the ratio of total mass transfer over diffusive mass transfer. The dimensionless Péclet number (Pe) is a measure for the ratio of convective mass transfer over diffusive mass transfer. These dimensionless numbers are employed to describe the transport dynamics of oxygen to

spheres and to calculate the oxygen partial pressure at the egg surface.

Intermezzo 4.4 gives a relation between the Sherwood number and the Péclet number for a sphere in Stokes flow:

$$Sh = 0.978Pe^{1/3} + 1.38 \quad (8.1)$$

For the spherical zebrafish egg, the Sherwood number can also be defined as (Daykin, 1965)

$$Sh = \frac{2a^2m}{3K(pO_2^{amb} - pO_2^s)} \quad (8.2)$$

where a is the egg radius [m], m is the volume-specific oxygen consumption [$\text{m}^3/(\text{m}^3 \text{ s})$], K is the oxygen permeability in water [$\text{m}^2/(\text{kPa s})$], pO_2^{amb} is the free water oxygen partial pressure [kPa] and pO_2^s is the (assumed constant) oxygen partial pressure at the egg surface [kPa]. Together, equations 8.1 and 8.2 present a relation between the Péclet number and the oxygen partial pressure at the egg surface, pending the oxygen consumption m .

Grunwald *et al.* (1988) showed that zebrafish embryos of 29 hpf (when blood circulation starts) bend their body about 7 times per minute. As it takes several minutes for the equilibrium in the diffusion of oxygen to settle (Kranenbarg *et al.*, 2000), it is safe to assume that these muscular contractions will stir and homogenize the perivitelline fluid with respect to oxygen partial pressure (Wickett, 1975). This stirring of the perivitelline fluid validates the assumption of a constant and equal oxygen partial pressure both at the egg capsule and the skin surface of the embryo. This partial pressure was calculated for a Péclet number of 100 (representing a flow velocity of several hundreds of micrometers per second (Kranenbarg *et al.*, 2001)) and used as a boundary condition in a numerical simulation of oxygen transport and consumption in the zebrafish embryo as essentially described by Kranenbarg *et al.* (2002). Except the boundary oxygen partial pressure, all parameter values are equal to Kranenbarg *et al.* (2002).

8.3 Results

8.3.1 *vegf* expression

Expression of *vegf* was detected in all stages analyzed. The spatial expression pattern of the normoxic group was comparable to that described previously by Liang *et al.*

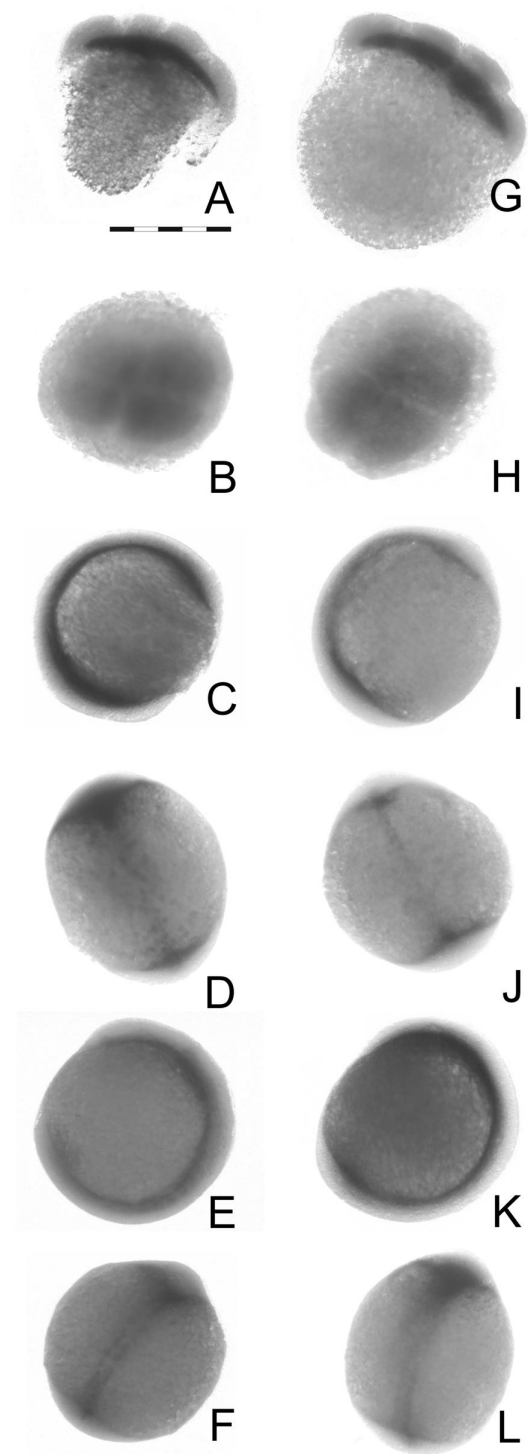


Figure 8.1: *veg*f expression in three embryonic stages of the zebrafish. Embryos raised under normoxic conditions (A-F) are compared with embryos raised under hypoxic conditions (G-L). A,B,G,H: 4-8 cell stage embryos in lateral (A,G) and top view (B,H); C,D,I,J: 10.5 hpf embryos in lateral (C,I) and dorsal view (D,J) and E,F,K,L: 12 hpf embryos in lateral (E,K) and dorsal view (F,L). Scale bar is 500 μ m.

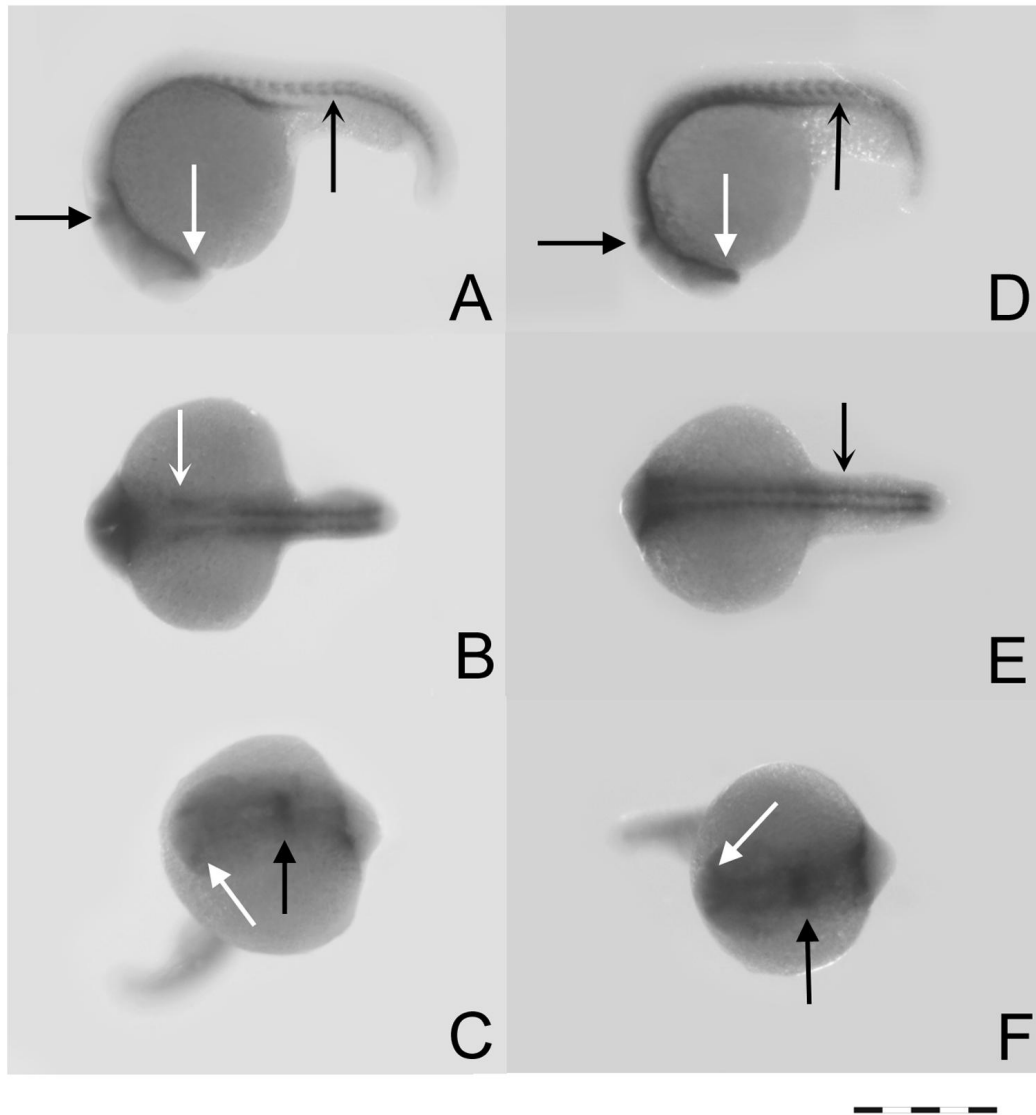


Figure 8.2: *vegf* expression in 18-19 hpf zebrafish embryos. Embryos raised under normoxic conditions (A-C) are compared with embryos raised under hypoxic conditions (D-F). Four regions of *vegf* expression can be determined: anterior forebrain (arrows with straight white heads), mesoderm underlining and lateral to the anterior hindbrain (arrows with straight black heads), mesoderm underlining and lateral to the posterior hindbrain (arrow with concave white head), and the ventro-medial portion of each somite, adjacent to the notochord (arrows with concave black heads). Scalebar is 500 μm .

(1998, 2001). In the 4 cell stage (1 hpf), all 4 cells showed *vegf* mRNA in the region adjacent to the yolk (Fig. 8.1 A,B). At 80% epiboly (8.75 hpf), *vegf* was expressed in the dorsal region of the embryo (data not shown). At 10.5 hpf, *vegf* is expressed throughout the embryo, adjacent to the yolk (Fig. 8.1 C,D). At 12 hpf, *vegf* is clearly expressed bilaterally along the entire length of the embryo in the region directly on top of the yolk (Fig. 8.1 E,F). At 18.5 hpf, *vegf* is expressed bilaterally in regions comparable to the four regions described by Liang *et al.* (1998) (anterior forebrain, mesoderm underlining and lateral to the anterior hindbrain, mesoderm underlining and lateral to the posterior hindbrain, and the ventro-medial portion of each somite, adjacent to the notochord (Fig. 8.2). In addition to the four regions described by Liang *et al.* (1998), we also found *vegf* expression in a region directly on top of the yolk at the beginning of the yolk sac extension (Fig. 8.2 A); the region of pronephros development (Drummond *et al.*, 1998). Cryosections confirmed the global localization of this expression pattern. A similar expression pattern was found in 24 hpf embryos, although the details of the *vegf* expression in the head region were not examined. In 30 hpf embryos, the somite expression was greatly reduced, while the expression in the region of pronephros development was extended posteriorly (Fig. 8.3). None of the control animals (in which the probe hybridization step was omitted) showed any coloring.

Both the spatial and temporal expression pattern of *vegf* under hypoxic conditions in the stages examined, were highly comparable to those in normoxic conditions (Fig. 8.1 G-L). Although some differences in color intensity of the whole mount embryos can be observed, these differences could not be attributed to the oxygen treatment since the variation in color intensity also existed within a treatment group. At 12 hpf, a bilateral expression as seen in the normoxic group was not found equally clear in the hypoxic group (Fig. 8.1 L). The consistency of this difference has yet to be determined in larger scale experiments.

The photographs of the 18.5 hpf embryos show a lagging behind of brain development in the hypoxic animals (Fig. 8.2). This difference was not observed consistently in the other hypoxic animals. However, from 18.5 hpf onwards hypoxic embryos did show a consistent lagging behind in pigmentation. In addition, at 30 hpf a pericardial edema was observed in 3 out of 6 hypoxic embryos.

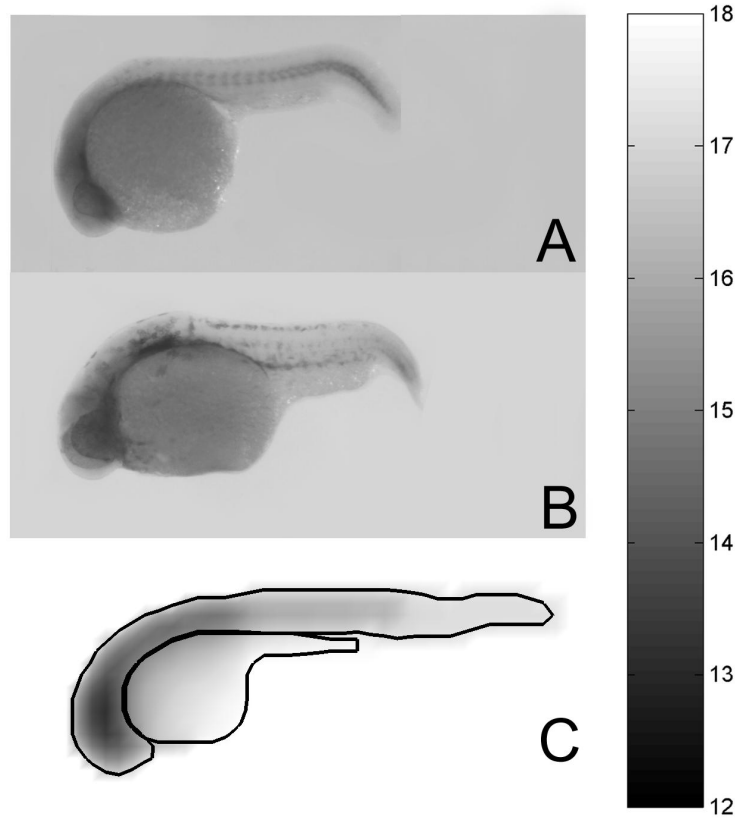


Figure 8.3: *vegf* expression in 24 hpf zebrafish embryo (A) and 30 hpf embryo (B), both with the tail curved upwards. Subfigure C shows the results of our numerical simulation of the oxygen dynamics. The colorbar on the right gives oxygen partial pressure in kPa.

8.3.2 Simulation of oxygen dynamics

We made a simulation of the oxygen transport and consumption dynamics in a zebrafish embryo with stirring of the perivitelline fluid. The oxygen partial pressure gradient between the bulk flow and the embryo surface was 3 kPa. The results of the numerical simulation are shown in Fig. 8.3, together with the ISH result of a 24 and 30 hpf normoxic embryo. The oxygen partial pressure at the body surface of the model embryo is constant. The lowest oxygen partial pressure can be observed in the head region, with a gradient of increasing oxygen pressure in posterior direction (Fig. 8.3 C). In the embryonic tissues on top of the yolk, the minimum oxygen partial pressure in dorso-ventral direction are located just ventral to the midline of the embryo.

8.4 Discussion

In tissues that are in active vascularization, *vegf* is known to be expressed and to play an important role (Beck and D'Amore, 1997; Liang *et al.*, 2001; Patan, 2000; Risau, 1997; Weinstein, 1999; Yancopoulos *et al.*, 2000). Furthermore, *Vegf* expression is sensitive to local oxygen conditions in mammals, with hypoxia increasing *vegf* mRNA levels (Boussat *et al.*, 2000; Gassmann *et al.*, 1996; Ladoux and Frelin, 1993; Namiki *et al.*, 1995; Shweiki *et al.*, 1992; Tufro-McReddie *et al.*, 1997). In order to clarify the role of local oxygen conditions in the vascularization of the early zebrafish embryo, we examined the effect of ambient oxygen partial pressure on the spatial and temporal expression pattern of *vegf* in the zebrafish embryo.

Not surprisingly, the expression pattern in normoxic embryos was highly comparable to that previously published by Liang *et al.* (1998, 2001). Low ambient oxygen partial pressure, however, changed neither the temporal nor the spatial *vegf* expression pattern in early zebrafish embryos, as far as can be judged from the current analysis of our *in situ* hybridizations.

We did, however, study the expression pattern on a whole embryo scale, with some preliminary cryosectioning to further localize the *vegf* expression. More detailed differences in the *vegf* expression pattern between the normoxic and hypoxic group have yet to be investigated. Furthermore, as *in situ* hybridization is not an adequate technique to quantify gene expression (Ikeda *et al.*, 1995; Levy *et al.*, 1995; Liu *et al.*, 1995), differences in the amount of *vegf* mRNA between the two experimental groups have not been detected. Quantitative polymerase chain reaction (PCR) techniques or RNase protection arrays could shed some light on this subject. The amount of *vegf* mRNA is determined by the transcription rate and its stability, both of which are potentially increased by hypoxia (Ikeda *et al.*, 1995; Levy *et al.*, 1995; Liu *et al.*, 1995; Shima *et al.*, 1995). As only the *Vegf protein* and not the mRNA can perform a functional task in vascularization, the effect of hypoxia on the actual amount of functional *Vegf* protein produced should be examined (Boussat *et al.*, 2000; Lee *et al.*, 2001).

Although several issues still have to be resolved, large differences in *vegf* expression patterns under normoxic and hypoxic conditions have not been found. During early organogenesis, the heart and blood vessels of the zebrafish embryo form by the process of vasculogenesis. This process is thought to be a mainly predetermined, genetically controlled developmental process. This idea is supported by our experiments.

We did see hypoxic embryos to lag behind in pigmentation with respect to normoxic embryos. This suggests that hypoxia slows down development. This effect of oxygen on early development has been shown *in extremo* by Padilla and Roth (2001), who found anoxia to completely stop zebrafish development and to elicit a state of suspended animation. In addition, the observed pericardial edema (common to many cardio-vascular and hematopoietic mutants (Chen *et al.*, 1996; Stainier *et al.*, 1996; Weinstein *et al.*, 1996)) in the hypoxia group suggests a more specific adverse effect of hypoxia on vascularization. The pathways through which hypoxia achieves this effect still have to be resolved. A similar phenotypic effect was found in both Vegf loss and gain of function studies in zebrafish embryos (Liang *et al.*, 2001; Nasevicius *et al.*, 2000).

Yet how does the *vegf* expression pattern compare with the local oxygen partial pressure in the embryo? We did not measure the local internal oxygen partial pressure of embryos raised in a well-stirred medium, though we did make a numerical simulation of the oxygen consumption and transport dynamics in a zebrafish embryo. When comparing the results of our numerical simulation with the actual *vegf* expression pattern, some interesting similarities emerge. The lowest oxygen pressure is predicted in the head region, which coincides with the most extensive expression of *vegf* found in the head. Furthermore, low oxygen pressures were predicted along the central axis in the trunk and tail region. And compared with the predictions in a stagnant medium (Kranenbarg *et al.*, 2002), the region of low oxygen partial pressure in the head is shifted towards the yolk. The same pattern can roughly be found in the *vegf* expression. This shows that vegf expression is roughly associated with relatively hypoxic regions.

A more detailed analysis of *vegf* expression is needed to elucidate smaller scale correlations. This analysis should be compared with the results of a more detailed numerical model, integrating a more differentiated representation of the animal tissues with local oxygen consumption differences. More detailed oxygen partial pressure measurements (with an oxygen micro-electrode or immuno-histo-chemical staining (Lee *et al.*, 2001)) can be employed to validate the model. This more detailed numerical-experimental procedure (Oomens *et al.*, 1993) might also detect small scale differences in oxygen partial pressure and *vegf* expression between the normoxic and hypoxic group.

Anticipating these more detailed studies, the following picture of early zebrafish

vascularization emerges. The heart and large vessels (such as the aorta) in the zebrafish are formed by a process called vascularization. This process seems largely determined by phylogenetic constraints. Smaller vessels, emerging later in development, are formed by the process of angiogenesis. This process appears to depend largely on environmental cues such as local oxygen pressure (Lee *et al.*, 2001), representing physical constraints. The regions in which vasculogenesis takes place coincide with regions of low oxygen pressure. Thus, the phylogenetic constraints regulating vasculogenesis can in fact be hypothesized to be physical constraints being trapped in the genome.

Acknowledgements

Dr. Ruowen Ge (School of Biological Sciences, Faculty of Science, National University of Singapore) is greatly acknowledged for generously providing the *vegf* plasmid.

Summary

The embryonic development of all more than 50,000 extant species of vertebrates (Harvey Pough *et al.*, 2002), is characterized by a period of remarkably low morphological variability between species. During this so-called phylotypic period, all embryos express the archetype of the vertebrate body plan. Development of the vascular system is one of the important and interesting processes taking place during the phylotypic period.

Knowledge on the genetic regulation of vascularization is vastly accumulating over the past decade. Regulation by environmental factors is also recognized (*e.g.* Maltepe and Simon (1998)), though a quantitative basis for a proper analysis appears to be lacking. The research described in this thesis aims to link qualitative and semi-quantitative molecular-genetic research on vascularization on the one hand with quantitative physical modelling on the other hand.

Fertilized vertebrate eggs lack a circulatory system and the early embryo relies solely on diffusion from the surrounding medium for its oxygen and nutrient supply. As diffusion can only be effective over short distances, the absence of a circulatory system limits the maximum size of embryos. Analytical models were employed to gain insight in the process of oxygen and nutrient diffusion and to predict the maximum size a vertebrate embryo can attain. The analysis showed that equilibrium between supply and consumption of oxygen can safely be assumed, which greatly facilitated further modelling (chapter 3).

Analytical models of oxygen diffusion in and around a specified shape showed that only three parameters are important in predicting the maximum size (based on oxygen requirements) of embryos living in either a stagnant or a very turbulent environment. Two of these three parameters are physical properties of the environment and embryo, *i.e.* the oxygen diffusivity and the oxygen solubility, while the third is a biological property of the embryo; the volume-specific oxygen consumption (chapter 3).

Values for these three parameters were found in the literature for several teleost

embryos and the predicted maximum size was compared with the actual size of the embryos. The equilibrium models (consumption equals supply) generally predicted maximum sizes larger than the actual ones and it was concluded that “diffusion across the body surface of teleost embryos is adequate for their oxygen supply even beyond the time a circulatory system is functional” (chapter 3).

The functional aspects of nutrient distribution in early blood vessel development were assessed in chapter 4. This chapter presents an application of the analytical models to the diffusion of nutrients, together with an implementation of the effect of a simplified vessel inside a zebrafish embryo. Since nutrient molecules are larger than oxygen molecules, the diffusivity of nutrients is much smaller than that of oxygen. The analysis suggested that “zebrafish embryos ... are restricted in their growth by nutrient but not by oxygen demand, and need their circulatory system for nutrient but not oxygen transport” (chapter 4).

These indications of physical constraints on body size from nutrient supply are very promising, but need further research to reach quantitative conclusions. The remainder of this thesis, however, focusses on the interplay between the supply and consumption of oxygen and vertebrate development. In the preceding chapters 3 and 4, the environment of the vertebrate embryo was either assumed stagnant or well stirred. As these conditions hardly occur in nature, the effects of forced convection with intermediate flow velocities were analyzed in chapter 5. Dimensionless number theory provided the framework for a theoretical relation between flow velocity and maximum size of the embryo, based on oxygen supply and demand. The shape of the embryo appeared to influence this relationship. At large flow velocities of the surrounding medium, a flattened shape is most favorable for gas exchange, while at very small flow velocities, a spherical shape is to be preferred. This can be explained as follows: since at high flow velocities, the oxygen diffusion boundary layer is continuously being refreshed at the body surface, a large surface-to-volume ratio, and thus a flattened shape, is favorable. At small flow velocities, however, an oxygen-poor boundary layer will develop around the embryo. Therefore, being able to obtain oxygen from as many directions as possible, and thus a spherical shape, is most favorable. Physical phenomena such as forced convection, free convection, thermal stirring and wind assure a certain minimum flow velocity of the surrounding medium of teleost embryos and thereby the flattened shape to be the most favorable (chapter 5).

The conjecture of changing optimal shapes with flow velocity was confirmed in

chapter 6. This chapter serves as a mathematical overview of the analytical modelling possibilities. In contrast with the models from previous chapters, the analytical model presented in this chapter integrates three important aspects of modelling oxygen transport to small organisms: variable shape, variable oxygen consumption pattern and variable external flow conditions. The combination of these aspects into one model allows an broad analysis of the constraints oxygen transport sets on the size and shape of organisms that do not have an active internal oxygen transport mechanism. The predictions from this integrative model support the main conclusions from chapters 3 and 5 (chapter 6).

With an overview of the analytical modelling possibilities of oxygen dynamics presented in chapter 6 and the preceding chapters, we had gained both qualitative and quantitative insight in the oxygen transport and consumption dynamics. Furthermore, we elucidated the constraints set on embryo size and morphology by oxygen diffusion and showed oxygen not to be a constraining factor. All analytical models, however, grossly simplified the morphology of the embryos. This shortcoming was alleviated in chapter 7, which presents a numerical model of the oxygen transport and consumption dynamics in a realistically shaped zebrafish embryo. The model predictions were compared with micro-electrode *in vivo* oxygen partial pressure measurements. This numerical-experimental procedure resulted in the spatial oxygen partial pressure profile in and around the zebrafish embryo. Lowest oxygen partial pressures were found in the head with a gradient of posteriorly increasing partial pressure along the midline of the embryo. The procedure further revealed that oxygen permeability in yolk material is remarkably high. This is very advantageous for the animal and prevents nearly anoxic conditions to develop inside the head region. Whereas the oxygen permeability of adult tissue of several vertebrate species has been found to be much lower than that of water, the permeability in embryonic tissues of zebrafish appears to be close to that of water (chapter 7).

Several angiogenic factors are known to respond to low oxygen partial pressures by stimulating vascularization. Therefore, detailed knowledge of the three-dimensional oxygen partial pressure profile is essential for a complete understanding of vertebrate vascularization.

In chapter 8, we showed the expression pattern of one such factors (vascular endothelial growth factor, *vegf*) under normoxic and under hypoxic conditions. Under normoxic conditions, *vegf* is expressed most extensively in the head of the embryo and

bilaterally in the ventro-medial part of the somites, as previously described (Liang *et al.*, 1998, 2001). Hypoxia did not noticeably affect the spatial and temporal expression pattern of *vegf* in the early zebrafish embryo, though it did slow down normal development. These results suggest the early vascularization of the zebrafish embryo (vasculogenesis) to be mainly determined by phylogenetic constraints.

The *in situ* hybridization results were compared with a numerical simulation of the oxygen transport and consumption dynamics. A spatial similarity could be observed between predicted regions of low oxygen partial pressure and the expression of *vegf*. This suggests the phylogenetic constraints to be physical constraints being trapped in the genome.

Taken together, chapters 7 and 8 help to understand the probable signalling pathways that actually bridge the gap between quantitative physical modelling and qualitative molecular genetic research. The combination of the two yields important insight in the process of vascularization and provides a promising new research field.

In the introduction, the general goal of this thesis was formulated as unravelling physical and phylogenetic constraints in the development of blood vessels in vertebrate embryos. Does the circulatory system develop to overcome oxygen shortage by the time it becomes functional in the growing embryo? It can now be concluded that the answer to this question must be negative. Both our analytical models and our numerical model shows that by the time a functional circulatory system is present, diffusion alone is still adequate for a proper oxygen supply (*cf.* chapters 3, 5, 6 and 7). The results of a hemoglobin ablation experiment by Pelster and Burggren (1996) also questioned the role of the early blood vessel system in oxygen transport and thus supports our conclusion. Apparently, ontogeny incorporates a safety factor to ensure a proper circulatory system to be present before its functioning is actually required.

Although the circulatory system does not develop to overcome acute anoxia, hypoxic conditions might still act as cues to regulate vessel development. This, however, could not be experimentally demonstrated and circulatory system development appears largely genetically determined (chapter 8), at least for the initial part of vascularization (vasculogenesis). Yet other studies show oxygen to influence vessel development and the onset and extent of environmental influences on vertebrate vascular development remains to be determined.

Another interesting aspect of vertebrate vascularization is the effect of other factors than oxygen as possible physical constraints on development (*e.g.* waste transport, transport of signalling molecules, hormones *etc.*). Nutrient distribution appears a promising candidate as the primary function of the functional circulatory system (chapter 4) though further research is needed to elucidate its effects.

Samenvatting

De embryonale ontwikkeling van alle meer dan 50.000 soorten gewervelde dieren, wordt gekenmerkt door een periode met weinig morfologische variatie. Gedurende deze zogenoemde fylotypische periode, vertonen alle embryo's het archetype van het bouwplan van de gewervelde dieren. De ontwikkeling van het bloedvatstelsel is een belangrijk en interessant proces dat plaatsvindt tijdens de fylotypische periode.

De kennis over genetische regulatie van bloedvatontwikkeling is het laatste decennium sterk toegenomen. Regulatie door omgevingsfactoren wordt nu erkend, maar een kwantitatieve basis voor verdere analyse ervan lijkt grotendeels afwezig. Het onderzoek dat in dit proefschrift beschreven wordt, is erop gericht om het kwalitatieve en semi-kwantitatieve moleculair-genetische onderzoek te koppelen aan kwantitatieve fysische modellering van dit proces.

Bevruchte eieren van gewervelde dieren bezitten nog geen bloedvatstelsel en het vroege embryo vertrouwt volledig op diffusie voor de aanvoer van zuurstof en voedingsstoffen. Aangezien diffusie alleen effectief is over kleine afstanden, zal de afwezigheid van een bloedvatstelsel de maximale grootte van de embryo's beperken. We hebben analytische modellen gemaakt om inzicht te krijgen in het diffusieproces en om de maximale grootte van de embryo's te kunnen voorspellen. Deze analyse toonde aan dat zeer snel evenwicht bereikt wordt tussen de aanvoer en consumptie van zuurstof, wat verdere modellering veel makkelijker maakte (hoofdstuk 3).

Analytische modellen van zuurstofdiffusie binnenin en rondom een bepaalde vorm, toonde aan dat slechts drie parameters belangrijk zijn voor het voorspellen van de maximale grootte (gebaseerd op zuurstofbehoefte) van embryo's in een ofwel stilstaand ofwel zeer snel stromend medium. Twee van deze drie parameters zijn fysische eigenschappen van de omgeving en het embryo (diffusiecoëfficiënt van zuurstof en de zuurstofoplosbaarheid), terwijl de derde parameter een biologische eigenschap van het embryo is (volumespecifieke zuurstofconsumptie, hoofdstuk 3).

Waarden van deze drie parameters hebben we in de literatuur gevonden voor

diverse soorten vissenembryo's. De daarmee voorspelde maximale grootte van deze embryo's hebben we vergeleken met de werkelijke grootte. De evenwichtsmodellen (waarin de consumptie gelijk is aan de toevoer) voorspelden over het algemeen een maximale grootte die groter was dan de werkelijke grootte van het embryo. Op basis hiervan hebben we geconcludeerd dat diffusie over het lichaamsoppervlak van vissenembryo's voldoende is voor de toevoer van zuurstof, zelfs nog als een functioneel bloedvatstelsel aanwezig is (hoofdstuk 3).

De functionele aspecten van het transport van voedingsstoffen in een vroeg bloedvatstelsel, hebben we onderzocht in hoofdstuk 4. Dit hoofdstuk beschrijft een toepassing van de analytische modellen op de diffusie van voedingsstoffen, gecombineerd met de effecten van een simpel bloedvat in een zebravisembryo. Aangezien voedingsstoffen bestaan uit grotere moleculen dan zuurstof, zullen ze over het algemeen minder makkelijk diffunderen. De analyse maakte aannemelijk dat zebravisembryo's in hun grootte beperkt worden door de toevoer van voedingsstoffen en niet door die van zuurstof. Het vroege bloedvatstelsel lijkt nodig voor het transport van voedingsstoffen en niet van zuurstof (hoofdstuk 4).

Deze aanwijzingen dat voedingsstoffen de lichaamsgrootte van embryo's kunnen beperken, zijn veelbelovend, maar behoeven nog verder onderzoek om kwantitatieve conclusies te kunnen trekken. De rest van het proefschrift gaat daarentegen over het samenspel tussen toevoer en consumptie van zuurstof aan de ene kant en de ontwikkeling van gewervelde dieren aan de andere kant. In de voorgaande hoofdstukken 3 en 4 werd aangenomen dat het medium rond het embryo ofwel helemaal stilstond of heel erg snel bewoog. Deze condities zijn echter in de natuur nauwelijks te vinden en daarom hebben we in hoofdstuk 5 de effecten van intermediaire stroomsnelheden onderzocht. Gebaseerd op de toevoer en consumptie van zuurstof, werd een theoretische relatie afgeleid tussen stroomsnelheid en maximale grootte van een embryo. De vorm van het embryo bleek deze relatie te beïnvloeden. Bij hoge stroomsnelheden van het medium bleek een platte vorm het gunstigst voor zuurstofopname, terwijl bij zeer lage stroomsnelheden een bolvorm juist gunstiger was. Dit kan als volgt worden verduidelijkt. Bij hoge stroomsnelheden wordt er continu zuurstofrijk water aangevoerd en zal dus continu aan de huid van het embryo een hoge zuurstofconcentratie heersen. Een relatief groot huidoppervlak, en dus een platte vorm, is in deze situatie zeer gunstig. Bij zeer geringe stroomsnelheden, zal zich een zuurstofarme grenslaag om het embryo heen ontwikkelen. In deze situatie is het juist gunstig om zuurstof

vanuit zoveel mogelijk richtingen te kunnen benutten en dus om bolvormig te zijn. Fysische fenomenen zoals externe stroming, vrije convectie, thermische beweging en wind zorgen in de natuur altijd voor een bepaalde minimale stroomsnelheid rondom vissenembryo's, waardoor een platte vorm het gunstigst is (hoofdstuk 5).

De vinding dat de meest optimale vorm voor gasuitwisseling afhangt van de stroomsnelheid, werd bevestigd in hoofdstuk 6. Dit hoofdstuk geeft een wiskundig overzicht van de analytische modelleermogelijkheden. In tegenstelling tot de voorgaande hoofdstukken incorporeert het analytische model uit dit hoofdstuk drie belangrijke aspecten van het zuurstoftransport naar kleine organismen: variabele vorm, variabel zuurstofconsumptiepatroon en variabele externe stromingscondities. De combinatie van deze drie aspecten in één model, maakt een zeer brede analyse mogelijk van de beperkingen die zuurstoftransport oplegt aan grootte en vorm van organismen die nog geen actief intern zuurstoftransportsysteem hebben. De conclusies van dit integratieve model onderschrijven de belangrijkste conclusie uit de hoofdstukken 3 en 5 (hoofdstuk 6).

Met het overzicht van de analytische mogelijkheden om het probleem van zuurstofdiffusie te modelleren uit hoofdstuk 6 en voorgaande hoofdstukken, hadden we zowel kwalitatief als kwantitatief inzicht gekregen in de dynamica van het zuurstoftransport en -consumptie. Verder hadden we de beperkingen die zuurstofdiffusie oplegt aan zowel grootte als vorm van embryo's geanalyseerd en ontdekt dat zuurstof geen beperkende factor lijkt. Alle analytische modellen vereenvoudigen echter in zeer sterke mate de vorm van het embryo. Dit nadeel werd aangepakt in hoofdstuk 7, dat een numeriek model laat zien van het transport en de consumptie van zuurstof in een realistisch gevormd zebravisembryo. De voorspellingen van dit model werden vergeleken met *in vivo* micro-elektrode metingen van de partiële zuurstofdruk. Deze numeriek-experimentele methode resulteerde in het drie-dimensionale partiële drukprofiel van zuurstof in en rondom het zebravisembryo. De laagste partiële zuurstofdruk werd gevonden in de kopregio, terwijl de partiële druk hoger werd richting de staart van het embryo. De procedure liet verder zien dat de permeabiliteit van zuurstof in de dooier verrassend hoog is. Dit is erg voordelig voor het embryo en voorkomt zelfs bijna-anoxische omstandigheden het kopgebied. Terwijl de zuurstofpermeabiliteit in weefsel van diverse soorten volwassen gewervelde dieren lager is dan die in water, lijkt deze permeabiliteit in weefsel van de embryonale zebravis niet te verschillen van die in water (hoofdstuk 7).

Van diverse factoren die belangrijk zijn bij de vorming van bloedvaten, is bekend dat zij gevormd worden onder invloed van lage zuurstofspanningen. Daarom is gedetailleerde kennis van het drie-dimensionale partiële drukprofiel van zuurstof belangrijk voor een compleet begrip van de bloedvatvorming in gewervelde dieren.

In hoofdstuk 8 lieten we het expressie-patroon zien van één van deze factoren (vascular endothelial growth factor, *vegf*) onder normoxische en hypoxische condities in een zebravisembryo. Onder normoxische omstandigheden komt *vegf* het sterkst tot expressie in de kop van het embryo en bilateraal in het ventro-mediale deel van de somieten (vgl. Liang *et al.* (1998, 2001)). Hypoxia had geen zichtbaar effect op het spatiële en temporele expressiepatroon van *vegf* in het vroege zebravisembryo. De lage zuurstofspanningen hadden echter wel een generieke verlaging van de ontwikkelingssnelheid tot gevolg. Op basis van deze resultaten kan gesteld worden dat de vroege bloedvatontwikkeling (vasculogenese) in het zebravisembryo voornamelijk door genetische factoren wordt bepaald.

De *in situ* hybridizatie-resultaten werden vergeleken met numerieke simulaties van zuurstoftransport en -consumptie. De plaatsen in het embryo waar de laagste zuurstofspanningen voorspeld werden, kwamen grofweg overeen met de plaatsen waar *vegf* tot expressie kwam. Dit pleit voor de stelling dat de eerder genoemde genetische factoren in principe fysische beperkingen zijn die zijn vastgelegd in het genoom.

Samen geven hoofdstukken 7 and 8 enige aanwijzingen die uiteindelijk moeten leiden tot het slaan van een brug tussen de kwantitatieve fysische modelvorming en het kwalitatief moleculair-genetisch onderzoek. De combinatie van deze twee velden levert belangrijke inzichten in het proces van bloedvatvorming en vormt daarmee een veelbelovend nieuw onderzoeksgebied.

Het algemene doel van dit proefschrift werd in de introductie omschreven als het ontrafelen van fysische en fylogenetische beperkingen tijdens de ontwikkeling van het bloedvatsysteem in gewervelde dieren. Ontwikkelt het bloedvatsysteem zich om tekorten aan zuurstof te ondervangen op het moment dat het begint te functioneren? We kunnen nu zeggen dat dit niet het geval is. Zowel de analytisch als de numerieke modellen laten zien dat via alleen diffusie nog steeds voldoende zuurstof naar de embryo's getransporteerd wordt op het moment dat er een functioneel bloedvatsysteem aanwezig is (vgl. hoofdstukken 3, 5, 6 en 7). De resultaten van een hemoglobine-ablatie experiment (Pelster and Burggren, 1996) gaven ook aanleiding tot het zetten van vraagtekens bij de rol van het vroege bloedvatstelsel in het transport van zuurstof

en onderschrijven dus onze conclusie. Blijkbaar bouwt de natuur een zekere veiligheidsmarge in om ervoor te zorgen dat het bloedvatsysteem in elk geval klaar is op de moment dat het daadwerkelijk nodig is.

Hoewel het bloedvatstelsel dus niet gevormd wordt om acuut zuurstofgebrek te verhelpen, kunnen lage zuurstofspanningen wel belangrijke regulerende factoren zijn voor de vorming van de vaten. Dit kon echter niet experimenteel worden bevestigd en de (initiële) vorming van het bloedvatstelsel (vasculogenese) van de zebravis lijkt voornamelijk genetisch bepaald (hoofdstuk 8). Andere studies tonen echter aan dat zuurstof wel invloed heeft op de bloedvatontwikkeling. Wanneer deze invloed begint en hoe uitgebreid hij is zal in vervolgonderzoek moeten worden vastgesteld.

Een ander interessant aspect van de vorming van het bloedvatstelsel bij gewervelde dieren is de mogelijke beperking die andere factoren dan zuurstof opleggen (*e.g.* transport van afvalstoffen, signaalmoleculen, hormonen *etc.*). Het transport van voedingsstoffen lijkt een belangrijke functie van het vroege bloedvatstelsel (hoofdstuk 4), maar verder onderzoek is nodig om dit duidelijk aan te tonen.

Bibliography

- ABRAMOWITZ, M. AND STEGUN, E. A. (eds.) (1965). *Handbook of mathematical functions with formulas, graphs and mathematical tables*. New York: Dover Publications, Inc.
- ALDERDICE, D. F., JENSEN, J. O. T. AND VELSEN, F. P. J. (1984). Measurement of hydrostatic pressure in salmonid eggs. *Can. J. Zool.* **62**, 1977–1987, *cited in*: Rombough, 1988.
- ALTMANN, P. L. AND DITTMER, D. S. (eds.) (1971). *Respiration and circulation*. Bethesda, Maryland: Federation of American Societies for Experimental Biology.
- BALINSKY, B. I. (1975). *An introduction to embryology*. Philadelphia: Saunders.
- BALLARD, W. W. (1976). Problems of gastrulation: real and verbal. *BioScience* **26**(1), 36–39.
- BECK, H., ACKER, T., WIESSNER, C., ALLEGRI, P. R. AND PLATE, K. H. (2000). Expression of angiopoietin-1, angiopoietin-2, and Tie receptors after middle cerebral artery occlusion in the rat. *Am. J. Pathol.* **157**(5), 1473–1483.
- BECK, L. AND D'AMORE, P. (1997). Vascular development: cellular and molecular regulation. *FASEB J.* **11**, 365–373.
- BEREZOVSKY, V. A., GOIDA, E. A., MUKALOV, I. O. AND SUSHKO, B. S. (1979). An experimental study of oxygen distribution. *Fiziol. Zh. SSSR* **25**(4), 379–389.
- BIRD, R. B., STEWART, W. E. AND LIGHTFOOT, E. N. (1960). *Transport phenomena*. New York: John Wiley & Sons, Inc.
- BLAXTER, J. H. S. (1988). Pattern and variety in development. In: W. S. Hoar and D. J. Randall (eds.) *The physiology of developing fish, part A Eggs and larvae*, vol. XI of *Fish physiology*, San Diego: Academic Press, Inc.

- BOUSSAT, S., EDDAHIBI, S., COSTE, A., FATACCIOLI, V., GOUGE, M., HOUSSET, B., ADNOT, S. AND MAITRE, B. (2000). Expression and regulation of vascular endothelial growth factor in human pulmonary epithelial cells. *Am. J. Physiol.* **179**, L371–L378.
- BRIAN, P. L. T. AND HALES, H. B. (1969). Effects of transpiration and changing diameter on heat and mass transfer to spheres. *A.I.Ch.E. J.* **15**(3), 419–425.
- BROGI, E., SCHATTEMAN, G., WU, T., KIM, E. A., VARTICOVSKI, L., KEYT, B. AND ISNER, J. M. (1996). Hypoxia-induced paracrine regulation of vascular endothelial growth factor receptor expression. *J. Clin. Invest.* **97**(2), 469–476.
- BROWDER, L. W. (1984). *Developmental biology*. 2nd edn., Philadelphia: Saunders College Publishing.
- BROWN, L. A., RODAWAY, A. R. F., SCHILLING, T. F., JOWETT, T., INGHAM, P. W., PATIENT, R. K. AND SHARROCKS, A. D. (2000). Insights into early vasculogenesis revealed by expression of the ETS-domain transcription factor Fli-1 in wild-type mutant zebrafish embryos. *Mech. Develop.* **90**, 237–252.
- BURGGREN, W. W. (1985). Gas exchange, metabolism, and “ventilation” in gelatinous frog egg masses. *Physiol. Zool.* **58**(5), 503–514.
- BURGGREN, W. W. AND TERRITO, P. R. (1995). Early development of blood oxygen transport. In: J. Houston and J. Coates (eds.) *Hypoxia and brain*, Burlington: Queen City Printer, *cited in*: Pelster and Burggren, 1996.
- BYATT-SMITH, J. G., LEESE, H. J. AND GOSDEN, R. G. (1991). An investigation by mathematical modelling of whether mouse and human preimplantation embryos in static culture can satisfy their demands for oxygen by diffusion. *Hum. Reprod.* **6**(1), 52–57.
- CAMBALIK, J. J., CHECKLEY, D. M. AND KAMYKOWSKI, D. (1998). A new method to measure the terminal velocity of small particles: A demonstration using ascending eggs of the Atlantic menhaden (*Brevoortia tyrannus*). *Limnol. Oceanogr.* **43**(7), 1722–1727.
- CARMELIET, P., FERREIRA, V., BREIER, G., POLLEFEYT, S., KIECKENS, L., GERTSENSTEIN, M., FAHRIG, M., VANDENHOECK, A., HARPAL, K., EBERHARDT, C., DECLERCQ, C., PAWLING, J., MOONS, L., COLLEN, D., RISAU,

- W. AND NAGY, A. (1996). Abnormal blood vessel development and lethality in embryos lacking a single VEGF allele. *Nature* **380**, 435–439.
- CARSLAW, H. S. AND JAEGER, J. C. (1959). *Conduction of heat in solids*. 2nd edn., Oxford: Clarendon Press.
- CETTA, C. M. AND CAPUZZO, J. M. (1982). Physiological and biochemical aspects of embryonic and larval development of the winter flounder *Pseudopleuronectes americana*. *Mar. Biol.* **71**, 327–337.
- CHEN, J.-N., HAFFTER, P., ODENTHAL, J., VOGELSANG, E., BRAND, M., VAN EEDEN, F. J. M., FURUTANI-SEIKI, M., GRANATO, M., HAMMER-SCHMIDT, M., HEISENBERG, C.-P., JIANG, Y.-J., KANE, D. A., KELSH, R. N., MULLINS, M. C. AND NÜSSLEIN-VOLHARD, C. (1996). Mutations affecting the cardiovascular system and other internal organs in zebrafish. *Development* **124**, 293–302.
- CHURCHILL, R. V. (1955). Extensions of operational mathematics. Proc. Conf. Diff. Eqns., University of Maryland.
- CLIFT, R., GRACE, J. R. AND WEBER, M. E. (1978). *Bubbles, drops, and particles*. New York: Academic Press.
- CRANK, J. (1975). *The mathematics of diffusion*. 2nd edn., Oxford: Clarendon Press.
- CURRIE, J. A. (1961). Gaseous diffusion in the aeration of aggregated soils. *Soil Sci.* **92**, 40–45.
- CUSSLER, E. L. (1997). *Diffusion, mass transfer in fluid systems*. 2nd edn., Cambridge: Cambridge University Press.
- DAYKIN, P. N. (1965). Application of mass transfer theory to the problem of respiration of fish eggs. *J. Fish. Res. Board Can.* **22**(1), 159–171.
- DESAULNIERS, N., MOERLAND, T. S. AND SIDELL, B. D. (1996). High lipid content enhances the rate of oxygen diffusion through fish skeletal muscle. *Am. J. Physiol.* **271**, R42–R47.
- DESILVA, C. D. AND TYTLER, P. (1973). The influence of reduced environmental oxygen on the metabolism and survival of herring and plaice larvae. *Neth. J. Sea Res.* **7**, 345–362.

- DOR, Y., PORAT, R. AND KESHET, E. (2001). Vascular endothelial growth factor and vascular adjustments to perturbations in oxygen homeostasis. *Am. J. Physiol.* **280**, C1367–C1374.
- DOWSE, H. B., NORTON, S. AND SIDELL, B. D. (2000). The estimation of the diffusion constant and solubility of O₂ in tissue using kinetics. *J. Theor. Biol.* **207**, 531–541.
- DROST, M. R. AND VAN DEN BOOGAART, J. G. M. (1986). A simple method for measuring the changing volume of small biological objects, illustrated by studies of suction feeding by fish larvae and of shrinkage due to histological fixation. *J. Zool.* **209**, 239–249.
- DRUMMOND, I. A., MAJUMDAR, A., HENTSCHEL, H., ELGER, M., SOLNICKA-KREZEL, L., SCHIER, A. F., NEUHAUSS, S. C. F., STEMPLE, D. L., ZWARTKRUIS, F., RANGINI, Z., DRIEVER, W. AND FISHMAN, M. C. (1998). Early development of the zebrafish pronephros and analysis of mutations affecting pronephric function. *Development* **125**, 4655–4667.
- DUBOULE, D. (ed.) (1994a). *Guidebook to the homeobox genes*. Oxford: Oxford University Press.
- DUBOULE, D. (1994b). Temporal colinearity and the phylotypic progression: a basis for the stability of a vertebrate Bauplan and the evolution of morphologies through heterochrony. *Development Supplement* **1994**, 135–142.
- DUFFY, D. G. (1994). *Transform methods for solving partial differential equations*. Boca Raton, FL: CRC Press.
- ELDRIDGE, M. B., ECHEVERRIA, T. AND WHIPPLE, J. A. (1977). Energetics of pacific herring (*Clupea harengus pallasii*) embryos and larvae exposed to low concentrations of benzene, a monoaromatic component of crude oil. *T. Am. Fish. Soc.* **106**(5), 452–461.
- ELINSON, R. P. (1987). Change in developmental patterns: embryos of amphibians with large eggs. In: R. A. Raff and E. C. Raff (eds.) *Development as an evolutionary process*, pp. 1–21, New York: Alan R. Liss, Inc.

- FAIRWEATHER, G. (1978). *Finite element Galerkin methods for differential equations*. New York: Dekker.
- FENN, W. O. (1927). The oxygen consumption of frog nerve during stimulation. *J. Gen. Physiol.* **10**, 767–779.
- FERRARA, N., CARVER-MOORE, K., CHEN, H., DOWD, M., LU, L., O'SHEA, K. S., POWELL-BRAXTON, L., HILLAN, K. J. AND MOORE, M. W. (1996). Heterozygous embryonic lethality induced by targeted inactivation of the VEGF gene. *Nature* **380**, 439–442.
- FEYNMAN, R. P. (1998). *The meaning of it all*. Harmondsworth, Middlesex, England: Penguin Books Ltd.
- FICK, A. (1855). Ueber diffusion. *Ann. Phys.* **170**, 59–86.
- FINN, R. N., FYHN, H. J. AND EVJEN, M. S. (1991). Respiration and nitrogen metabolism of Atlantic halibut eggs (*Hippoglossus hippoglossus*). *Mar. Biol.* **108**, 11–19.
- FONG, G.-H., ROSSANT, J., GERTSENSTEIN, M. AND BREITMAN, M. L. (1995). Role of the Flt-1 receptor tyrosine kinase in regulating the assembly of vascular endothelium. *Nature* **376**, 66–70.
- FRIEDLANDER, S. K. (1957). Mass and heat transfer to single spheres and cylinders at low Reynolds numbers. *A.I.Ch.E. J.* **3**(1), 43–48.
- FRIEDLANDER, S. K. (1961). A note on transport to spheres in Stokes flow. *A.I.Ch.E. J.* **7**(2), 347–348.
- GASSMANN, M., FANDREY, J., BICHET, S., WARTENBERG, M., MARTI, H. H., BAUER, C., WENGER, R. H. AND ACKER, H. (1996). Oxygen supply and oxygen-dependent gene expression in differentiating embryonic stem cells. *P. Natl. Acad. Sci. USA* **93**, 2867–2872.
- GERARD, R. W. (1931). Oxygen diffusion into cells. *Biol. Bull.* **60**(3), 245–268.
- GERBER, H.-P., CONDORELLI, F., PARK, J. AND FERRARA, N. (1997). Differential transcriptional regulation of the two vascular endothelial growth factor receptor genes. *J. Biol. Chem.* **272**(38), 23659–23667.

- GIELEN, J. L. W. (2000). The general packed column: an analytical solution. *IMA J. Appl. Math.* **65**, 123–146.
- GIELEN, J. L. W. AND KRANENBARG, S. (2002). Oxygen balance for small organisms: an analytical model. *B. Math. Biol.* **64**(1), 175–207.
- GILBERT, S. F. (1991). *Developmental biology*. 3rd edn., Sunderland, Massachusetts: Sinauer Associates, Inc.
- GILBERT, S. F. (1994). *Developmental biology*. 4th edn., Sunderland: Sinauer Associates Inc.
- GOLTERMAN, H. L., CLYMA, R. S. AND OHNSTAD, M. A. M. (1978). *Methods for physical and chemical analysis of fresh waters*, vol. 8 of *IBP handbook*. 2nd edn., Oxford: Blackwell Scientific Publications.
- GRAHAM, J. B. (1988). Ecological and evolutionary aspects of integumentary respiration: body size, diffusion, and the invertebrata. *Am. Zool.* **28**, 1031–1045.
- GROTE, J. AND THEWS, G. (1962). Die Bedingungen für die Sauerstoffversorgung des Herzmuskelgewebes. *Pflüg. Arch. Ges. Phys.* **276**, 142–165.
- GRUNWALD, D. J., KIMMEL, C. B., WESTERFIELD, M., WALKER, C. AND STREISINGER, G. (1988). A neural degeneration mutation that spares primary neurons in the zebrafish. *Dev. Biol.* **126**, 115–128.
- HAECKEL, E. (1877). *Anthrophogenie oder Entwicklungsgeschichte des Menschen*. Leipzig: Verlag von Wilhelm Engelmann.
- HAECKEL, E. (1902). *Natürliche Schöpfungs-Geschichte*. 10th edn., Berlin: Georg Reimer.
- HALL, B. K. (1992). *Evolutionary developmental biology*. London: Chapman & Hall.
- HARVEY, E. N. (1928). The oxygen consumption of luminous bacteria. *J. Gen. Physiol.* **11**, 469–475.
- HARVEY, R. P. (1996). NK-2 Homeobox genes and heart development. *Dev. Biol.* **178**, 203–216.

- HARVEY POUGH, F., JANIS, C. M. AND HEISER, J. B. (2002). *Vertebrate life*. 6th edn., Upper Saddle River, New Jersey: Prentice Hall.
- HEMING, T. A. AND BUDDINGTON, R. K. (1988). Yolk absorption in embryonic and larval fishes. In: W. S. Hoar and D. J. Randall (eds.) *Fish Physiology*, vol. XI A, pp. 407–446, New York: Academic Press.
- HÜFFNER, G. (1897). Ueber die Bestimmung der Diffusionscoefficienten einiger Gase für Wasser. *Ann. Phys. Chem. Neue Folge* **60**, 134–168.
- HYNES, H. B. N. (1970). *The ecology of running waters*. Liverpool: Liverpool University Press.
- IKEDA, E., ACHEN, M. G., BREIER, G. AND RISEAU, W. (1995). Hypoxia-induced transcriptional activation and increased mRNA stability of vascular endothelial growth factor in C6 glioma cells. *J. Biol. Chem.* **270**(34), 19761–19766.
- ISOgai, S., Horiguchi, M. AND WEINSTEIN, B. M. (2001). The vascular anatomy of the developing zebrafish: an atlas of embryonic and early larval development. *Dev. Biol.* **230**, 278–301.
- IYER, N. V., KOTCH, L. E., AGANI, F., LEUNG, S. W., LAUGHNER, E., WENGER, R. H., GASSMANN, M., GEARHART, J. D., LAWLER, A. M., YU, A. Y. AND SEMENZA, G. L. (1997). Cellular and developmental control of O₂ homeostasis by hypoxia-inducible factor 1 α . *Gene. Dev.* **12**, 149–162.
- JAKOB, M. (1949). *Heat transfer*, vol. I. New York: John Wiley & Sons, Inc, reprint Status: On Request 970115.
- JOHNSON, R. A. (1980). Oxygen transport in salmon spawning gravels. *Can. J. Fish. Aquat. Sci.* **37**, 155–162.
- KAMLER, E. (1992). *Early life history of fish. An energetics approach*. London: Chapman & Hall.
- KAMLER, E., SZLAMINSKA, M., KUCZYNSKI, M., HAMÁCKOVÁ, J., KOURIL, J. AND DABROWSKI, K. (1994). Temperature-induced changes of early development and yolk utilization in the African catfish *Clarias gariepinus*. *J. Fish Biol.* **44**, 311–326.

- KAUSHIK, S. J., DABROWSKI, K. AND LUQUET, P. (1982). Patterns of nitrogen excretion and oxygen consumption during ontogenesis of common carp (*Cyprinus carpio*). *Can. J. Fish. Aquat. Sci.* **39**, 1095–1105.
- KIMMEL, C. B., BALLARD, W. W., KIMMEL, S. R., ULLMAN, B. AND SCHILLING, T. F. (1995). Stages of embryonic development of the zebrafish. *Dev. Dynam.* **203**, 253–310.
- KRANENBARG, S., MULLER, M., GIELEN, J. L. W. AND VERHAGEN, J. H. G. (2000). Physical constraints on body size in teleost embryos. *J. Theor. Biol.* **204**, 113–133.
- KRANENBARG, S., VAN DEN BOOGAART, J. G. M. AND VAN LEEUWEN, J. L. (2002). Oxygen profile in zebrafish embryo (*Danio rerio*) elucidated by theory and experiment **in prep.**
- KRANENBARG, S., VERHAGEN, J. H. G., MULLER, M. AND VAN LEEUWEN, J. L. (2001). Consequences of forced convection for the constraints on size and shape in embryos. *J. Theor. Biol.* **212**, 521–533.
- KROGH, A. (1919). The rate of diffusion of gases through animal tissues, with some remarks on the coefficient of invasion. *J. Physiol. London* **52**, 391–408.
- KROGH, A. (1941). *The comparative physiology of respiratory mechanisms*. Philadelphia: University of Pennsylvania Press.
- LADOUX, A. AND FRELIN, C. (1993). Hypoxia is a strong inducer of vascular endothelial growth factor mRNA expression in the heart. *Biochem. Bioph. Res. Co.* **195**(2), 1005–1010.
- LEE, C. E. AND STRATHMANN, M. F. (1998). Scaling of gelatinous clutches: effects of siblings' competition for oxygen on clutch size and parental investment per offspring. *Am. Nat.* **151**(4), 293–310.
- LEE, Y. M., JEONG, C.-H., KOO, S.-Y., SON, M. J., SONG, M. S., BAE, S.-K., RALEIGH, J. A., CHUNG, H.-Y., YOO, M.-A. AND KIM, K.-W. (2001). Determination of hypoxic region by hypoxia marker in developing mouse embryos in vivo: a possible signal for vessel development. *Dev. Dynam.* **220**, 175–186.

- LEVY, A. P., LEVY, N. S. AND GOLDBERG, M. A. (1996). Post-transcriptional regulation of vascular endothelial growth factor by hypoxia. *J. Biol. Chem.* **271**(5), 2746–2753.
- LEVY, A. P., LEVY, N. S., WEGNER, S. AND GOLDBERG, M. A. (1995). Transcriptional regulation of the rat vascular endothelial growth factor gene by hypoxia. *J. Biol. Chem.* **270**(22), 13333–13340.
- LIANG, D., CHANG, J. R., CHIN, A. J., SMITH, A., KELLY, C., WEINBERG, E. S. AND GE, R. (2001). The role of vascular endothelial growth factor (VEGF) in vasculogenesis, angiogenesis, and hematopoiesis in zebrafish development. *Mech. Develop.* **108**, 29–43.
- LIANG, D., XU, X., CHIN, A. J., BALASUBRAMANIAN, N. V., TEO, M. A. L., LAM, T. J., WEINBERG, E. S. AND GE, R. (1998). Cloning and characterization of vascular endothelial growth factor (VEGF) from zebrafish, *Danio rerio*. *Biochim. Biophys. Acta* **1397**, 14–20.
- LIU, Y., COX, S. R., MORITA, T. AND KOUREMBANAS, S. (1995). Hypoxia regulates vascular endothelial growth factor gene expression in endothelial cells. *Circ. Res.* **77**(3), 638–643.
- LONGMUIR, I. S. (1957). Respiration rate of rat-liver cells at low oxygen concentrations. *Biochem. J.* **65**, 378–382.
- MAHLER, M., LOUY, C., HOMSHER, E. AND PESKOFF, A. (1985). Reappraisal of diffusion, solubility, and consumption of oxygen in frog skeletal muscle, with applications to muscle energy balance. *J. Gen. Physiol.* **86**, 105–134.
- MALTEPE, E. AND SIMON, M. C. (1998). Oxygen, genes, and development: An analysis of the role of hypoxic gene regulation during murine vascular development. *J. Mol. Med.* **76**, 391–401.
- MCADAMS, W. H. (1951). *Heat transmission*. London: McGraw-Hill Publishing Company Ltd.
- McFARLAND, W. N., HARVEY POUGH, F., CADE, T. J. AND HEISER, J. B. (1979). *Vertebrate life*. New York: Macmillan Publishing Co., Inc.

- MCNEILL ALEXANDER, R. (1971). *Size and shape*, vol. 29 of *Studies in biology*. London: Edward Arnold.
- MCNOWN, J. S. AND MALAIKA, J. (1950). Effects of particle shape on settling velocity at low Reynolds numbers. *EOS T. Am. Geophys. Un.* **31**(1), 74–82.
- MILLINGTON, R. J. (1955). Diffusion constant and diffusion coefficient. *Science* **122**, 1090–1091.
- MINAMI, S. (1923). Versuche an überlebendem Carcinomgewebe. *Biochem. Z.* **142**, 334–350.
- MOSER, H. G. (ed.) (1996). *The early stages of fishes in the California current region*, vol. Atlas no. 33 of *California cooperative oceanic fisheries investigations*. Lawrence, KA: Allen Press, Inc.
- NAKATANI, T. AND MAEDA, T. (1993). Early life history of the walleye pollock. *Sci. Rep. Hokkaido Fish. Exp. Stn.* **42**, 15–22.
- NAMIKI, A., BROGI, E., KEARNEY, M., KIM, E. A., WU, T., COUFFINHAL, T., VARTICOVSKI, L. AND ISNER, J. M. (1995). Hypoxia induces vascular endothelial growth factor in cultured human endothelial cells. *J. Biol. Chem.* **270**(52), 31189–31195.
- NASEVICIUS, A., LARSON, J. AND EKKER, S. C. (2000). Distinct requirements for zebrafish angiogenesis revealed by a *VEGF-A* morphant. *Yeast* **17**, 294–301.
- NELSON, S. G. AND WILKINS, S. D. (1994). Growth and respiration of embryos and larvae of the rabbitfish *Siganus randalli* (Pisces, Siganidae). *J. Fish Biol.* **44**, 513–525.
- NEUDECKER, T. (1976). Die Embryonalentwicklung des Karpfens (*Cyprinus carpio* L.). *Arch. Fischereiwiss.* **27**(1), 25–35.
- O'BRIEN, R. N., VISAISOUK, S. AND RAINE, R. (1978). Natural convection: A mechanism for transporting oxygen to incubating salmon eggs. *J. Fish. Res. Board Can.* **35**, 1316–1321.
- OOMENS, C. W. J., VAN RATINGEN, M. R., JANSSEN, J. D., KOK, J. J. AND HENDRIKS, M. A. N. (1993). A numerical-experimental method for a mechanical characterization of biological materials. *J. Biomech.* **26**(4/5), 617–621.

- OSSE, J. W. M. AND VAN DEN BOOGAART, J. G. M. (1994). Resistive and reactive components in swimming of carp larvae. In: *SEB Symposium Biological Fluid Dynamics*, University of Leeds.
- PADILLA, P. A. AND ROTH, M. B. (2001). Oxygen deprivation causes suspended animation in the zebrafish embryo. *P. Natl. Acad. Sci. USA* **98**(13), 7331–7335.
- PATAN, S. (2000). Vasculogenesis and angiogenesis as mechanisms of vascular network formation, growth and remodelling. *J. Neuro-Oncol.* **50**, 1–15.
- PELSTER, B. AND BURGGREN, W. W. (1996). Disruption of hemoglobin oxygen transport does not impact oxygen-dependent physiological processes in developing embryos of zebra fish (*Danio rerio*). *Circ. Res.* **79**, 358–362.
- PINDER, A. W. AND FRIET, S. C. (1994). Oxygen transport in egg masses of the amphibians *Rana sylvatica* and *Ambystoma maculatum*: convection, diffusion and oxygen production by algae. *J. Exp. Biol.* **197**, 17–30.
- POTTS, W. T. W. AND RUDY, P. P. (1969). Water balance in the eggs of the atlantic salmon *Salmo salar*. *J. Exp. Biol.* **50**, 223–237.
- PURCELL, E. M. (1977). Life at low Reynolds number. *Am. J. Phys.* **45**(1), 3–11.
- RAFF, R. A. (1996). *The shape of life; genes, development, and the evolution of animal form*. Chicago: The University of Chicago Press.
- RAFF, R. A., WRAY, G. A. AND HENRY, J. J. (1991). Implications of radical evolutionary changes in early development for concepts of developmental constraint. In: L. Warren and M. Meselson (eds.) *New perspectives in evolution*, New York: Liss/Wiley, cited in: Gilbert, 1991.
- RAPPOLDT, C. (1992). *Diffusion in aggregated soil*. Ph.D. thesis, Landbouwniversiteit Wageningen.
- RICHARDSON, M. K. (1995). Heterochrony and the phylotypic period. *Dev. Biol.* **172**, 412–421.
- RICHARDSON, M. K. (1999). Vertebrate evolution: the developmental origins of adult variation. *BioEssays* **21**(7), 604–613.

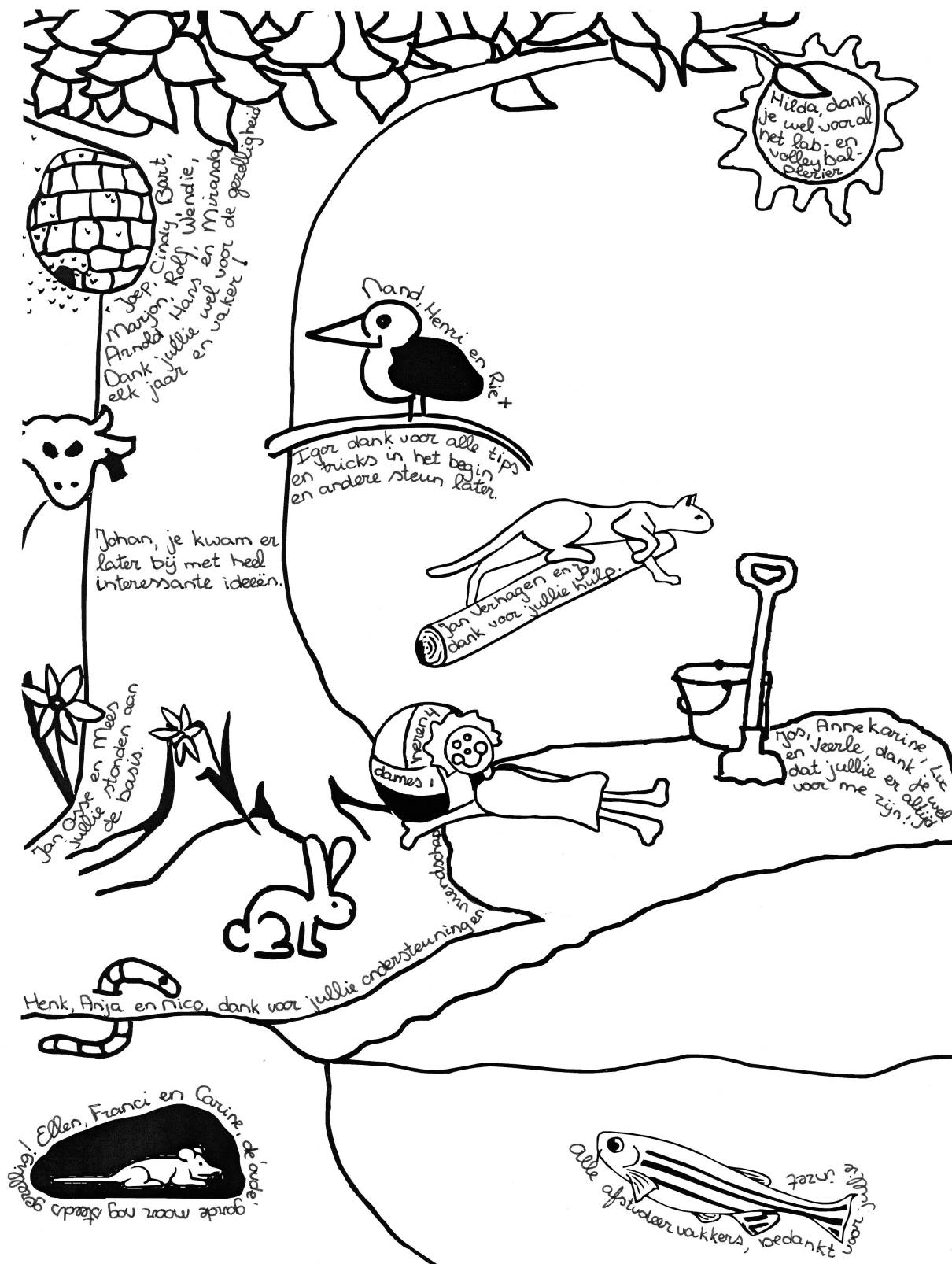
- RICHARDSON, M. K., HANKEN, J., GOONERATNE, M. L., PIEAU, C., RAYNAUD, A., SELWOOD, L. AND WRIGHT, G. M. (1997). There is no highly conserved embryonic stage in the vertebrates: implications for current theories of evolution and development. *Anat. Embryol.* **196**, 91–106.
- RICHARDSON, M. K., HANKEN, J., SELWOOD, L., WRIGHT, G. M., RICHARDS, R. J. AND PIEAU, C. (1998). Haeckel, embryos, and evolution. *Science* **280**, 983–984.
- RIEB, J.-P. (1973). La circulation sanguine chez l'embryon de *Brachydanio rerio* (Téléostéens, Cyprinidae). *Ann. Embryol. Morph.* **6**(1), 43–54.
- RISAU, W. (1997). Mechanisms of angiogenesis. *Nature* **386**, 671–674.
- RISAU, W. AND FLAMME, I. (1995). Vasculogenesis. *Annu. Rev. Cell Dev. Biol.* **11**, 73–91.
- ROMBOUGH, P. J. (1988). Respiratory gas exchange, aerobic metabolism, and effects of hypoxia during early life. In: W. S. Hoar and D. J. Randall (eds.) *The physiology of developing fish, part A Eggs and larvae*, vol. XI of *Fish physiology*, pp. 59–161, San Diego: Academic Press, Inc.
- ROMBOUGH, P. J. (1998). Partitioning of oxygen uptake between the gills and skin in fish larvae: a novel method for estimating cutaneous oxygen uptake. *J. Exp. Biol.* **201**, 1763–1769.
- ROMBOUGH, P. J. AND MOROZ, B. M. (1990). The scaling and potential importance of cutaneous and branchial surfaces in respiratory gas exchange in young chinook salmon (*Oncorhynchus tshawytscha*). *J. Exp. Biol.* **154**, 1–12.
- ROSEN, J. B. (1952). Kinetics of a fixed bed system for solid diffusion into spherical particles. *J. Chem. Phys.* **20**, 378–394.
- ROSSO, J. AND LUKINS, S. (1986). *Het delicatessenkookboek*. Utrecht: Het Spectrum B.V.
- SCHWERTE, T. AND PELSTER, B. (2000). Digital motion analysis as a tool for analysing the shape and performance of the circulatory system in transparent animals. *J. Exp. Biol.* **203**, 1659–1669.

- SCOTT, W. B. AND CROSSMAN, E. J. (1973). *Freshwater fishes of Canada*. Ottawa: Fisheries Research Board of Canada, Bulletin 184.
- SEMENZA, G. L. (2001). Regulation of hypoxia-induced angiogenesis: a chaperone escorts VEGF to the dance. *J. Clin. Invest.* **108**(1), 39–40.
- SEYMOUR, R. S. (1994). Oxygen diffusion through the jelly capsules of amphibian eggs. *Israel J. Zool.* **40**, 493–506.
- SEYMOUR, R. S. AND BRADFORD, D. F. (1987). Gas exchange through the jelly capsule of the terrestrial eggs of the frog, *Pseudophryne bibroni*. *J. Comp. Physiol. B* **157**, 477–481.
- SEYMOUR, R. S. AND BRADFORD, D. F. (1995). Respiration of amphibian eggs. *Physiol. Zool.* **68**(1), 1–25.
- SHALABY, F., HO, J., STANFORD, W. L., FISCHER, K.-D., SCHUH, A. C., SCHWARTZ, L., BERNSTEIN, A. AND ROSSANT, J. (1997). A requirement for Flk1 in primitive and definitive hematopoiesis and vasculogenesis. *Cell* **89**, 981–990.
- SHALABY, F., ROSSANT, J., YAMAGUCHI, T. P., GERTSENSTEIN, M., WU, X.-F., BREITMAN, M. L. AND SCHUH, A. C. (1995). Failure of blood-island formation and vasculogenesis in Flk-1-deficient mice. *Nature* **376**, 62–66.
- SHIMA, D. T., DEUTSCH, U. AND D'AMORE, P. (1995). Hypoxic induction of vascular endothelial growth factor (VEGF) in human epithelial cells is mediated by increases in mRNA stability. *FEBS Lett.* **370**, 203–208.
- SHWEIKI, D., ITIN, A., SOFFER, D. AND KESHET, E. (1992). Vascular endothelial growth factor induced by hypoxia may mediate hypoxia-initiated angiogenesis. *Nature* **359**, 843–845.
- SIRE, M.-F., BABIN, P. J. AND VERNIER, J.-M. (1994). Involvement of the lysosomal system in yolk protein deposit and degradation during vitellogenesis and embryonic development in trout. *J. Exp. Zool.* **269**, 69–83.
- SKIDMORE, J. F. (1967). Oxygen uptake by zebrafish (*Brachydanio rerio*) of different ages in relation to zinc sulphate resistance. *J. Fish. Res. Board Can.* **24**(6), 1253–1267.

- SLACK, J. M. W., HOLLAND, P. W. H. AND GRAHAM, C. F. (1993). The zootype and the phylotypic stage. *Nature* **361**, 490–492.
- SPOOR, W. A. (1977). Oxygen requirements of embryos and larvae of the largemouth bass, *Micropterus salmoides* (Lacépède). *J. Fish Biol.* **11**(77–86).
- STAINIER, D. Y. R., FOUQUET, B., CHEN, J.-N., WARREN, K. S., WEINSTEIN, B. M., MEILER, S. E., MOHIDEEN, M.-A. P. K., NEUHAUSS, S. C. F., SOLNICA-KREZEL, L., SCHIER, A. F., ZWARTKRUIS, F., STEMPEL, D. L., MALICKI, J., DRIEVER, W. AND FISHMAN, M. C. (1996). Mutations affecting the formation and function of the cardiovascular system in the zebrafish embryo. *Development* **123**, 285–292.
- STEVENS, C., SCHIPPER, H., SAMALLO, J., STROBAND, H. W. J. AND TE KRONNIE, G. (1998). Blastomeres and cells with mesendodermal fates of carp embryos express *cth1*, a member of the *TIS11* family of primary response genes. *Int. J. Dev. Biol.* **42**, 181–188.
- STRATHMANN, R. R. AND CHAFFEE, C. (1984). Constraints on egg masses. II. Effect of spacing, size, and number of eggs on ventilation of masses of embryos in jelly, adherent groups, or thin-walled capsules. *J. Exp. Mar. Biol. Ecol.* **84**, 85–93.
- STROBAND, H. W. J., STEVENS, C., TE KRONNIE, G., SAMALLO, J., SCHIPPER, H., KRAMER, B. AND TIMMERMAN, L. P. M. (1995). Expression of *carp-cdx1*, a caudal homolog, in embryos of the carp, *Cyprinus carpio*. *Roux's Arch. Dev. Biol.* **204**, 369–377.
- SUMOY, L., KEASEY, J. B., DITTMAN, T. D. AND KIMELMAN, D. (1997). A role for notochord in axial vascular development by analysis of phenotype and the expression of VEGF-2 in zebrafish *flh* and *ntl* mutant embryos. *Mech. Develop.* **63**, 15–27.
- SUZUKI, T. AND SUYAMI, M. (1983). Free amino acids and phosphopeptides in the extracts of fish eggs. *B. Jpn. Soc. Sci. Fish.* **49**(11), 1747–1753.
- TUFRO-MCREDDIE, A., NORWOOD, V. F., AYLOR, K. W., BOTKIN, S. J., CAREY, R. M. AND GOMEZ, R. A. (1997). Oxygen regulates vascular endothelial growth factor-mediated vasculogenesis and tubulogenesis. *Dev. Biol.* **183**, 139–149.

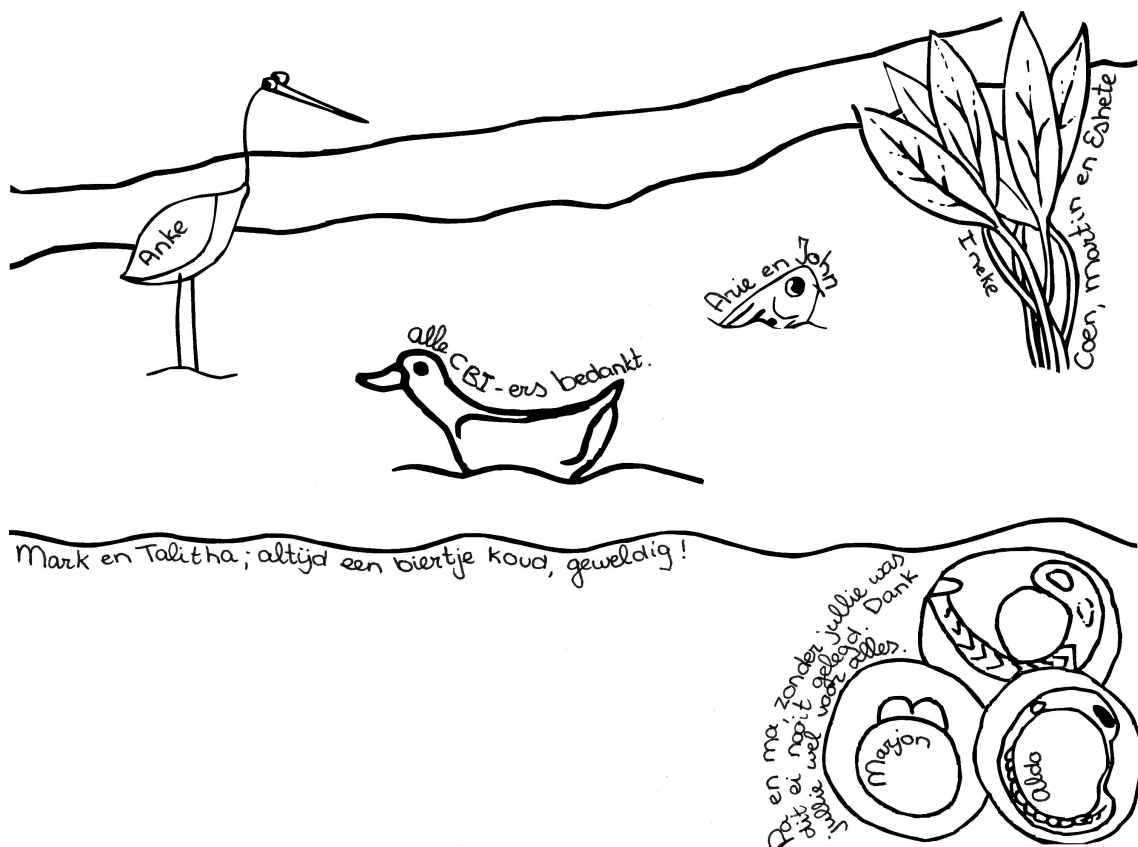
- VAN STROE, A. J. AND JANSSEN, L. J. J. (1993). Determination of the diffusion coefficient of oxygen in sodium chloride solutions with a transient pulse technique. *Analytica chim. Acta* **279**, 213–219.
- VOGEL, S. (1994). *Life in moving fluids - the physical biology of flow*. 2nd edn., Princeton: Princeton University Press.
- VON BAER, K. E. (1828). *Über Entwicklungsgeschichte der Thiere. Beobachtung und Reflexion*. Königsberg: Borntrager.
- WARBURG, O. (1923). Versuche an überlebendem Carcinomgewebe. *Biochem. Z.* **142**, 317–333.
- WEAST, R. C. (ed.) (1976). *Handbook of chemistry and physics*. 57th edn., Cleveland: CRC Press.
- WEIHS, D. (1980). Respiration and depth control as possible reasons for swimming of northern anchovy, *Engraulis mordax*, yolk-sac larvae. *Fish. B.* **78**(1), 109–117.
- WEINSTEIN, B. M. (1999). What guides early embryonic blood vessel formation? *Dev. Dynam.* **215**, 2–11.
- WEINSTEIN, B. M., SCHRIER, A. F., ABDELILAH, S., MALICKI, J., SOLNICKA-KREZEL, L., STEMPLE, D. L., STAINIER, D. Y. R., ZWARTKRUIS, F., DRIEVER, W. AND FISHMAN, M. C. (1996). Hematopoietic mutations in the zebrafish. *Development* **123**, 303–309.
- WESTRIN, B. A. AND AXELSSON, A. (1991). Diffusion in gels containing immobilized cells: a critical review. *Biotechnol. Bioeng.* **38**, 439–446.
- WICKETT, W. P. (1975). Mass transfer theory and the culture of fish eggs. In: W. A. Adams, G. Greer, J. E. Desnoyers, G. Atkinson, G. S. Kell, K. B. Oldham and J. Walkley (eds.) *Chemistry and physics of aqueous gas solutions*, pp. 419–434, Princeton: The Electrochemical Society, Inc.
- WILLMER, M. A. (1933). Some observations on the respiration of certain tropical fresh-water fishes. *J. Exp. Biol.* **11**, 283–306.
- WOLPERT, L. (1991). *The triumph of the embryo*. Oxford: Oxford University Press.

- WOODS, H. A. (1999). Egg-mass size and cell size: effects of temperature on oxygen distribution. *Am. Zool.* **39**, 244–252.
- YANCOPOULOS, G. D., DAVIS, S., GALE, N. W., RUDGE, J. S., WIEGAND, S. J. AND HOLASH, J. (2000). Vascular-specific growth factors and blood vessel formation. *Nature* **407**, 242–248.
- YUE, X. AND TOMANEK, R. J. (1999). Stimulation of coronary vasculogenesis/angiogenesis by hypoxia in cultured embryonic hearts. *Dev. Dynam.* **216**, 28–36.
- ZAKI, M. I. AND ABDULA, A. (1983). The reproduction and development of *Clarias gariepinus* (Clariidae) from lake Manzala (Egypt). *J. Ichthyol.* **23**(6), 48–58.



Dankwoord

Met weemoed terugkijkend op de afgelopen vier jaar, kan ik zeggen dat promoveren een leerzame maar vooral leuke onderneming is. Hoewel slechts mijn naam prijkt op de titelpagina van dit proefschrift, hebben aan de totstandkoming ervan velen een belangrijke bijdrage geleverd. Ik ben er trots op dat zoveel mensen mij op zowel wetenschappelijk als op sociaal gebied hebben willen ondersteunen en hoop dat ze dat blijven doen! Om niet te verzanden in te lange stukken tekst, wil ik iedereen, geïnspireerd door een kookboek van Rosso and Lukins (1986), een plaatsje geven in het geheel en hen op die manier bedanken voor de onuitwisbare indruk die ze hebben achtergelaten. Thank you very much, we enjoyed ourselves! (naar Feynman (1998))



Curriculum Vitae

Sander Kranenbarg werd op 26 augustus 1974 geboren te Ede. In 1992 behaalde hij zijn VWO diploma aan het Christelijk Streek-Lyceum Ede en in datzelfde jaar begon hij met de studie Biologie aan de Landbouwniversiteit te Wageningen. Tijdens zijn eerste afstudeervak, uitgevoerd in Ethiopië en bij de vakgroep Experimentele Diermorfologie en Celbiologie onder leiding van Nand Sibbing, werden de grootte- en smaakselectiecapaciteiten van verschillende barbelen uit het Tanameer (Ethiopië) onderzocht. Hierbij werd de bouw van de dieren gerelateerd aan hun functioneren (Functionele Diermorfologie). In zijn tweede afstudeervak, uitgevoerd bij de afdeling biologie van de Rijksuniversiteit Groningen onder leiding van Joost Tinbergen, werd een ecologische benadering gekozen. Het effect van handicapping op de voederfrequentie van koolmezen werd in het veld onderzocht en gemodelleerd in een wiskundig model. Zijn derde afstudeervak werd wederom bewerkt aan de vakgroep Experimentele Diermorfologie en Celbiologie, nu onder leiding van Mees Muller. De beperking die diffusie oplegt aan het groter worden van embryo's vormde het onderwerp van dit afstudeervak. In 1997 studeerde hij met lof af. Dit examen werd gevolgd door diverse aanstellingen als studentassistent en toegevoegd docent aan de leerstoelgroep experimentele dierkunde, waarin verschillende biologische practica werden begeleid en ontwikkeld. Met de hulp van Jan Osse en Mees Muller werd het onderwerp van zijn derde afstudeervak uitgewerkt tot een project-voorstel. Dit project werd goedgekeurd door de onderzoeksschool WIAS en op 16 april 1998 trad hij in dienst bij de leerstoelgroep experimentele dierkunde als assistent in opleiding (aio). De resultaten van het in dit proefschrift beschreven promotieonderzoek verschenen in diverse internationale vakbladen en werden gepresenteerd tijdens diverse internationale congressen. In 2000 werd het artikel dat de basis vormt voor hoofdstuk drie bekroond met de 'WIAS PhD Student's Publication Prize', terwijl in datzelfde jaar een mondelinge voordracht over dit onderwerp goed was voor de Bolk-prijs van de Nederlandse Anatomen Vereniging.

Publication List

GIELEN, J.L.W. AND KRANENBARG, S. (2002). Oxygen balance for small organisms: an analytical model. *Bulletin of Mathematical Biology* **64**(1), 175-207.

KRANENBARG, S. (1997). Inland-strayed Long-tailed Skua *Stercorarius longicaudus* victim of Goshawk *Accipiter gentilis*. *Limosa* **70**(2), 76-77.


KRANENBARG, S. (2000). The phylotypic egg timer. *Netherlands Journal of Zoology* **50**(2), 289-294.

KRANENBARG, S., MULLER, M., GIELEN, J.L.W. AND VERHAGEN, J.H.G. (2000). Physical constraints on body size in vertebrate embryos. *Journal of Theoretical Biology* **204**(1), 113-133.

KRANENBARG, S., VERHAGEN, J.H.G., MULLER, M. AND VAN LEEUWEN, J.L. (2001). Consequences of forced convection for the constraints on size and shape in embryos. *Journal of Theoretical Biology* **212**(4), 521-533.

SANZ, J.J., KRANENBARG, S. AND TINBERGEN, J.M. (2000). Differential response by males and females to manipulation of partner contribution in the great tit (*Parus major*). *Journal of Animal Ecology* **69**, 74-84.

Printing of this thesis was financially supported by FEMLAB®.

- Omslag: De omslag verbeeldt de volgende gedachten bij de inhoud van dit proefschrift. 'Eindelijk zien ze het licht. De embryo's. Net bevrucht en nu samen zwevend in hun veilige leefruimte. Allemaal zijn ze gelijk; als identieke meerlingen. En allemaal dragen ze nieuw leven mee. Bruisende energie die zich wil ontwikkelen. De een zal uitgroeien tot dit en de ander tot dat. Maar dat beseffen ze nog niet. Nu is alles mooi en nu is er nog geen onderscheid. De toekomst lonkt als een opening in de verte. Ze zijn onderweg.'
- Omslagontwerp: Jan Kranenbarg
- Inkleuring:  van den Boogaart, 5 jaar
- Dankwoordontwerp: Talitha van der Meulen